



FIRE EFFECT ON NON-LOADBEARING LIGHT STEEL FRAMING WALLS – NUMERICAL AND SIMPLE CALCULATION METHODS

Larissa Lourdes Luz Ferreira

Thesis Presented to the School of Technology and Management of
Polytechnic Institute of Bragança to the Fulfilment of the
Requirements for the Master of Science Degree in Industrial
Engineering (Mechanical Engineering branch)

Supervised by:

Prof. Doctor Paulo Alexandre Gonçalves Piloto

Prof. Doctor Giovanni Bratti

Bragança

November 2019



FIRE EFFECT ON NON-LOADBEARING LIGHT STEEL FRAMING WALLS – NUMERICAL AND SIMPLE CALCULATION METHODS

Larissa Lourdes Luz Ferreira

Thesis Presented to the School of Technology and Management of
Polytechnic Institute of Bragança to the Fulfillment of the Requirements
for the Master of Science Degree in Industrial Engineering (Mechanical
Engineering branch)

Supervised by:

Prof. Doctor Paulo Alexandre Gonçalves Piloto

Prof. Doctor Giovanni Bratti

Bragança

November 2019

Acknowledgment

Firstly, I would like to thank God for providing me this opportunity to come so far as to follow a dream and learn about how to be a better person and professional.

Special thanks to the Federal University of Technology – Paraná (UTFPR) for guiding me in this path towards knowledge and to the Polytechnic Institute of Bragança (IPB) for receiving me so well and accepting me to learn and grow a lot more. I want to thank Prof. Robson Gonçalves Trentin, Prof. Maria Nalu Verona Gomes and Prof Giovanni Bratti for trusting me and allowing me to come for the double diploma.

Thanks to Prof. Paulo Alexandre Gonçalves Piloto and Prof. Giovanni Bratti for guiding me and supervising me in this work.

I want also to thank the people who stayed with me throughout this work, although not directly, but giving me support and strength to continue until the end. Thanks to my mom, Dulce Helena Luz, who beared with me through everything and to my boyfriend, Itan Alan Marinho de Oliveira, for always being there for me from Brazil. I want to thank my family for all the support and many letters I received throughout this journey. Thanks to all of my friends, those in Bragança and also those in Brazil for listening to me and helping me when necessary. Also, thanks to Ana Marques, who became my portuguese mom and took care of me through this time.

Every person in this list made it possible for me to finish this thesis and carry on towards my future, so I want them to know that I will never forget their help and support.

Abstract

This work presents a study on the effects of fire in non-loadbearing Light Steel Framing (LSF) walls. Since there is still a desire to use a much more simplified method in routine fire resistance design, the objective of this study is to propose an equation that describes the effective width for calculating the fire resistance through one dimensional simplified analysis also described in this study. The one dimensional analysis was possible by considering fourteen layers, where five layers are presented on the gypsum exposed wall, four layers on the cavity and five more layers on the gypsum unexposed wall. The heat flow is considered as one path in both of the gypsum layers but divided into five different paths in the cavity, considering heat transfer between different materials, only in the y direction. Two different methods for the calculation of the effective width were proposed and validated with eleven different configurations of LSF walls, with experimental and numerical two-dimensional results, in order to find which method is more effective. Lastly, parametric studies were made using seven different cavity insulation materials, five different spacing between studs and five different cavity spacing, maintaining every other specification as constant, to understand their role in fire resistance of LSF non-loadbearing walls.

Keywords: LSF Walls, Fire Resistance, Ansys APDL, Advanced Calculation Method, One Dimensional Analysis, Effective Width.

Resumo

Este trabalho apresenta um estudo nos efeitos de incêndios em estruturas de paredes leves em aço enformado a frio não portantes. Como há ainda um desejo de usar um método muito mais simplificado para encontrar um design de resistência ao fogo, o objetivo deste estudo é propor uma equação que descreva a largura efetiva para o cálculo da resistência ao fogo através de análise uni-dimensional que também é descrita neste estudo. A análise uni-dimensional foi possível considerando quatorze camadas, onde cinco camadas estão apresentadas na parede de gesso exposta ao fogo, quatro camadas na cavidade e mais cinco camadas na parede de gesso não exposta ao fogo. O fluxo de calor é considerado com um único caminho em ambas as paredes de gesso, porém dividido em cinco caminhos diferentes na cavidade, considerando transferência de calor entre materiais diferentes, apenas na direção y. Dois diferentes métodos para o cálculo da largura efetiva foram propostos e validados com onze diferentes configurações de paredes leves em aço enformado a frio, com resultados experimentais e numéricos de duas dimensões, a fim de encontrar qual método é mais eficaz. Por fim, estudos paramétricos foram realizados utilizando sete diferentes materiais de isolamento na cavidade, cinco diferentes espaçamentos entre os montantes verticais e cinco diferentes espaçamentos de cavidade, mantendo todas as outras especificações constantes, a fim de entender seu papel na resistência ao fogo de paredes leves em aço enformado a frio não portantes.

Palavras chave: Paredes de LSF, Resistência ao Fogo, Método Avançado de Cálculo, Análise Uni-dimensional, Largura Efetiva.

Contents

Acknowledgment.....	i
Abstract.....	iii
Resumo	v
1. Introduction.....	1
1.1. Objectives.....	1
1.2. Light Steel Framing Constructions.....	2
1.3. Plan of Thesis	4
2. State of the Art.....	5
2.1. Preliminary Studies.....	5
2.2. Light Steel Frame Studies.....	6
2.3. Cavities and Composites: the new concept	7
3. Analitical Methods.....	9
3.1. Multilayered Plane Walls.....	9
3.2. Parallel Path Method	11
3.3. Isothermal Planes (Serie-Parallel Path) Method	12
3.4. Zone Method.....	14
3.5. Ashrae Modified Zone Method.....	15
3.6. ISO 6946 Method.....	17
4. Fire	20
4.1. Heat Transfer Theory.....	20
4.2. Natural Fire Curve	23
4.3. Standard Fire Curves.....	25
4.4. Fire Resistance Requirements.....	26
5. Numerical Simulation	28

5.1.	Proposed Approach for Calculating the Effective Width	29
5.1.1.	Calculation Method 1.....	37
5.1.2.	Calculation Method 2.....	39
5.2.	Advanced Calculation Method	41
5.2.1.	ANSYS Mechanical APDL.....	41
6.	Validation of the Numerical Models	45
6.1.	Experimental Studies	45
6.1.1.	University of Manchester	45
6.1.2.	Queensland University of Technology – 1.....	47
6.1.3.	Queensland University of Technology – 2.....	50
6.1.4.	Polytechnic Institute of Bragança	52
7.	Parametric Studies	55
7.1.	Parametric Analysis of the Cavity Insulation	55
7.2.	Parametric Analysis of the Spacing Between Studs	56
7.3.	Parametric Analysis of the Cavity Spacing	57
8.	Comparison of Results	59
8.1.	University of Manchester	59
8.2.	Queensland University of Technology – 1	61
8.3.	Queensland University of Technology – 2	66
8.4.	Polytechnic Institute of Bragança.....	70
8.5.	Parametric Studies	76
9.	Conclusions and Future Work.....	78
9.1.	Conclusions	78
9.2.	Future Work.....	79

List of Figures

Fig. 1 – Examples of cold-formed cross-section profiles. [7].....	3
Fig. 2 – Thermal resistance network for heat transfer through a two-layer plane wall subjected to convection on both sides [18].	10
Fig. 3 – Calculation schematic for the parallel path method [4].....	12
Fig. 4 – Calculation schematic for the isothermal plane method [4].	13
Fig. 5 – Calculation schematic for the zone method [4].	15
Fig. 6 – Modified Zone Method R-value Calculation Representation for Metal Stud Walls. [19].....	16
Fig. 7 – Modified Zone Factor for Calculating R-value of Metal Stud Walls with Cavity Insulation. [19].....	17
Fig. 8 – Heat conduction through a large plane wall of thickness Δx and area A . [24].....	21
Fig. 9 – Heat transfer from a hot surface to air by convection. [24].....	22
Fig. 10 – Blackbody radiation represents the maximum amount of radiation that can be emitted from a surface at a specified temperature. [24]	23
Fig. 11 – Natural fire curve compared to ISO 834 fire curve.[25]	24
Fig. 12 – Standard Fire Curve (ISO 834).	25
Fig. 13 – (a) Actual temperature distribution; (b) Acceptable temperature distribution according to Feng et al. [34]	28
Fig. 14 – One dimensional heat transfer. a) Layers and nodes for heat transfer; b) Heat flow pattern.....	30
Fig. 15 – Heat resistance from layer 5 to 10, based on Shahbazian [36].....	32
Fig. 16 – Heat capacitance for each layer of the panel, based on Shahbazian [36].....	33
Fig. 17 – Diagram of the Matlab application program.	34
Fig. 18 – Proposed geometry for heat transfer calculation.....	35
Fig. 19 – Maximum and minimum values for the effective width (WL).	35
Fig. 20 – Graph of TI as a function of SP according to analysis made by the author.....	38
Fig. 21 – Number of element divisions for each section.....	42

Fig. 22 – Finite Element mesh used for specimen 10 from Polytechnic Institute of Bragança.	42
Fig. 23 – PLANE55 element description.	42
Fig. 24 – PLANE55 2-D Thermal Solid.	43
Fig. 25 – Boundary conditions of the advanced calculation method.	44
Fig. 26 – Experimental tests for the Mineral wool cavity insulation made by Feng et al. [15].	46
Fig. 27 – Experimental tests for the (a) glass fibre, (b) rock fibre and (c) cellulose fibre cavity insulation made by Kolarkar et al. [39].....	49
Fig. 28 – Experimental tests for the (a) glass fibre, (b) rock fibre and (c) cellulose fibre cavity insulation made by Kolarkar [41] and studied by Rusthi et al. [40]	51
Fig. 29 – Experimental tests for Spec. 3, 10, 15 and 16, respectively, made by Khetata et al. [37], [42], [43] and Piloto [44].	53
Fig. 30 – Configuration in scale for Spec. 10 used and the variation of the cavity insulation material.	55
Fig. 31 – Configuration in scale for Spec. 10 used and the variation of the spacing between studs.	56
Fig. 32 – Configuration in scale for Spec. 10 used and the variation of the cavity spacing.	57
Fig. 33 – Configuration and discrete points of analysis for the University of Manchester	59
Fig. 34 – Graph of experimental and numerical results for the University of Manchester.	60
Fig. 35 – Graph of the unexposed wall temperature compared to the insulation criterion (I) for University of Manchester.	61
Fig. 36 – Configuration and discrete points of analysis for the Queensland University of Technology – 1.....	62
Fig. 37 – Graph of experimental and numerical results for Spec. 4 of Queensland University of Technology – 1.	63
Fig. 38 – Graph of the unexposed wall temperature compared to the insulation criterion (I) for Spec. 4 of Queensland University of Technology – 1.	63
Fig. 39 – Graph of experimental and numerical results for Spec. 5 of Queensland University of Technology – 1.	64

Fig. 40 – Graph of the unexposed wall temperature compared to the insulation criterion (I) for Spec. 5 of Queensland University of Technology – 1.	64
Fig. 41 – Graph of experimental and numerical results for Spec. 6 of Queensland University of Technology – 1.	65
Fig. 42 – Graph of the unexposed wall temperature compared to the insulation criterion (I) for Spec. 6 of Queensland University of Technology – 1.	65
Fig. 43 - Configuration and discrete points of analysis for the Queensland University of Technology – 2.....	66
Fig. 44 – Graph of experimental and numerical results for Spec. 3 of Queensland University of Technology – 2.	67
Fig. 45 – Graph of the unexposed wall temperature compared to the insulation criterion (I) for Spec. 3 of Queensland University of Technology – 2.	68
Fig. 46 – Graph of experimental and numerical results for Spec. 4 of Queensland University of Technology – 2.	68
Fig. 47 – Graph of the unexposed wall temperature compared to the insulation criterion (I) for Spec. 4 of Queensland University of Technology – 2.	69
Fig. 48 – Graph of experimental and numerical results for Spec. 5 of Queensland University of Technology – 2.	69
Fig. 49 – Graph of the unexposed wall temperature compared to the insulation criterion (I) for Spec. 5 of Queensland University of Technology – 2.	70
Fig. 50 – Configuration and discrete points of analysis for the Polytechnic Institute of Bragança.	71
Fig. 51 – Graph of experimental and numerical results for Spec. 3 of Polytechnic Institue of Bragança.	71
Fig. 52 – Graph of the unexposed wall temperature compared to the insulation criterion (I) for Spec. 3 of Polytechnic Institute of Bragança.	72
Fig. 53 – Graph of experimental and numerical results for Spec. 10 of Polytechnic Institue of Bragança.	72
Fig. 54 – Graph of the unexposed wall temperature compared to the insulation criterion (I) for Spec. 10 of Polytechnic Institute of Bragança.	73
Fig. 55 – Graph of experimental and numerical results for Spec. 15 of Polytechnic Institue of Bragança.	73
Fig. 56 – Graph of the unexposed wall temperature compared to the insulation criterion (I) for Spec. 15 of Polytechnic Institute of Bragança.	74

Fig. 57 – Graph of experimental and numerical results for Spec. 16 of Polytechnic Institute of Bragança.....74

Fig. 58 – Graph of the unexposed wall temperature compared to the insulation criterion (I) for Spec. 16 of Polytechnic Institute of Bragança.75

List of Tables

Table 1 – Details of heat transfer and thermal resistance.....	32
Table 2 – The best effective width used for the calculation method 1.....	37
Table 3 – The best effective width used for the calculation method 2.....	40
Table 4 – Feng[15] studies considered in this research.....	46
Table 5 – Fire resistance values for Manchester University.....	47
Table 6 - Kolarkar [39] studies considered in this research.	47
Table 7 – Fire resistance values for Queensland University of Technology – 1.	50
Table 8 –Rusthi [40] studies considered in this research.....	50
Table 9 – Fire resistance values for Queensland University of Technology – 2.	52
Table 10 – Khetata et al. [42], [43] and Piloto[44] studies considered in this research.....	52
Table 11 - Fire resistance values for Polytechnic Institute of Bragança for rock fibre.....	54
Table 12 – Fire resistance values for Polytechnic Institute of Bragança for superwool.	54
Table 13 – Fire resistance of the wall assemblies used for parametric analysis of the cavity insulation.....	56
Table 14 –Fire resistance of the wall assemblies used for parametric analysis of the spacing between studs.	57
Table 15 – Characteristics and fire resistance of the wall assemblies used for parametric analysis of the web size.	58
Table 16 – Relative error of results by University of Manchester.....	61
Table 17 – Relative error of results by Queensland University of Technology – 1.....	66
Table 18 - Relative Error of results by Queensland University of Technology – 2.....	70
Table 19 – Relative Error of results by Polytechnic Institute of Bragança.....	75
Table 20 – Relative error for the cavity insulation material study.....	76

Table 21 – Relative error for the spacing between studs study.77
Table 22 – Relative error for the cavity spacing study.77

Nomenclature

WL	effective width
BW	length of the web
BL	length of the lip
BF	length of the flange
TS	thickness of the steel section
TG	thickness of the gypsum board
α	convection coefficient of the fire side
ε_f	emissivity coefficient of the fire side
ε_G	emissivity coefficient of the sheathing material (gypsum)
σ	Stefan-Boltzmann constant ($5.67 \times 10^{-8} \text{ W/m}^2\text{K}^4$)
λ_s	thermal conductivity of steel
ρ_s	density of steel
Cp_s	specific heat of steel
λ_i	thermal conductivity of insulation
ρ_i	density of insulation
Cp_i	specific heat of insulation
λ_G	thermal conductivity of gypsum board
ρ_G	density of gypsum board
Cp_G	specific heat of gypsum board
\dot{Q}_n	heat transfer rate on the n layer
$\dot{Q}_{CONDa,b}$	heat conduction between layers a and b
\dot{Q}_{CAPn}	heat capacity for layer n
T_{fire}	temperature of the fire side, which is defined by ISO 834
T_n	temperature in the n layer
T_n^{i-1}	temperature of the n layer in the previous timestep
Δt	timestep of the simulation

1. Introduction

Finite Element simulation methods for heat transfer are now sufficiently mature and accessible, however there is still a desire to use a much more simplified method in routine fire resistance design. For this purpose, it is necessary to present more about the structure of the wall in this study.

According to Santos [1], buildings in Europe are responsible for 40% of the energy consumption, having the space conditioning (heating and cooling systems) an important share, which also depends on climate. Alternatives to traditional structural systems for buildings have emerged, e.g. lightweight steel framing (LSF) systems. The LSF construction systems have as base-material a steel structure, made of bended cold formed steel plates, which are usually prismatic and have a thin-walled cross section.

The use of steel as a construction material has grown greatly in the last few years, due to its advantages: cost efficiency, reduced weight, exceptionally solid in relation to weight, stability of shape in case of humidity, rapid on-site erection, excellent acoustic properties, easy to prefabricate, great potential for recycling and reuse and incombustibility (category A material) [2]. However, if not addressed correctly, thermal bridges could penalize the thermal behaviour and energy efficiency of steel buildings. Thermal bridges is the name given for highly conductive members spaced along the wall, which allow higher heat transfer than that through less conductive areas [3], [4]. Therefore, in recent years, there has been an effort to assess and improve the thermal behaviour of constructive solutions with steel structures. Although such adverse conditions can be easily avoided by proper thermal design of wall systems, these effects have not been well understood and thermal data has been lacking.

1.1. Objectives

This work presents a study of the fire effects on a non-loadbearing wall Light Steel Frame (LSF) structure through numerical and simple calculation methods for a thermal analysis.

Special numerical tasks aim to develop an accurate one-dimensional model to predict fire resistance using Matlab programming. The validation of the Matlab program

with experiments and a 2D finite element model using ANSYS Mechanical APDL is presented.

Specific tasks are included to be investigated by three parametric studies, where the first one is used to evaluate the influence of cavity insulation materials on the fire resistance using seven different configurations, the second one is used to evaluate the influence of the spacing between studs on the fire resistance using five different configurations and the last one is used to evaluate the influence of the cavity spacing on the fire resistance using five different configurations.

1.2. Light Steel Framing Constructions

Steel is now in use for over 100 years. Although the immediate thought when considering steel is associated with skyscrapers and bridges, the choice for this material is emerging in industrial, commercial and institutional buildings. Light steel framing has been an increasing choice in low to medium rise structures, such as schools, shopping malls, box stores, stacked row houses, hotels, assisted care residences and office buildings. LSF can be used in either the floor, roof or wall assemblies in buildings from one to six stories in height. It can be used alone to provide all necessary structural elements or in combination with other materials for a greater building diversity and scope

LSF is a novel construction technology that has been considered vastly for cold climate countries due to its good thermal and structural behavior [5]. The main advantages of lightweight steel frame is their weight, their incombustibility, their high load-bearing capacity and a wide range of possible uses. Light steel frames if combined with improved plating and insulation materials can be an interesting option to achieve different applications in modern constructions [2].

Steel can be practically used in an unlimited number of ways, since it has a variety of sections, assembly techniques, associations with other materials and forming methods. Its different finishes and wide range of forms makes it a good choice for all requirements. Besides being environmentally safe, this material is also magnetic, which makes it easy to be extracted from disparate waste heaps. Every single piece collected, including scraps, can be fully recycled to produce extremely fine qualities [2].

Steel can be used to make members that are durable, separable, dismantlable and reusable, which makes it a type of building that protects natural resources, since it uses very little of the earth's non-renewable reserves.

The material and thickness of the sheathing used to cover the steel structure is usually dependable on the physical constraints of the member. Plasterboards or fiberplaster plates are preferred for internal partitions because they provide good acoustic properties when they are used to cover thin sections, are easy to paint and wallpaper and provide some type of heat resistance in the event of a fire. Lightweight steel construction can be used to build up to four storey buildings at low cost [2].

As pointed out by Gunalan [6], there are two main families in steel construction: hot-rolled shapes and members built up of plates and girders, and cold-formed sections from steel sheet, strip, plates or flat bars in roll-forming machines or by press brake or bending brake operations, which are known as cold-formed steel structural members.

According to Soares et. al. [7], the Light Steel Framing (LSF) constructions are composed of studs and tracks made from thin C, U, Z, Σ , Top-hat and I-shaped cold-formed sections and the thickness of the sheet can range between 0.45 to 6 mm.

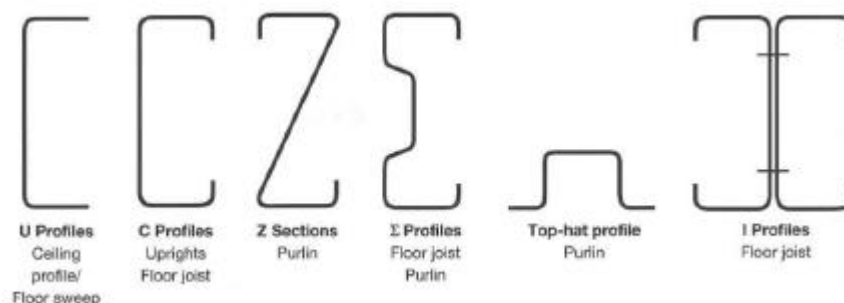


Fig. 1 – Examples of cold-formed cross-section profiles. [7]

Light steel wall frame systems are commonly used in a variety of contemporary building constructions, especially as a non-loadbearing wall. Fire resistance of LSF walls is an important factor to prevent the spread of fire and eventually the building collapse. One or more layers of the proper combination of certain materials and members usually provide the fire protection. The thin steel sections must be covered by a sheathing to protect them from the fire. Gypsum plates have been approved as fire protection materials, as well as insulation materials such as rockwool, glassfiber and mineral fiber, which are going to be taken into account in this research [7].

Two distinct numerical methods were considered in this investigation. The two dimensional finite element model uses incremental and nonlinear transient thermal analysis (ANSYS). The one dimensional strip model uses incremental and nonlinear transient solution and was developed for comparison, assuming that heat flows across the section by well-defined patterns.

1.3. Plan of Thesis

The second chapter of this thesis presents the state of the art, which is a retrospective about the studies related with the fire resistance of LSF structures.

The third chapter brings an explanation about the analytical methods studied with the purpose of helping to create an equation to describe the effective width, which is the main objective of this study.

The fourth chapter presents the fire, the fire curves and the fire resistance requirements considered in this study.

The fifth chapter presents the specifications of the simplified calculation method and the proposed equations for the calculation of the effective width, as well as the specifications of the advanced calculation method.

The sixth chapter shows the validation of both the simple and advanced calculation methods, compared to experimental analysis made by several authors.

Three parametric analysis, to study the effect of the materials of the cavity insulation, the spacing between studs and the cavity spacing, are all presented in the seventh chapter.

The eighth chapter presents the comparison between every result, most importantly comparing both of the simple calculation methods proposed in this study.

The conclusions and future work are given in the ninth chapter. More information about the materials and methods used are presented in the appendix pages.

2. State of the Art

This chapter presents a review of the research of the LSF walls. Both experimental and numerical investigation of LSF wall panels under fire conditions achievements are going to be presented. The state of the art explores the current knowledge of the LSF wall panels on a time line basis, including the behavior of all the components, failure modes, temperature fields and displacement behavior.

2.1. Preliminary Studies

In 1946, the American Iron and Steel Institute (AISI) introduced the first design principles. A research made by Prof. G. Winter on cold formed steel elements at Cornell University in 1963 analyzed the effects of cold-straining on structural sheet steels and corner properties of cold-formed steel shapes. AISI then sponsored a research investigation at Cornell University with the objective of identifying the effects of cold-forming on the mechanical properties, as well as on structural behaviour of members.

In 1961, the British steel standard was modified to include the design of cold formed steel members, based on the work of Prof. A. H. Chilver. The Australian standard for the design of cold formed steel structural members was first published in 1974. It was based on the American specifications of the 1968 edition, but with modifications to beams and columns design curves to keep them in line with the Australian Steel Structures Code [8].

In 1970, Chajes et al. [9] studied the cold working to which steel sheets are subjected when being cold-formed into structural shapes for light-gauge steel construction, presenting good results for the mechanical resistance and properties strong enough to handle a structure. Several cold-forming processes are used for the production of light-gauge steel construction structural members, such as cold-rolling and brakeforming, and it is well known that stretching and bending cold working affects the mechanical properties of mild structural steel. The work by Chajes et al. verified that the cold-forming causes a significant increase in yield strength of corners and a

smaller increase on flat surfaces of thin-walled steel members, validating the LSF construction model.

In 1985, Schwartz and Lie [10] studied the resistance of exposed surfaces under fire conditions guided by the ASTM E119 criterion for the unexposed surface. The information and data increased the knowledge between the unexposed surface temperature rise criterion of ASTM E119 and the ignition temperature of common combustible materials, assuming three different modes of failure: structural collapse of the assembly, openings in the assembly allowing hot gases and flames to pass through, or excessive heat transfer through the assembly, making the temperature of the unexposed surface hot enough to ignite materials in contact or in close proximity. The conclusion of this study is that the standard have a large safety factor included and more economic solutions could be performed.

In 1994, Mehaffey et al. [11] presented the finite difference numerical model to perform studies across heat transfer in surfaces and between surfaces and cavities. The model was validated with experimental tests. A similar study is presented in this work, in which it is assumed an one-dimensional finite difference numerical model and proposed an equation for the effective width to be considered. Also, the results are validated with experimental tests.

2.2. Light Steel Frame Studies

In 1994, Barbour [3] decided to make twenty three different tests in Light Steel Framing walls since until then the available data was obtained by different researchers, using various measurement methods, under diverse conditions, and therefore were inconsistent.

With steel framing, the heat transfer in the y-direction (laterally in the plane of the wall normal to the x-direction) can be as significant as the heat transfer in the x-direction. As heat is transferred along the y-direction, the other materials of the non-homogeneous wall are exposed to different temperature distributions, thereby changing the heat transfer characteristics of the wall. However, the capacity of the adjacent facing materials to transmit heat to the metal is limited. Also, contact between materials limits heat transfer through contact resistance. Contact resistance is the change attributed to the temperature drop across the interface between materials, and

for steel framing, can be a large factor. Most contact resistances between materials are small, but since the area of metal in contact with other materials is larger than the thickness of the metal through the layer of insulation, it does have a large effect on the heat transfer characteristics of the wall [3].

According to Barbour [3], the insulation is much more effective on the external than on the cavity. Small differences in flange size have little effect on the overall wall R-value. Temperatures did not vary considerably from the web side of the stud to the open side of the stud. The temperature gradients on the sheathing material are larger in LSF walls with a material with low R-value for sheathing, than that of materials with high R-value as sheathing. In his studies, no condensation was noted on the warm surface, interior or exterior, and although some condensation was noted on the interior of the cold side, it shouldn't be considered as an effect of the steel framing.

Another discover made by Barbour [3] is that, by comparing both interior and exterior surface temperatures of the warm side of the sheathing material, as the R-value of the sheathing increases, the temperature over the cavity is mostly constant, but the temperature over the stud increases. This is an indication of a reduction of heat flowing through the stud for larger R-value sheathing and a reduction in possible thermal bridging effects.

In 1995, McGowan and Desjarlais [12] conclude that neither the parallel-path nor the isothermal-planes method should be used exclusive of the other. These are intended to be complementary methods that provide the upper and lower limites of the actual result.

According to several authors [12], [3] the addition of a higher R-value sheathing material (or insulated sheathing) makes the thermal resistance of the whole wall increase, since it probably reduces the thermal bridging effect.

2.3. Cavities and Composites: the new concept

In 1994, Sultan and Loughheed [13] performed several small scale fire tests of gypsum board clad steel wall assemblies (914 x 914 mm) using different cavity insulations, such as glass fibers, rock fibers and cellulose fibers. Their conclusions were that the rock and cellulose fiber cavity insulations both improved the fire resistance by approximately 30 minutes, in comparison to non-insulated wall

assemblies, whereas there was only a small benefit for specimens using glass fiber as cavity insulation. On the warm side of the wall assembly with insulated cavities, the internal side of the gypsum board heated up more rapidly, reaching temperatures of 700°C much earlier in comparison to non-insulated wall assemblies. Same as the exposed plasterboard, the exposed side of the cavity also reached high temperatures in comparison to non-insulated assemblies.

In 1995, Sultan [14] performed full scale fire resistance tests on non-load bearing gypsum board wall assemblies and concluded that when rock fiber insulation was used, there is a noted increase in the fire resistance rating by 54% over the non-insulated wall assembly. However, the use of glass fiber as insulation cavity did not affect the fire performance whereas the cellulose fiber insulation reduced the fire resistance of the wall.

In 2003, Feng et al. [15] conducted fire tests on non-load bearing small scale wall systems and noted that the thermal performance of wall panels improved with the use of cavity insulation.

Kosny and Yarbrough, 2006 [16], also provided the conclusion that fiberglass batts used for cavity insulation in the internal areas between steel-stud flanges doesn't bring significant improvements of the steel-stud wall thermal performance.

Kolarkar and Mahendran, 2008 [17], show that the use of glass fiber as cavity insulation led to poor thermal performance of stud walls, whereas the thermal performance of externally insulated steel stud walls was superior than the traditionally built stud walls with or without cavity insulation.

Because of the contradicting results seen in previous researches about the benefits of cavity insulation to the fire rating of stud wall systems, further research is required.

3. Analitical Methods

This section will present a few different analitical methods that shows the calculation of the R-value of a LSF wall in a simplified process. The study of these methods is relevant for this work as being helpful for the analysis of the simplified method proposed.

According to McGowan and Desjarlais [12], the best method for analysis of the R-value of a steel framed wall is by physical testing, followed by computer simulation, the ASHRAE 90.1, ISO 6946, and lastly, the modified zone method.

3.1. Multilayered Plane Walls

Çengel, 2002 [18] presents plane walls, having several layers of different materials, so the easiest way to determine the rate of steady heat transfer through such composite walls is by using the termal resistance concept. That way, the conduction resistance to heat flow of each wall is defined by L/kA , where L is the thickness of the wall, k is its thermal conductivity and A is the area, connected in series, or in other words dividing the temperature difference between two surfaces at known temperatures by the total thermal resistance between them.

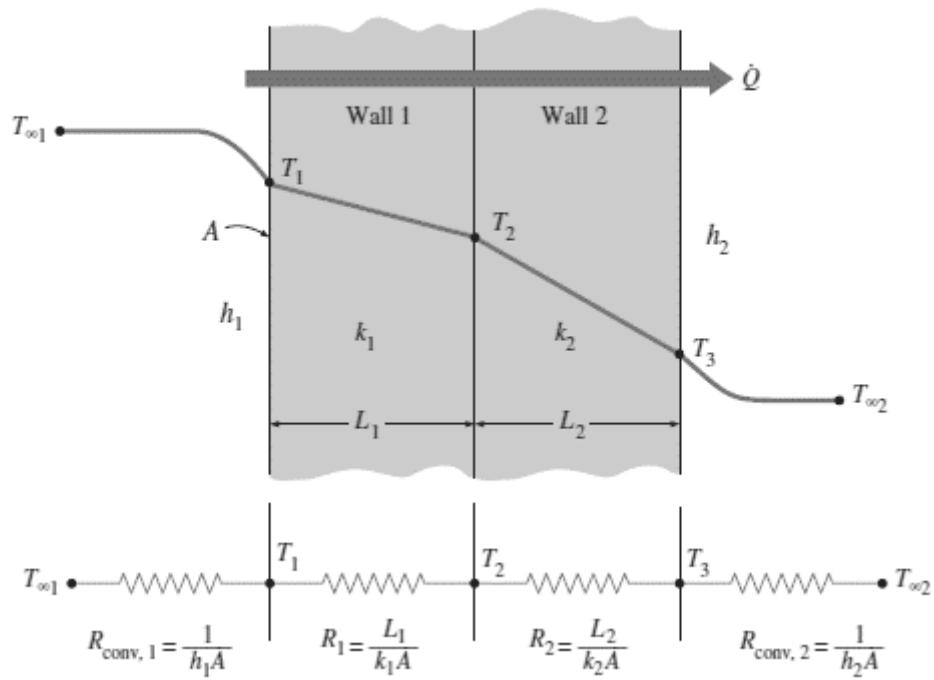


Fig. 2 – Thermal resistance network for heat transfer through a two-layer plane wall subjected to convection on both sides [18].

Using a concept of walls with a layer of insulation, when there is two layers, the rate of steady heat transfer can be expressed by Eq. 1, see Fig. 2.

$$\dot{Q} = \frac{T_{\infty 1} - T_{\infty 2}}{R_{total}} \quad \text{Eq. 1}$$

where $T_{\infty 1}$ is the temperature of side 1, $T_{\infty 2}$ is the temperature of the side 2 and R_{total} is the total thermal resistance, which can be expressed as

$$R_{total} = R_{conv,1} + R_{wall,1} + R_{wall,2} + R_{conv,2}$$

$$R_{total} = \frac{1}{h_1 A} + \frac{L_1}{k_1 A} + \frac{L_2}{k_2 A} + \frac{1}{h_2 A} \quad \text{Eq. 2}$$

where $R_{conv,1}$ represents the convection resistance of side 1, $R_{wall,1}$ represents the thermal resistance of layer 1, $R_{wall,2}$ represents the thermal resistance of layer 2 and $R_{conv,2}$ represents the convection resistance of side 2.

On plane walls of three or more layers, an additional resistance should be added for each additional layer.

3.2. Parallel Path Method

For calculations of this method, a component wall can be divided into parallel heat flow paths of different conductances that extend from surface to surface. The heat flows through these paths are assumed to be independent from one another, and the thermal conductance for each path is calculated using a series relationship analogous to electrical resistance. The average resistance is found by multiplying the resistance of each path by the fraction of the total area over which the heat flow path acts [3], [4].

This method shows relatively accurate results for one-dimensional heat flow transfer, where there is little or no heat exchange between the “parallel” paths in the assembly. The parallel-path calculation is most useful in cases of simple sandwich constructions or wood-frame assemblies, as shown in Eq. 3. The equations below are given for both R-values and U-factors, considering the concept of thermal transmission (U) or the concept of thermal resistance (R).

$$Q = (A_1 / R_{T1} + A_2 / R_{T2} + A_3 / R_{T3} + \dots) \Delta T, \quad \text{Eq. 3}$$

$$Q = (U_1 \cdot A_1 + U_2 \cdot A_2 + U_3 \cdot A_3 + \dots) \Delta T$$

where Q is the heat flow through a defined area with multiple adjacent assemblies; R_{Ti} is the thermal resistance for assembly “i”, generally obtained by summing the resistance of each layer of material in the assembly including inner and outer air films; U_i is the heat transmission coefficient in $W/(m^2 \cdot K)$ for assembly “i” including the effect of the interior and exterior surface films; A_i is the area of assembly “i”, in m^2 and ΔT is the difference between the internal and external air temperatures.

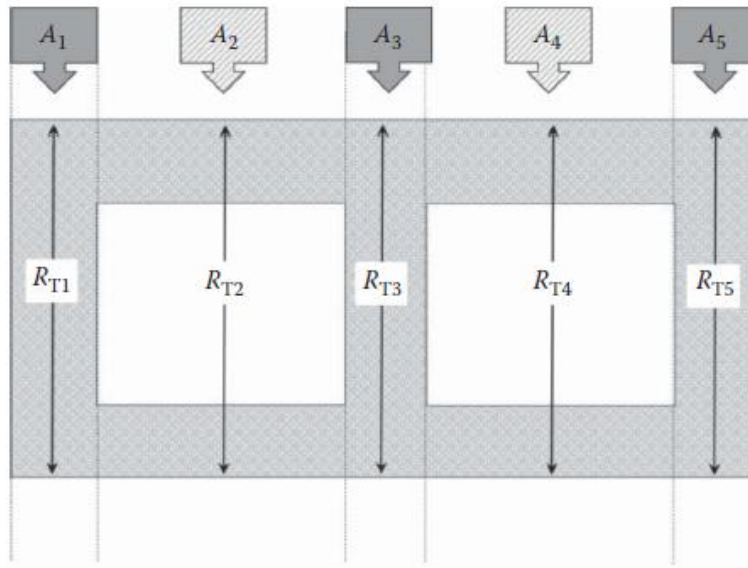


Fig. 3 – Calculation schematic for the parallel path method [4].

For a region as shown in Fig. 3, the following equation may be used.

$$R_{eff} = \frac{1}{U} = \left(\frac{A_1}{R_{T1}} + \frac{A_2}{R_{T2}} + \frac{A_3}{R_{T3}} + \dots \right) / A_{total} \quad \text{Eq. 4}$$

3.3. Isothermal Planes (Serie-Parallel Path) Method

Differently from the parallel-path method, if one assumes that heat can flow laterally in any component, this creates isothermal planes parallel to the building surfaces, which is the concept of this method. Resistances of adjacent components are combined in parallel, resulting in effective resistances acting in series. The thermal resistance equals the sum of these effective series. Typically, this number is smaller than that obtained using the parallel path method [3].

The concept of parallel-path method is not likely to provide reliable results in buildings with highly conductive structural members or other components, such as steel, aluminium or glass. In such cases, the isothermal planes method is an alternate for calculating the U-value.

This method uses an uniform temperature (isothermal) for the high conductive planes separating less conductive layers, therefore it is used to analyze heat flow through wood-framed assemblies or masonry walls, since the method divides the

construction assembly into series of layers. A good example of use for this method are hollow masonry units. The solid webs connecting the face shells are quite conductive compared to the air spaces in the hollow cores, and the face shells conduct heat laterally. Usually, the thermal resistance through the isothermal planes method is smaller than the one obtained through the parallel-path method. [3]

For a two-core masonry wall, as shown in Fig. 4, the layer with the webs and cores is calculated using the parallel-path method to get to an average R-value for the layer, and then this result is added to the R-values of the two face shells in series. That way, in the isothermal planes method, the air-to-air R-value is calculated through Eq. 5.

$$R_{air-to-air} = \frac{1}{U} = R_e + R_{fe} + \left[\frac{a_w}{R_w} + \frac{a_c}{R_c} \right] + R_{fi} + R_i \quad \text{Eq. 5}$$

where R_e and R_i are exterior and interior air-film resistances; R_{fe} and R_{fi} are exterior and interior face resistances; a_w and a_c are fractions of the total heat flow area for the webs and air-cores; R_w and R_c are R-values (calculated for the space between faces) for all webs and air-filled cores.

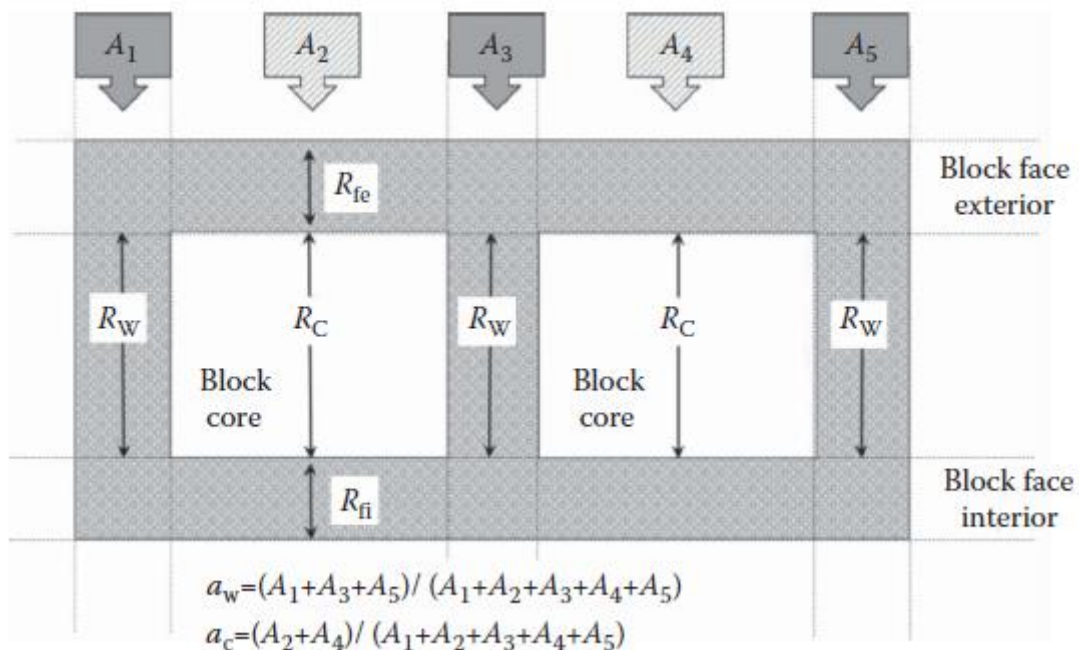


Fig. 4 – Calculation schematic for the isothermal plane method [4].

3.4. Zone Method

Both the previous described methods assume the heat flow as being perpendicular to the wall. However, if a thermal bridge, such as a steel framing member, is placed in the wall component next to a material with low thermal conductivity, then there is a need for a two-dimensional effects analysis. One of the first methods to be developed to overcome this problem and provide a simplified solution was the American Society of Heating, Refrigeration, and Air Conditioning Engineers (ASHRAE) Zone method [19]. An area “weighing factor” is applied to the section of the wall with the thermal bridge, and this section is known as Zone A, the area affected by thermal bridge. The width of this zone is overstated compared to the one used in the usual parallel path calculation and is calculated from equation Eq. 6 [3].

The zone method is ideal for structures with widely spaced metal members of substantial cross-section area, since the isothermal planes method calculation results in values that are too low in this case [19].

The zone method calculation involves two separate computations – one for a chosen limited portion, Zone A, in which contains the highly conductive element, and the other for the remaining portion of simpler construction, Zone B. Then, these two computations should be combined using the parallel flow method and the average transmittance per unit overall area should be calculated. Due to the basic laws of heat transfer, the conductances CA of elements are added in parallel and the resistances R/A of elements are added in series.

The metal element determines the surface shape of Zone A, for example, for a rod perpendicular to panel surfaces, the Zone A is a circle of diameter W ; for a steel stud, as seen in Fig. 5 , it is a strip of width W that is centered on the stud.

The difference between this method and the parallel path method is how W is estimated. Using the parallel method, $W = L$, whereas using the zone method, W is calculated empirically though Eq. 6. The value of d should not be less than 13 mm for still air [19].

$$W = m + 2d \quad \text{Eq. 6}$$

where m is the width or diameter of metal heat path terminal in millimeters and d is the distance from panel surface to metal in millimeters.

The dissimilarity between this calculation and the parallel-path method is the way of estimating the area of the wall that is thermally affected by thermal bridging. According to several authors, the accuracy of above methods are unsatisfactory [20].

This method is not applicable to steel profiles perpendicular to one another and according to Barbour [3], it should be used for large spacemens between largely conductive materials. Also, this method is limited to cases in which there is insulation.

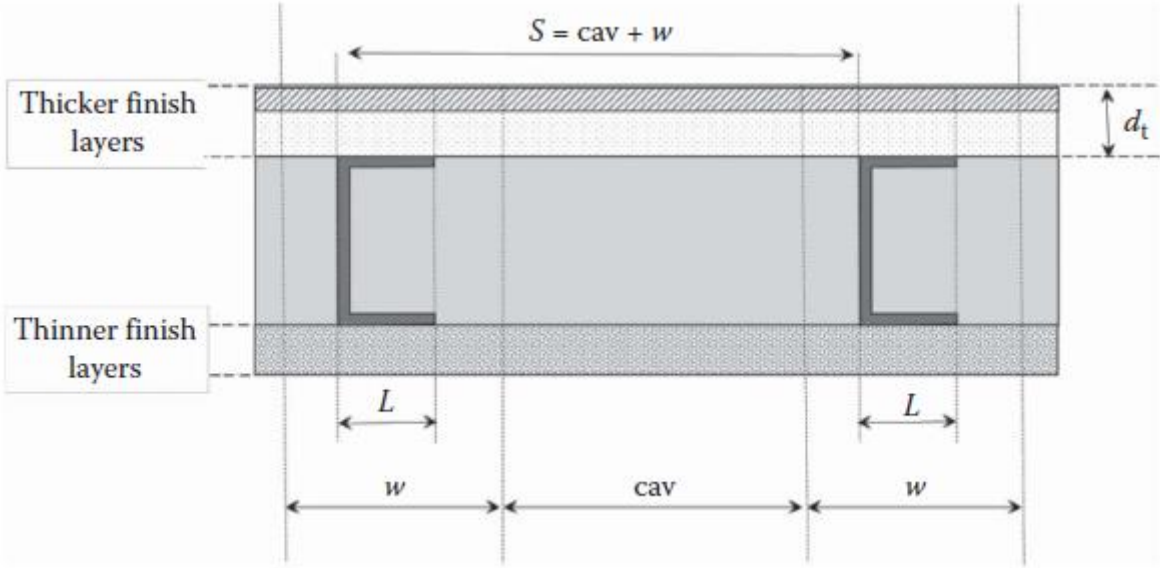


Fig. 5 – Calculation schematic for the zone method [4].

3.5. Ashrae Modified Zone Method

Similarly to the parallel path method and the zone method, the modified zone method is based on parallel-path calculations. As in parallel method, this zone can be assumed to be equal the length of the stud flange L , or it can be calculated as a sum of the length of the stud flange and a distance doubled from wall surface to metal $\sum d_i$, such as in zone method. In the modified zone method, the width of the zone depends on three parameters: ratio between thermal resistivity of sheathing material and cavity insulation, size (depth) of stud and thickness of sheathing material [19].

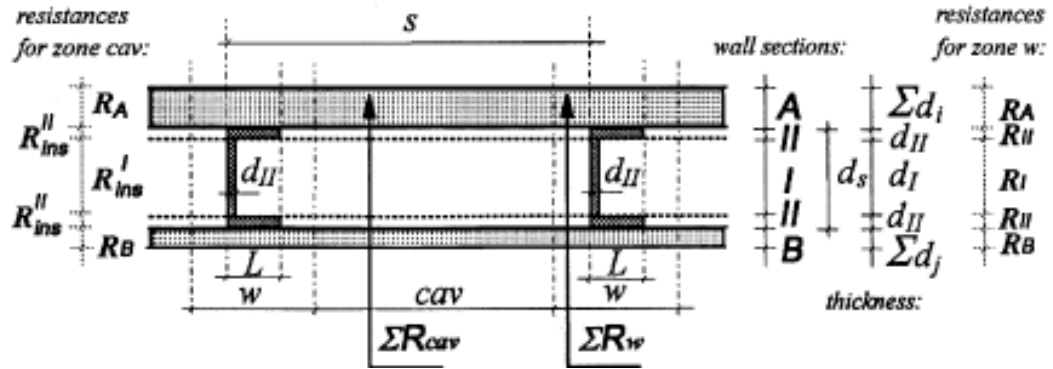


Fig. 6 – Modified Zone Method R-value Calculation Representation for Metal Stud Walls. [19]

The Fig. 6 shows the width W of the zone of thermal bridge around a steel stud. The wall cross section is divided into two zones: w and the cavity zone cav . Layers of wall materials are grouped into an exterior and interior surface sections, being A for sheathing and siding and B for wallboard, as well as interstitial sections I (cavity insulation) and II (steel stud flange). In ASHRAE [19], there is a form which can be copied and used as a calculation form.

If it is assumed that the layers of wall materials in wall section A is thicker than those of section B, than they can be described as:

$$\sum_{i=1}^n d_i \geq \sum_{j=1}^m d_j \quad \text{Eq. 7}$$

where n is the number of material layer (of thickness d_i) between steel stud flange and wall surface for section A and m is the number of material layer (of thickness d_j) for section B [19].

Then, the width of the zone of thermal anomalies around the metal stud w can be estimated by

$$w = L + z_f \sum_{i=1}^n d_i \quad \text{Eq. 8}$$

where L is the stud flange size, d_i is the thickness of material layer in section A and z_f is the zone factor, which can be obtained from Fig. 7 ($z_f = 2$ for zone method).

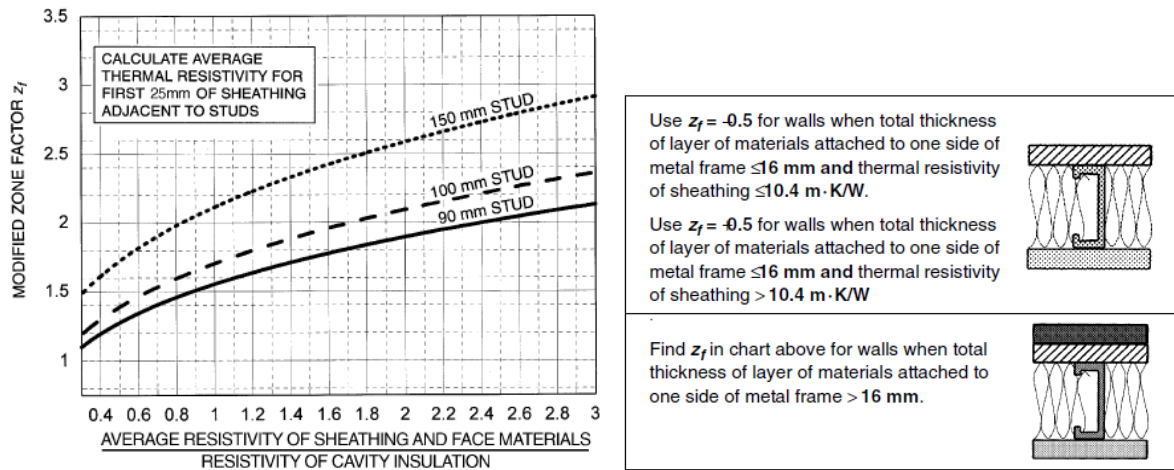


Fig. 7 – Modified Zone Factor for Calculating R-value of Metal Stud Walls with Cavity Insulation. [19]

3.6. ISO 6946 Method

The International Organization for Standardization (ISO) 6946 method is a numerical simulation carried out in accordance with ISO 10211. It is valid for components consisting of thermally homogenous or inhomogeneous layers and which may contain air layers up to 0.3 m thick and metal fasteners. [21]

This method is used for steady-state conditions and assumed to be independent of actual conditions, such as indoor temperature or effect of wind or solar radiation.

The thermal transmittance is given by Eq. 9.

$$U = \frac{1}{R_{tot}} \quad \text{Eq. 9}$$

where U is the thermal transmittance ($W/(m^2 \cdot K)$); R_{tot} is the total thermal resistance ($m^2 \cdot K/W$), obtained from Eq. 12.

If the total correction is less than 3% of U , there is no need to be applied. However, if it is higher than 3% of U , then it should be applied in accordance with Annex E of ISO 6949 [21].

The thermal resistance of opaque components is given by Eq. 10.

$$R_{c;op} = \frac{1}{U} - R_{si} - R_{se} \quad \text{Eq. 10}$$

where $R_{c;op}$ is the thermal resistance of opaque component ($\text{m}^2\cdot\text{K}/\text{W}$); R_{si} is the thermal resistance of internal surface ($\text{m}^2\cdot\text{K}/\text{W}$); R_{se} is the thermal resistance of external surface ($\text{m}^2\cdot\text{K}/\text{W}$); e U is the thermal transmittance, determined by Eq. 9.

The surface resistances are the same as used to calculate the thermal transmittance.

If thermal conductivity is given, the thermal resistance of the layer can be obtained from Eq. 11.

$$R = \frac{d}{\lambda} \quad \text{Eq. 11}$$

where R is the thermal resistance ($\text{m}^2\cdot\text{K}/\text{W}$); d is the thickness of the material layer in the component (m); λ is the design thermal conductivity of the material ($\text{W}/(\text{m}\cdot\text{K})$).

Values of λ should be calculated in accordance to ISO 10456 is based on measured data; in any other case, values of λ are obtained from tables A.1 and B.1 of ISO 6946 [21].

The total thermal resistance, R_{tot} , of a plane building component consisting of thermally homogeneous layers perpendicular to the heat flow shall be calculated by Eq. 12.

$$R_{tot} = R_{si} + R_1 + R_2 + \dots + R_n + R_{se} \quad \text{Eq. 12}$$

where $R_1, R_2 \dots R_n$ are the design thermal resistances of each layer ($\text{m}^2\cdot\text{K}/\text{W}$).

When calculating the resistance of internal building components (partitions, etc.), or a component between the internal environment and an unheated space, R_{si} applies on both sides.

This method is not valid for cases where the ratio of the upper limit of thermal resistance to the lower limit of thermal resistance exceeds 1.5 [21]. The method is not applicable to cases where insulation is bridged by metal. For metal fasteners, the

method can be used as if there were no metal fasteners and the result corrected in accordance with E.3 of ISO 6946 [21].

4. Fire

This chapter presents the thermal behaviour of the LSF wall assembly during a fire and some considerations that are proved to be necessary to perform numerical and experimental studies in this field of investigation.

To present a fire, there is a need of three important factors: a heat source, fuel and a oxidizing, starting when the mix of fuel and oxidizer is hot enough to ignite [22].

4.1. Heat Transfer Theory

Çengel [18] pointed out that the science of thermodynamics deals with the amount of heat transfer as a system undergoes a process from one equilibrium state to another, and makes no reference to how long the process will take. However, engineering often takes more interest in knowing the rate in heat transfer, which is the topic of the science of heat transfer.

Although thermodynamics and heat transfer are different concepts, the laws of thermodynamics lay the framework for the science of heat transfer. The first law requires that the rate of energy transfer into a system be equal to the rate of increase of the energy of that system. The second law requires that heat be transferred in the direction of decreasing temperature [18].

According to Çengel [18], the first law of thermodynamics states that the “energy can neither be created nor destroyed; it can only change forms”. Therefore, every bit of energy must be accounted for during the process. The principle of conservation of energy (or energy balance) may be expressed as the Eq. 13.

$$\left(\begin{array}{c} \textit{Total energy} \\ \textit{entering} \\ \textit{the system} \end{array} \right) - \left(\begin{array}{c} \textit{Total energy} \\ \textit{leaving} \\ \textit{the system} \end{array} \right) = \left(\begin{array}{c} \textit{Change in the} \\ \textit{total energy of} \\ \textit{the system} \end{array} \right) \quad \text{Eq. 13}$$

Considering that energy can be transferred to or from a system by heat, work and mass flow, and that the total energy of a simple compressible system consists of internal, kinetic and potential energies, the energy balance for any system undergoing any process can be expressed as Eq. 14 or, in the rate form, as Eq. 15.

$$E_{in} - E_{out} = \Delta E_{system} \quad \text{Eq. 14}$$

$$\dot{E}_{in} - \dot{E}_{out} = \frac{dE_{system}}{dt} \quad \text{Eq. 15}$$

There are three basic mechanisms of heat transfer: conduction, convection and radiation. Conduction is defined as the transfer of energy from one more energetic particles of a substance to the less energetic ones as a result of interactions between the particles; Convection is the mode of heat transfer between a solid surface and a liquid or gas that is in motion and involves the combined effects of conduction and fluid motion; Lastly, radiation is the energy emitted by matter in the form of electromagnetic waves as a result of the changes in the electronic configurations of the atoms or molecules [18], [23].

For conduction, consider steady heat conduction through a large plane wall of thickness $\Delta x = L$ and area A , as shown in Fig. 8. The temperature difference across the wall is $\Delta T = T_2 - T_1$. Experiments have shown that the rate of heat transfer \dot{Q} through the wall is doubled when the temperature difference ΔT across the wall of the area A normal to the direction of heat transfer is doubled, but is halved when the wall thickness L is doubled. Thus it can be concluded that the rate of heat conduction through a plane is proportional to the temperature difference across the layer and the heat transfer area, but is inversely proportional to the thickness of the layer, which can be expressed as Eq. 16 [18], [23].

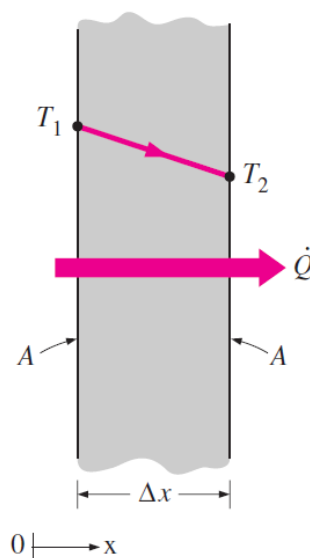


Fig. 8 – Heat conduction through a large plane wall of thickness Δx and area A . [24]

$$\dot{Q}_{cond} = \lambda A \frac{T_1 - T_2}{\Delta x} = -kA \frac{\Delta T}{\Delta x} \quad \text{Eq. 16}$$

where the constant of proportionality λ is the thermal conductivity of the material (W/m°C), which is a measure of the ability of a material to conduct heat.

As for convection, consider the cooling of a hot block by blowing cool air over its top surface, as presented in Fig. 9. Energy is first transferred to the air layer next to the block through conduction. This energy is then carried away from the surface of the block through convection, that is, by the combined effects of conduction within the air that is due to random motion of air molecules and the bulk or macroscopic motion of the air that removes the heated air near the surface and replaces it by the cooler air. Despite the complexity of convection, the rate of convection heat transfer is observed to be proportional to the temperature difference, and is expressed by Newton's law of cooling as Eq. 17 [17], [19].

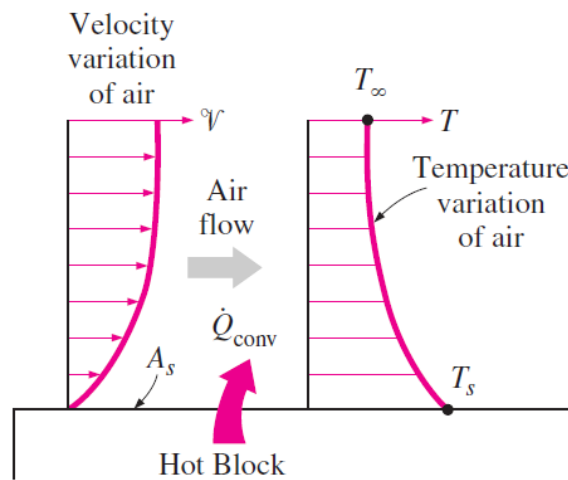


Fig. 9 – Heat transfer from a hot surface to air by convection. [24]

$$\dot{Q}_{conv} = hA_s(T_s - T_\infty) \quad \text{Eq. 17}$$

where h is the convection heat transfer (W/m².°C), A_s is the surface area through which convection heat transfer happens, T_s is the surface temperature and T_∞ is the temperature of the fluid sufficiently far from the surface.

Unlike conduction and convection, the transfer of energy by radiation does not require the presence of an intervening medium. It is fastest and suffers no attenuation in a vacuum, as this is how the energy of the sun reaches the earth.

Radiation is usually considered to be a surface phenomenon for solids that are opaque to thermal radiation such as metals, wood, and rocks since the radiation emitted by the interior regions of such material can never reach the surface, and the radiation incident on such bodies is usually absorbed within a few microns from the surface. The maximum rate of radiation that can be emitted from a surface at an absolute temperature T_s is given by the Stefan-Boltzmann law as Eq. 18 describes [18], [23].

$$\dot{Q}_{emit,max} = \sigma A_s T_s^4 \tag{Eq. 18}$$

where σ is the Stefan-Boltzmann constant ($= 5.67 \cdot 10^{-8} \text{ W/m}^2 \cdot \text{K}^4$). The idealized surface that emits radiation at this maximum rate is called blackbody, which is represented in Fig. 10.

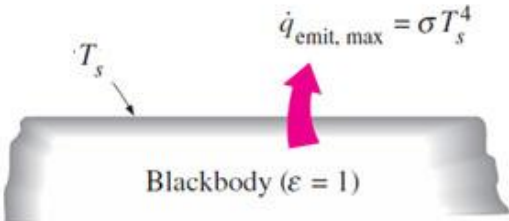


Fig. 10 – Blackbody radiation represents the maximum amount of radiation that can be emitted from a surface at a specified temperature. [24]

4.2. Natural Fire Curve

According to Truong et. al. [25], natural fire models include the heating and cooling phase, while standard fires considers the heating phase only. In literature, most researches on building structures in fire conditions only focus on the behavior of structures during the heating phase, however recent authors have examined the possibility of structural collapse during the cooling phase, but their focus is mainly on the possibility of structural collapse and the minimum value of heating time that the structures fail.

The natural fire curve is composed of some periods: the ignition-smouldering, the flashover, heating and cooling phases.

As presented by some authors [26], [27], the ignition period is not included in the standard models of fire because of its low temperatures and the fact that it does not have significant influence in the fire resistance of the structures. Although this period does not have a structural significance, it is the period where the toxic gases are produced.

The flashover period is when the fire is expanded to the compartment, which occurs when the temperature near the ceiling is between 450°C and 600°C or when the heat flux in the floor reaches 20 W/m². The continuous combustion period is the period immediately after the flashover and it is the period when the maximum temperature is obtained and this value remains approximately constant. This period is when high levels of carbon dioxide (CO₂) and carbon monoxide (CO) are verified, which is caused by the heat release of most of the fuel [26], [27].

Lastly, the cooling period is when the rest of the fuel is burned and the heat of combustion decreases until the complete end of fire [26], [27].

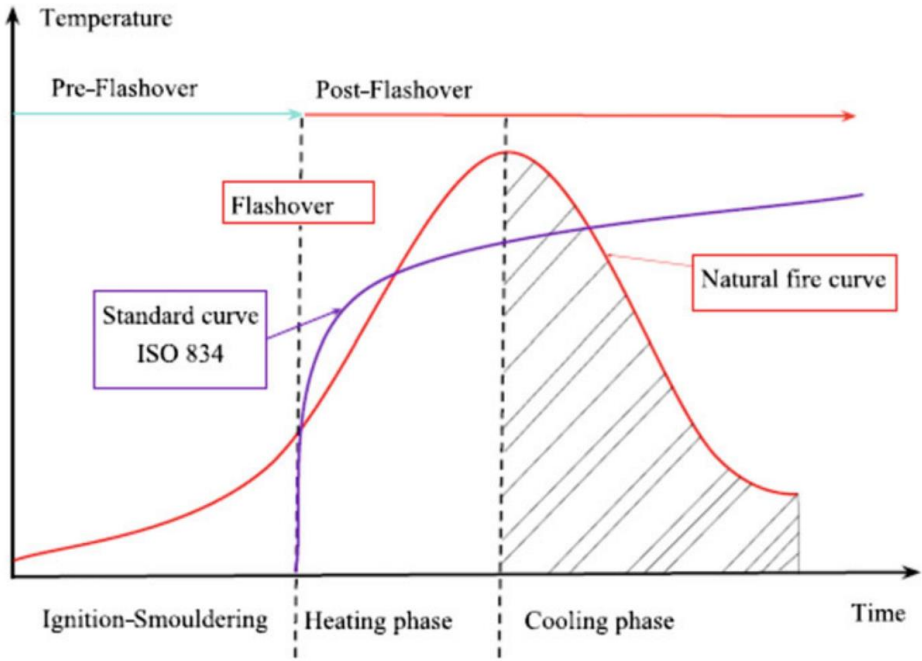


Fig. 11 – Natural fire curve compared to ISO 834 fire curve.[25]

4.3. Standard Fire Curves

The standard models of fire considers the natural fire curve and have an independent nature of space and fire load density. These curves normally is an approximation of the flashover and the continuous combustion, which are the most critical periods of fire in both structural and termal studies.

The Eurocode 1 [28], presents three nominal curves of fire: the standard curve, which is ISO834 [29] (same as BS 476 part 20 [30]), the external elements curves and the curve of fire caused by hydrocarbons. The standard curve is represented in Eq. 19, where θ_g is temperature of the gas in Celsius and t is time in seconds, and plotted in Fig. 12. For this case, the coefficient of heat transfer is $\alpha_c = 25 \text{ W/m}^2 \cdot \text{K}$.

$$\theta_g = 20 + 345 \log_{10}(8t + 1) \quad \text{Eq. 19}$$

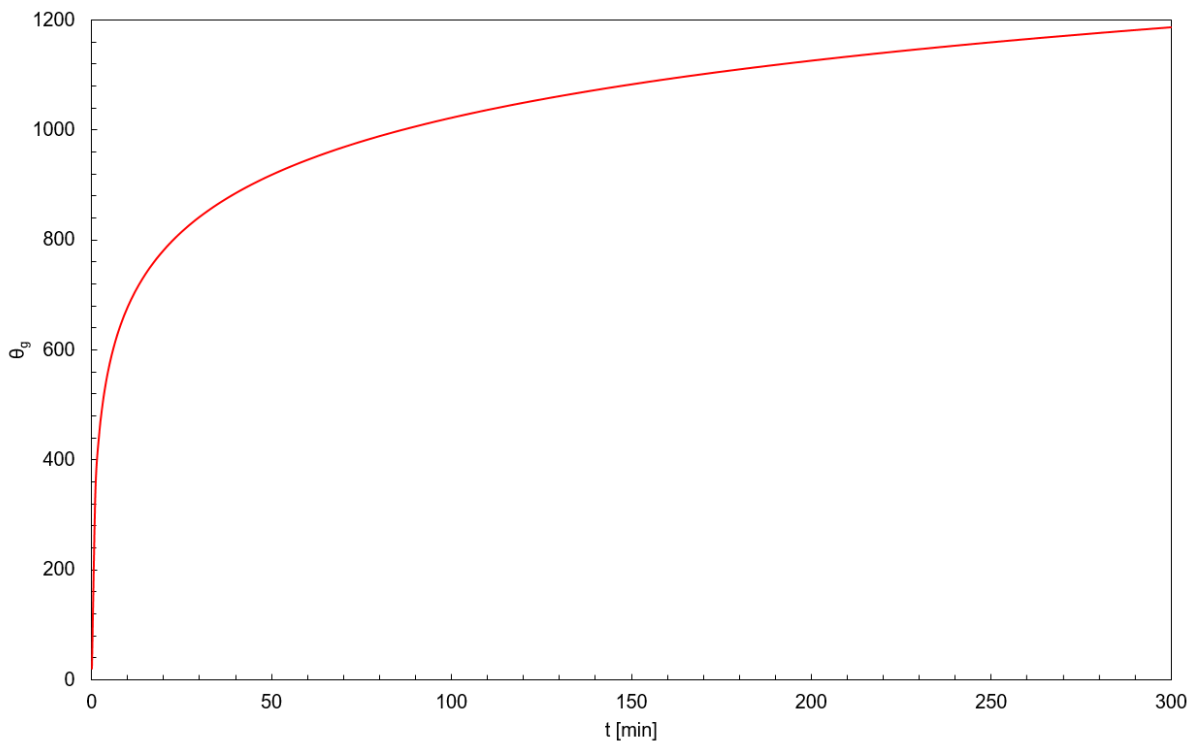


Fig. 12 – Standard Fire Curve (ISO 834).

However, since the initial temperature of different articles analyzed in this study varied greatly, it was decided to use a variation of ISO834, which is defined by Australian Standard AS1530.4 [31]. This fire curve is also used in Queensland University of Technology, whose works are presented in this study for validation. The

equation that describes the fire curve for this standard is presented in Eq. 20, where θ_g is temperature of the gas in Celsius, θ_0 is initial temperature in Celsius and t is time in seconds

$$\theta_g = \theta_0 + 345 \log_{10}(8t + 1) \quad \text{Eq. 20}$$

4.4. Fire Resistance Requirements

Each component of the non-loadbearing wall system, such as the panels, insulation, lightweight steel structure and its location determines the whole member's fire resistance category. The classification of the member is decided especially by the spacing of plates, the thickness and number of coating layers, the thermal properties of the materials as well as the width of the insulation material.

The fire resistance of non-load bearing LSF walls is obtained by standards such as the EN 1363-1 (Fire Resistance Tests – General Requirements) [32], EN 1364-1 (Fire Resistance Tests for Non-load Bearing Elements – Walls) [33].

- **EN 1363-1**

When subjected to standard fire exposure conditions, this standard establishes the general principles for determining the fire resistance of different elements of construction. According to this standard, fire resistant construction should satisfy three fire resistance requirements, namely stability, insulation and integrity [32].

Load-bearing capacity (Stability - R): For load-bearing elements of a structure, they shall not collapse in such a way that they no longer perform the load-bearing function for which they were constructed.

Insulation (I): For elements of a structure such as walls and floors which have a function of separating two parts of a building, the average temperature of the unexposed face of the element shall not increase above the initial temperature by more than 140°C while the maximum temperature at any point of this face shall not exceed the initial temperature by more than 180°C.

Integrity (E): Initial integrity failure shall be deemed to have occurred when a cotton pad is ignited or when sustained flaming, having duration of at least 10s, appears on the unexposed face of the elements.

The performance criterion used to validate the fire resistance of non-load bearing walls in this study is the insulation criterion (I). The insulation (I) criterion shall automatically be assumed not to be satisfied when the integrity (E) criterion ceases to be satisfied.

The main performance criterion given by this standard is the stability criterion (R), although this criterion is not analyzed in this study, since it concerns about the fire resistance of non-load bearing walls.

- **EN 1364-1**

This standard contains the procedures to perform experimental tests to measure the fire resistance of a non-loadbearing wall to resist the fire propagation from one side to another [33].

This standard requires that a rigid frame with high stiffness and low thermal expansion is needed to fix the specimen. The dimension of the specimen should follow the rule that if the width or height of the construction element is smaller than 3 m, the specimen should be tested in its actual size. However, if one of the dimensions of the construction element is bigger than 3 m, the dimension of the specimen tested should not be less than 3 m. All the specimens used in this study follows the rules of this standard.

5. Numerical Simulation

Since physical tests are usually expensive, numerical methods can be used to estimate the insulation-I criterium of fire resistance. For this purpose, this study presents an analysis in both one-dimensional simplified calculation method and two-dimensional advanced calculation method. This section of the research presents the one-dimensional simplified calculation method with a proposed approach for calculating the effective width to be analyzed.

Ignoring heat transfer in the longitudinal direction of the LSF wall panel, the heat transfer can then be considered 2-dimensional, in both thickness and width directions. Nevertheless, Feng et al. [34] and Shahbazian et al. [35] presented numerical simulations with results that suggest that for compressive resistance of the steel stud, it is acceptable to assume the temperature distribution on the thickness direction to be linear using the average temperatures in the two flanges of the cross-section. Fig. 13 shows the actual temperature distribution in the flange section and the acceptable simplified temperature distribution based on Feng et al [34].

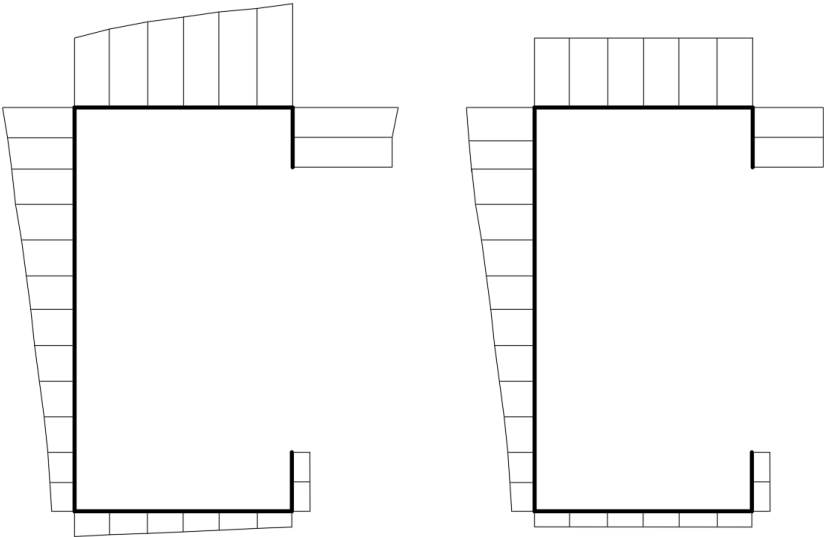


Fig. 13 – (a) Actual temperature distribution; (b) Acceptable temperature distribution according to Feng et al. [34]

If heat transfer in the panel width direction is not dealt with explicitly, then this allows for a considerable simplification to be made. However, as demonstrated by some authors [36], [37], there is a strong heat transfer in the width direction between

steel flanges and the adjacent materials, so it is important to include this effect in the temperature calculation method for the steel section. One way of including this effect is to use the weighted average of thermal resistances in the wall panel width direction. The method for calculating the weighted average of thermal resistances is presented in Section 5.1. The accuracy of the proposed temperature calculation method will be assessed by comparing the simulation results using the advanced calculation method finite element software ANSYS APDL for steel temperatures.

5.1. Proposed Approach for Calculating the Effective Width

All methods presented in Section 3 are one-dimensional numerical solutions for calculating the R-value of the composite wall. However, for steel framing, it frequently is necessary to account for multi-dimensional effect, e.g. consider heat transfer in the width direction. One method of including this effect is finite-difference computer solution. Differently from analytical solutions, which allow temperature determination at any point in the wall, the finite-difference solution allows for determination of temperature only at discrete points. These points, or nodes, are defined by dividing the wall into small control volumes and placing a node in the center. The node represents the average temperature of the control volume. From this selection, an appropriate energy conservation equation can be chosen for each node. The complete set of equations is then solved simultaneously for the temperature at each node.

One way of accounting for the width direction without the need of making a two dimensional analysis is to use the weighted average of thermal resistances in the wall panel width direction.

For the research made in this study, the reference construction element model is described by Eq. 27 as follows.

$$\frac{\partial}{\partial y} \left(\lambda \frac{\partial T}{\partial y} \right) = \rho C_p \frac{\partial T}{\partial t} \quad \text{Eq. 21}$$

This model is based on the heat balance of each layer, taking into consideration the amount of heat flux entering the layer and the amount of heat flux leaving the layer, as represented in the following.

$$\left(\begin{array}{c} \textit{heat} \\ \textit{entering} \\ \textit{the layer} \end{array} \right) - \left(\begin{array}{c} \textit{heat} \\ \textit{leaving} \\ \textit{the layer} \end{array} \right) = \left(\begin{array}{c} \textit{heat change} \\ \textit{to change layer} \\ \textit{temperature} \end{array} \right)$$

If it is considered a small time interval, the heat transfer between any two layers can be written as Eq. 22. The amount of heat required to increase the temperature of a layer from the previous time step T_i^{t-1} to the current one T_i is defined by Eq. 23.

$$\dot{Q} = \frac{\Delta T}{\Sigma R} \quad \text{Eq. 22}$$

where ΔT is temperature difference between these two layers and ΣR is the total thermal resistance in the heat transfer path.

$$\dot{Q} = \Sigma R_{\textit{capacity}} \frac{dT}{dt} \quad \text{Eq. 23}$$

where t is time and $\Sigma R_{\textit{capacity}}$ is the total capacitance (mass times specific heat) of the layer.

The thermal resistance calculated in this study uses the weighted average of the materials within the heat transfer path. Table 1 details how this analysis is made.

Table 1 – Details of heat transfer and thermal resistance.

Heat transfer	Thermal resistance
Between fire and gypsum board on the fire exposed side (layer 1)	Total of the thermal boundary layer and ½ of the gypsum layer.
Heat conduction between two adjacent gypsum layers (2-3, 3-4, 4-5, 10-11, 11-12, 12-13)	Total of the 2 halves each layer.
Between slice of gypsum board on the air side with the air layer (layer 14)	Total of the air layer and ½ the gypsum layer.
Between a gypsum slice and a steel or between two adjacent steel slices	Should include different materials that are present in these slices. Fig. 15 shows the materials to be considered for layers 5 to 10. For each layer, the thermal resistances are in parallel, therefore they should be calculated using $\frac{1}{R_{total}} = \frac{1}{R_1} + \frac{1}{R_2} + \dots + \frac{1}{R_n}$ where n is the layer of thermal resistances in parallel.

To calculate the heat capacitance of each layer, all the materials within that layer must be included. In Fig. 15 it is shown the parallel heat resistance terms and in Fig. 16 it is shown the thermal capacitance terms for different multi-material layers.

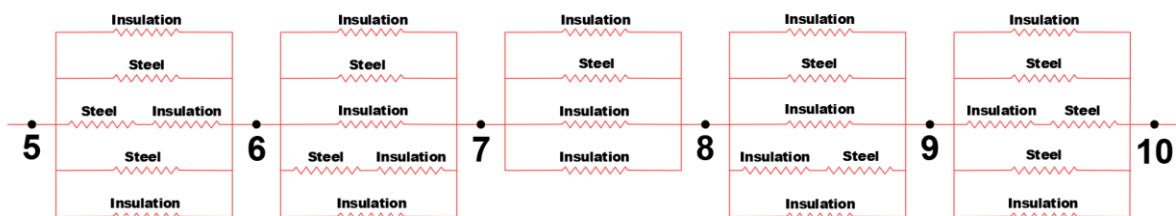


Fig. 15 – Heat resistance from layer 5 to 10, based on Shahbazian [36].

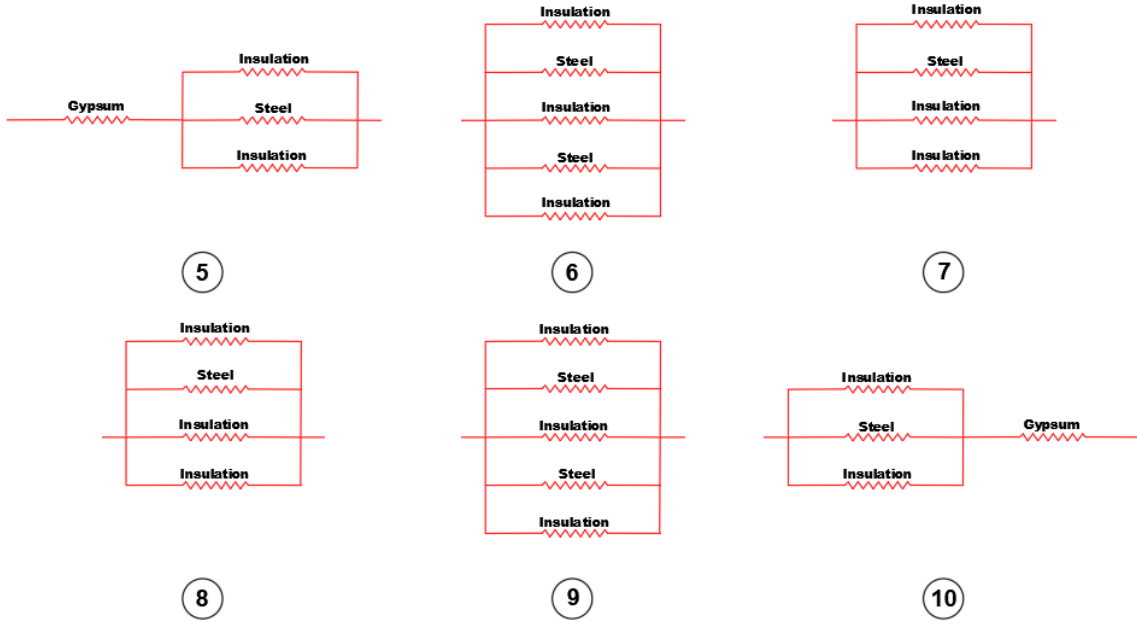


Fig. 16 – Heat capacitance for each layer of the panel, based on Shahbazian [36].

Equations 25-38 are the representation of this concept in each of the 14 layers used in this study. Eq. 24 was linearized to solve a system of linear equations.

$$\alpha(T_{fire} - T_1)WL + \varepsilon_f \varepsilon_G \sigma (T_{fire} + T_1)(T_{fire}^2 + T_1^2)(T_{fire} - T_1)WL - \lambda_G / (TG/4)(T_1 - T_2)WL - \rho_G Cp_G (TG/8)(T_1 - T_1^{t-1}) / \Delta t WL \quad \text{Eq. 24}$$

$$\lambda_G / (TG/4)(T_1 - T_2)WL - \lambda_G / (TG/4)(T_2 - T_3)WL - \rho_G Cp_G (TG/4)(T_2 - T_2^{t-1}) / \Delta t WL \quad \text{Eq. 25}$$

$$\lambda_G / (TG/4)(T_2 - T_3)WL - \lambda_G / (TG/4)(T_3 - T_4)WL - \rho_G Cp_G (TG/4)(T_3 - T_3^{t-1}) / \Delta t WL \quad \text{Eq. 26}$$

$$\lambda_G / (TG/4)(T_3 - T_4)WL - \lambda_G / (TG/4)(T_4 - T_5)WL - \rho_G Cp_G (TG/4)(T_4 - T_4^{t-1}) / \Delta t WL \quad \text{Eq. 27}$$

$$\lambda_G / (TG/4)(T_4 - T_5)W_l - (T_5 - T_6) / R_{COND56} - (T_5 - T_5^{t-1}) / R_{CAP5} \quad \text{Eq. 28}$$

$$(T_5 - T_6) / R_{COND56} - (T_6 - T_7) / R_{COND67} - (T_6 - T_6^{t-1}) / R_{CAP6} \quad \text{Eq. 29}$$

$$(T_6 - T_7) / R_{COND67} - (T_7 - T_8) / R_{COND78} - (T_7 - T_7^{t-1}) / R_{CAP7} \quad \text{Eq. 30}$$

$$(T_7 - T_8) / R_{COND78} - (T_8 - T_9) / R_{COND89} - (T_8 - T_8^{t-1}) / R_{CAP8} \quad \text{Eq. 31}$$

$$(T_8 - T_9) / R_{COND89} - (T_9 - T_{10}) / R_{COND910} - (T_9 - T_9^{t-1}) / R_{CAP9} \quad \text{Eq. 32}$$

$$(T_9 - T_{10}) / R_{COND910} - \lambda_G / (TG/4)(T_{10} - T_{11})W_l - (T_{10} - T_{10}^{t-1}) / R_{CAP10} \quad \text{Eq. 33}$$

$$\lambda_G / (TG/4)(T_{10} - T_{11})WL - \lambda_G / (TG/4)(T_{11} - T_{12})WL - \rho_G Cp_G (TG/4)(T_{11} - T_{11}^{t-1}) / \Delta t WL \quad \text{Eq. 34}$$

$$\lambda_G / (TG/4)(T_{11} - T_{12})WL - \lambda_G / (TG/4)(T_{12} - T_{13})WL - \rho_G Cp_G (TG/4)(T_{12} - T_{12}^{t-1}) / \Delta t WL \quad \text{Eq. 35}$$

$$\lambda_G / (TG/4)(T_{12} - T_{13})WL - \lambda_G / (TG/4)(T_{13} - T_{14})WL - \rho_G Cp_G (TG/4)(T_{13} - T_{13}^{t-1}) / \Delta t WL \quad \text{Eq. 36}$$

$$\lambda_G / (TG/4)(T_{13} - T_{14})WL - \alpha_c (T_{14} - T_{amb})WL - \rho_G Cp_G (TG/8)(T_{14} - T_{14}^{t-1}) / \Delta t WL \quad \text{Eq. 37}$$

The parameter R_{CONDij} represents the resistance to heat flow by conduction expected from node i to node j due to parallel heat flow pattern and should be calculated as the equivalent resistance. This parameter should be evaluated at the average temperature of both nodes i and j . The parameter R_{CAPi} represents the inverse of the thermal capacitance of layer i and should be evaluated at the temperature of layer i .

The thermal conductivity of gypsum λ_G should be evaluated at the average temperature of the nodes involved, while the density ρ_G and the specific heat Cp_G should be evaluated at the temperature level of the corresponding layer [36]. The time step was defined to be 1 s and validate the stability criterion [38].

A full description and exact solution procedure of the discretisation of this method as adopted in the present work, applied to multi-layer construction elements, can be found in Appendix A and the matrix input for the one-dimensional analysis can be found in Appendix B.

To auxiliate on the calculation of this method, it was used the Matlab R2016a software. The diagram of the application of this program is presented in Fig. 17. Appendix E will present the program of the Specimen 10 of the Polytechnic Institute of Bragança as reference for every other program, since for each wall configuration there is the need to change the variables defined and the material properties.

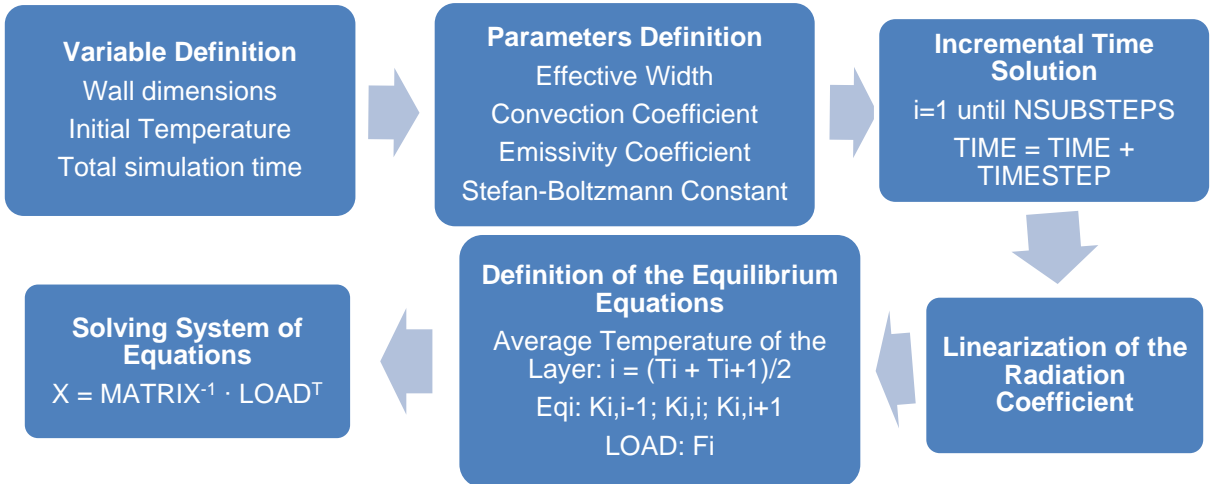


Fig. 17 – Diagram of the Matlab application program.

To calculate the thermal resistance and heat capacitance, it is necessary to determine the effective width of the panel that should be included in the calculations.

Fig. 18 shows the model of the proposed geometry for this heat transfer calculation method. Fig. 19 shows the cases studied in this research, in which WL_{max} considers the effective width as being the whole width between two steel sections and WL_{min} considers only the width of the flange as the effective width. The WL_{max} will over-predict the temperatures in the flange of the steel stud on the exposed side and under-predict the temperatures in the flange on the unexposed side, while WL_{min} will have an opposite result.

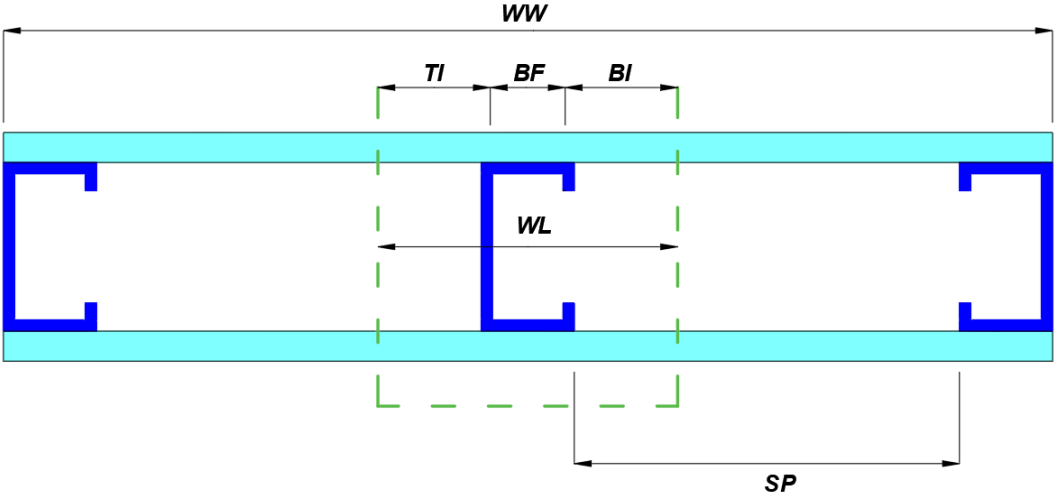


Fig. 18 – Proposed geometry for heat transfer calculation.

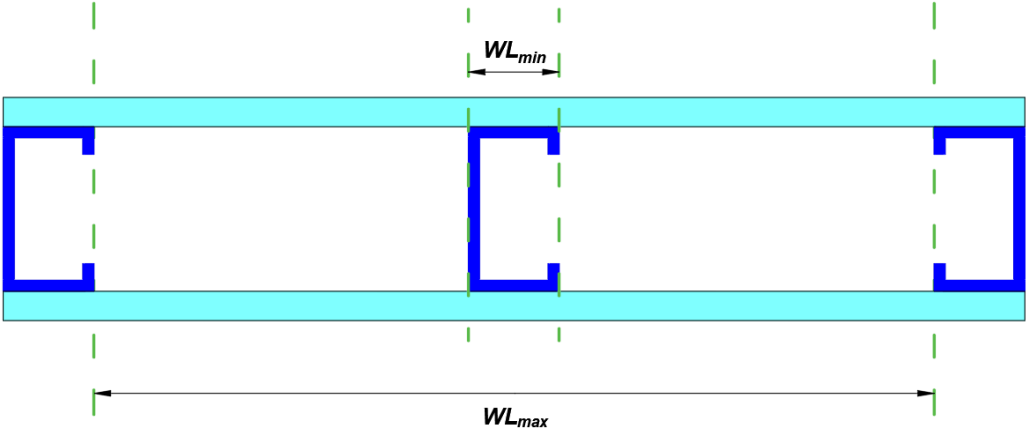


Fig. 19 – Maximum and minimum values for the effective width (WL).

First, it was proposed both the maximum and minimum values for the effective width possible, presented in Fig. 19 to find a relative good choice for the effective width for each case and configuration. After that, it was proposed different dimensions for the effective width by adding 50 by 50 mm to the minimum width (which is the flange size, BF) until it reached the maximum width (which is two times the spacing between studs plus the flange size, or in other words, $2 \cdot SP + BF$) to gather the unexposed side

curve of temperature as a function of time and compare it to the results of both the experimental and the advanced method calculation analysis, the latter specially for those cases where the experimental test did not reach the fire resistance insulation criterion (I).

To find the best effective width from the proposed widths, it was used two different comparison methods: the Pearson Correlation and the Relative Error.

The Pearson Correlation is calculated by Eq. 38. It varies from -1 to 1, where -1 means that the values being compared are inversally proportional to one another (if one is going up, the other is going down, and vice-versa) and 1 positive means that both sets of data are moving accordingly to one another.

$$r_{XY} = \frac{\sum_{i=1}^n (X_i - \bar{X})(Y_i - \bar{Y})}{\sqrt{\sum_{i=1}^n (X_i - \bar{X})^2} \sqrt{\sum_{i=1}^n (Y_i - \bar{Y})^2}} \quad \text{Eq. 38}$$

The Relative Error is presented by Eq. 39 and provides the error between each temperature in time. It was made an arithmetic mean of every value for Relative Error to find the best effective width when comparing to the experimental test or advanced calculation method.

$$RE = \frac{T_{\text{experimental}} - T_{\text{simulated}}}{T_{\text{experimental}}} [\%] \quad \text{Eq. 39}$$

The Manchester University specimen was not analyzed in this study because it does not consider a small scale of the whole wall.

For achieving the best effective width equation, some different approaches were made. These approaches are presented in the following sections and are going to be compared to every validation result further in this study. Each method used a different comparison method, and therefore the results for each is going to be presented in their sections.

5.1.1. Calculation Method 1

This method used the comparison with the experimental results for the specimens made in Polytechnic Institute of Bragança and with the advanced calculation results for every other specimen.

After analyzing roughly the best possible effective width for each case presented using the Relative Error, it was possible to observe the results presented in Table 2.

Table 2 – The best effective width used for the calculation method 1.

Case	University	Cavity Insulation	Minimum Width (<i>BF</i>) [mm]	Maximum Width ($2 \cdot SP + BF$) [mm]	Best Effective Width Advanced [mm]	Best Effective Width Experimental [mm]
Spec. 4	Queensland University - 1	Rock fibre	40	1040	225	–
Spec 5	Queensland University - 1	Glass fibre	40	1040	150	–
Spec 6	Queensland University - 1	Cellulose fibre	40	1040	1040	–
Spec. 3	Queensland University - 2	Rock fibre	40	1240	145	–
Spec. 4	Queensland University - 2	Glass fibre	40	1240	175	–
Spec. 5	Queensland University - 2	Cellulose fibre	40	1240	40	–
Spec. 3	Polytechnic Institute of Bragança	Rock fibre	43	423	–	300
Spec. 10	Polytechnic Institute of Bragança	Rock fibre	43	889	–	150
Spec. 15	Polytechnic Institute of Bragança	Superwool	43	889	–	225
Spec. 16	Polytechnic Institute of Bragança	Superwool	43	889	–	200

Since the effective width values encountered by both of the Cellulose fibre analysis are inconsistent (either the minimum or maximum value for the effective width), and also it does not have a linear growth pattern (it goes up and down while the effective width is either constantly increasing or decreasing), it was assumed that the thermal properties for the Cellulose fibre was not corresponding to the real behavior

and therefore the values for the effective width of both tests for the Cellulose fibre were not considered for the calculation of the equation for the effective width.

Spec. 16 from the Polytechnic Institute of Bragança was also not considered in the final equation for the effective width because of its geometry, which includes two studs in the middle of the wall, as shown in section 6.1.4, and this effect is not considered by the equations for heat transfer used in this study.

While different values for roughly the best effective width was found for each case, the first idea is to make the effective width a variable of the spacing between studs and the flange size, not considering the material for the insulation cavity. Therefore, an average for each best effective width was made, grouping the best effective widths for the same size of walls, where the specimens with wall width of 975 mm, 1120 mm and 1960 mm, would have an effective width of 225 mm, 187.5 mm and 160 mm, respectively.

From these results, it was possible to make an approximation value that would satisfy every geometry and material, and the graph for this approximation is presented in Fig. 20.

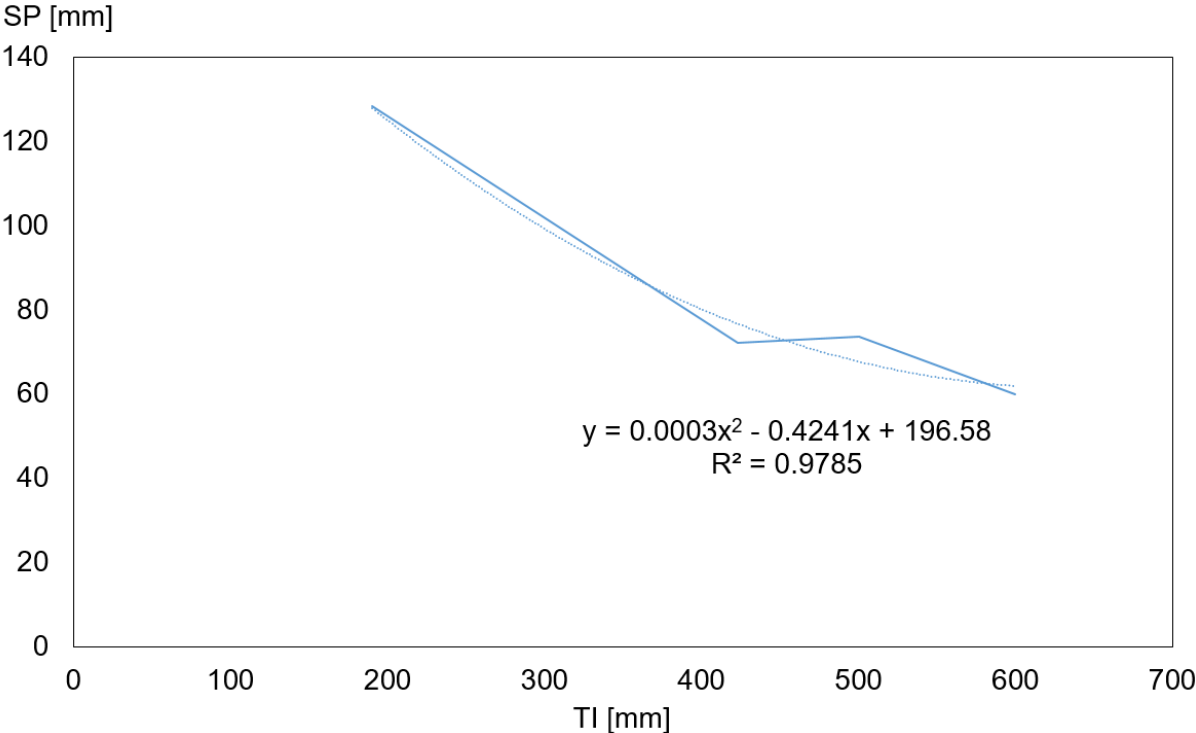


Fig. 20 – Graph of TI as a function of SP according to analysis made by the author.

This graph presents TI as a function of the spacing between studs SP and the equation is represented by Eq. 40, in millimeters.

$$TI = 0.0003 \cdot SP^2 - 0.4241 \cdot SP + 196.58 \quad \text{Eq. 40}$$

Through Eq. 40, it is possible to write an equation that describes the effective width (WL) as being 2 times the equation for TI as a function of SP plus the flange size BF . This equation is demonstrated in Eq. 41 and should be used in millimeters.

$$WL = 2(0.0003 \cdot SP^2 - 0.4241 \cdot SP + 196.58) + BF \quad \text{Eq. 41}$$

5.1.2. Calculation Method 2

For this method, the analysis for each effective width used mostly the results from the Pearson Correlation and can be seen in Table 3.

Table 3 – The best effective width used for the calculation method 2.

Case	University	Cavity Insulation	Minimum Width (BF) [mm]	Maximum Width ($2 \cdot SP + BF$) [mm]	Best Effective Width Advanced [mm]	Best Effective Width Experimental [mm]
Spec. 4	Queensland University - 1	Rock fibre	40	1040	225	–
Spec. 5	Queensland University - 1	Glass fibre	40	1040	150	–
Spec. 6	Queensland University - 1	Cellulose fibre	40	1040	1040	–
Spec. 3	Queensland University - 2	Rock fibre	40	1240	350	–
Spec. 4	Queensland University - 2	Glass fibre	40	1240	350	–
Spec. 5	Queensland University - 2	Cellulose fibre	40	1240	40	–
Spec. 3	Polytechnic Institute of Bragança	Rock fibre	43	423	155	350
Spec. 10	Polytechnic Institute of Bragança	Rock fibre	43	889	165	230
Spec. 15	Polytechnic Institute of Bragança	Superwool	43	889	145	250
Spec. 16	Polytechnic Institute of Bragança	Superwool	43	889	150	165

Just like in the calculation method 1, values for the specimens which used cellulose fibre were discarded, as were the values for the specimen 16 of the Polytechnic Institute of Bragança.

From this values presented in Table 3, it was decided to use only the values from the advanced calculation method, since the experimental value for Spec. 3 from the Polytechnic Institute of Bragança seems to be very different from the advanced calculation value, while the other studies from the same university show closer values for both the advanced calculation method and the experimental tests.

For that same reason, it was decided not to consider the spacing between studs as a variable, since the advanced calculation results from Spec. 3 of the Polytechnic Institute of Bragança, which has a spacing of 190 mm, and Spec. 10 from the same university, which has a spacing of 423 mm, are not very far from each other.

The next step was grouping the values from the same wall width, since the idea is to consider every material in a single equation and not different equations for

different materials, and an average of these values were used, where for the walls of widths of 975 mm, 1120 mm and 1960 mm, it was considered the effective width of 155 mm, 187.5 mm and 350 mm, respectively.

From the results gathered, it was possible to understand a pattern between the effective width and the wall width of each specimen. These results made it possible to consider equation Eq. 42, in which the effective width (WL) is equal to 15% of the wall width (WW).

$$WL = 0.15 \cdot WW \quad \text{Eq. 42}$$

5.2. Advanced Calculation Method

Another method used for this analysis is the advanced calculation method, using a 2D analysis of the heat transfer and considering the whole width of the wall. Although this method still does not consider the 3D effect of heat transfer, it is a close approximation of the physical tests results. This method is used for the validation of the Simple Calculation Method proposed in this study.

5.2.1. ANSYS Mechanical APDL

This study presents an analysis in 2D using ANSYS Mechanical APDL to provide comparison with the proposed simplified method from Matlab. In this study, it was considered the same small-scale wall assembly used in the physical tests from the validation articles.

Differently from the simplified calculation method, the advanced calculation method considers in between studs interference, the heat not following a linear path and possible thermal bridges. Nevertheless, both advanced and simplified calculation methods do not consider the 3D effect of heat transfer that exists in the physical tests.

The convergence criterion for this method is based on the heat flow, with a tolerance of 1E-3 and a minimum reference value of 1E-6. The mesh was defined with different numbers of element divisions in each section, which are represented in Fig. 21.

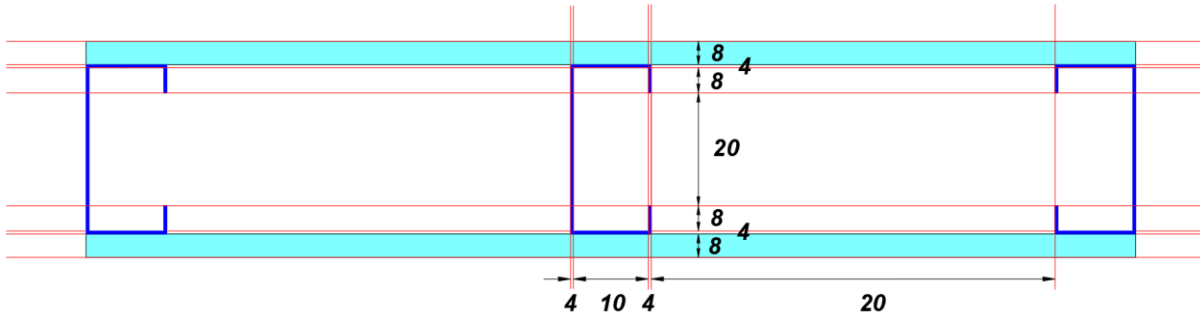


Fig. 21 – Number of element divisions for each section.

. This numerical model considers perfect thermal contact between materials and the mesh of Specimen 10 from Polytechnic Institute of Bragança is represented in Fig. 22

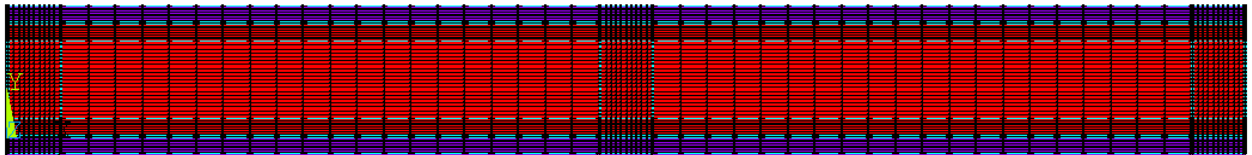


Fig. 22 – Finite Element mesh used for specimen 10 from Polytechnic Institute of Bragança.

5.2.1.1. Element Description

PLANE55 is an element in Ansys Mechanical APDL which is represented in Fig. 23 and will be used in this study because of its 2D thermal conduction capability. The element has four nodes with a single degree of freedom, temperature, at each node.

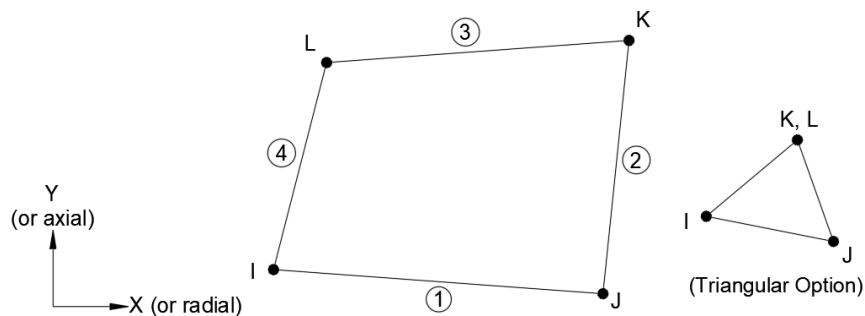


Fig. 23 – PLANE55 element description.

It is applicable to a 2D, steady-state or transient thermal analysis and can also compensate for mass transport heat flow from a constant velocity field.

There is an option that allows the element to model nonlinear steady-state fluid flow through a porous medium. With this option, the thermal parameters are interpreted as analogous fluid flow parameters.

In this study, it will be used PLANE55 2D Thermal Solid, represented by Fig. 24, in which there is a matrix of conductivity and heat generation load vector, with the quad geometry and 2 x 2 integration points. Therefore, the equation to be used is that for the 2-D 4-node and axisymmetric quadrilateral solid elements without extra shape functions, represented by Eq. 43.

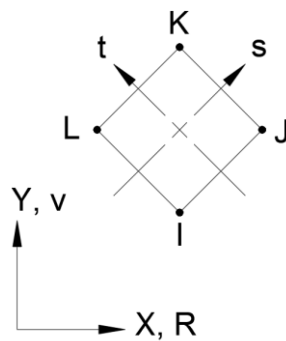


Fig. 24 – PLANE55 2-D Thermal Solid.

$$T = \frac{1}{4}(T_i(1-s)(1-t) + T_j(1+s)(1-t) + T_k(1+s)(1+t) + T_l(1-s)(1+t)) \quad \text{Eq. 43}$$

5.2.1.2. Boundary Conditions

For the boundary conditions of this method, it is considered convection in the exposed side with a coefficient of $\alpha_{fire} = 25.0 \text{ W/m}^2\text{K}$ and a convection in the unexposed side, with a coefficient of $\alpha_{unex} = 9.0 \text{ W/m}^2\text{K}$ which considers also the radiation on the unexposed side. For the radiation, it is considered a coefficient of $\epsilon_{fire} = 1.0$ for the exposed side.

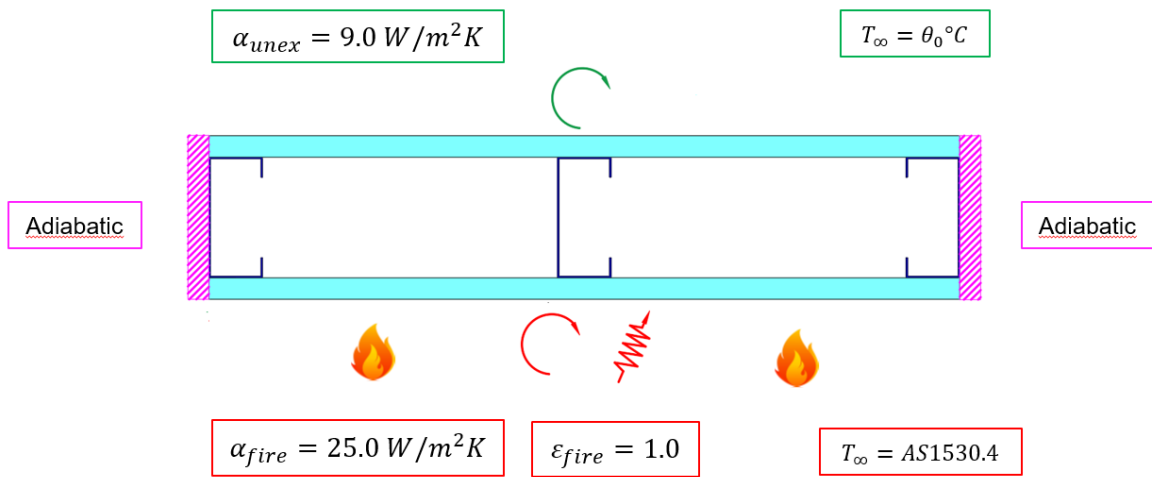


Fig. 25 – Boundary conditions of the advanced calculation method.

The initial temperature changes with each analysis, from 14°C to 28.5°C, along with the geometry of the wall specimens. The gypsum and steel properties can be found in Appendix C, along with the insulation materials.

6. Validation of the Numerical Models

To validate the analysis made in this study, both the results from the advanced calculation method and tests developed by authors were used, such as Kolarkar et al. [39], Rusthi et al. [40], [41], Feng et al. [15], Khetata et al. [42], [43] and Piloto [44].

The tests were separated by the Universities where they were made, being Kolarkar and Rusthi at Queensland University of Technology identified as tests 1 and 2, respectively, Feng at University of Manchester, and Khetata and Piloto at Polytechnic Institute of Bragança.

Most researches made by other authors are presented only with the average of temperatures on different places of the wall to consider it a point. Since the results made by the simplified calculation method considers only a region of one stud, the maximum value is considered (or, in other words, it is the critical stud in the wall). To make a fair comparison between results, those results in which there is not a maximum value for each point, the simplified calculation results are compared to the advanced calculation results, in which it is possible to obtain the maximum value.

The Relative Error presented in Eq. 39 is used for the validation of the results in this topic.

6.1. Experimental Studies

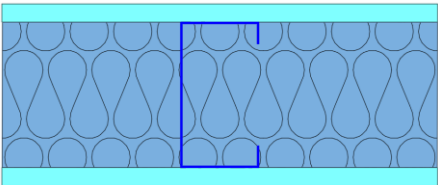

This Section presents the experimental studies made by different authors that were used for the validation of the methods described in this study.

6.1.1. University of Manchester

This study made by Feng et al. [15], in 2003, was developed in the fire-testing laboratory of the Manchester Centre for Civil and Construction Engineering. Only Specimen of ID Tlip12-a3 was used for the analysis in this study. The overall size of the panel was 300 x 300 mm. The parameters of this experimental investigation include the types of steel cross-section (lipped channel 100 x 54 x 15 x 1.2 mm), one gypsum board on both sides (12.5 mm on each side), and mineral wool as insulation material.

All channels were pre-hot dip galvanised to BS EN 10147 with a G275 coating. The gypsum boards used were Fireline Gyproc board manufactured by British Gypsum Limited and the interior mineral wool was the 100 mm thick Isowool 1000, also manufactured by British Gypsum Limited.

Table 4 – Feng[15] studies considered in this research.

Spec.	Geometry	Cavity Insulation	Gypsum Boards
Tlip12-a3		Mineral wool	12.5 mm
			

Tests were carried out in the small gas fired furnace which is lined with stack bonded cermaic wool with a working volume of 1.5 x 1.5 x 1.5 m. The test panels were positioned in the four 300 x 300 mm apertures located on the front panel of the furnace. The furnace was computer controlled and the average temperature rise in the furnace, which was obtained from four control thermocouples inside the furnace, was according to the BS: 476 Part 20 – Cellulosic fire curve [30]. Numerous thermocouples were placed in each test specimen in order to monitor its temperature distributions. Detailed locations of thermocouples are shown in Table 1. All fire tests were terminated after 2 hours of fire exposure.

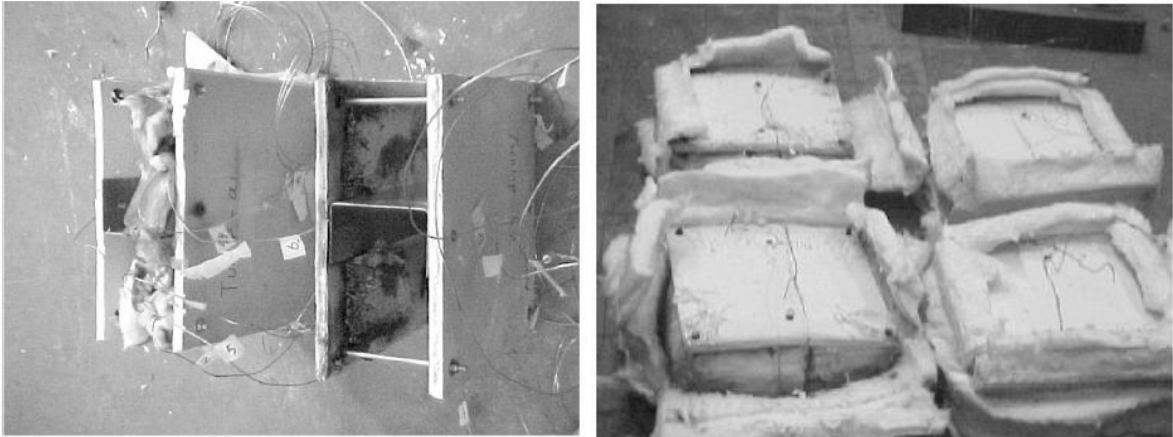


Fig. 26 – Experimental tests for the Mineral wool cavity insulation made by Feng et al. [15].

The material properties used in this study were: steel, as presented by Eurocode 3 Part 1.2 [45], gypsum as presented by Sultan [38] and mineral wool as the cavity insulation, as presented by Feng et al. [15]. Further information about the material properties can be found in Appendix C.

Table 5 – Fire resistance values for Manchester University.

Spec.	Fire Res. Exp. (Ave) [min]	Fire Res. Num. Simple Method 1 [min]	Fire Res. Num. Simple Method 2 [min]	Fire Res. Num. Adv. (Max) [min]	Fire Res. Num. Adv. (Ave) [min]
Tlip12-a3	>120	>1200	84	105	768

6.1.2. Queensland University of Technology – 1

In 2012, Kolarkar and Mahendran [39] made a research in which they used various configurations of wall panels to predict their resistance to fire through physical tests.

Table 6 - Kolarkar [39] studies considered in this research.

Spec. Kolarkar.	Geometry	Cavity Insulation	Gypsum Boards
4		Glass fiber	2 x 16 = 32 mm
5		Rock fiber	2 x 16 = 32 mm
6		Cellulose fiber	2 x 16 = 32 mm

The specimens used for analysis in this study were specimens 4, 5 and 6, presented in Table 6. They were made using small scale steel wall frame assemblies of 1280 mm x 1015 mm. The wall assemblies consisted of three cold-formed steel lipped channel section studs (90 mm x 40 mm x 15 mm x 1.15 mm) spaced at 500 mm. The studs were fabricated from G500 steel sheets with a minimum yield strength of 500 MPa. Test frames were built by attaching the studs to the top and bottom tracks made of 1.15 mm G500 steel unlipped channel sections (92 mm x 50 mm) using 12 mm long self-drilling wafer head screws. Test specimens were built by lining the test frames with two layers of gypsum plasterboards (FireSTOP) manufactured by Boral Plasterboard. These plasterboards were 1280 mm x 1015 mm with a thickness of 16 mm and a mass density of 13 kg/m².

K type thermocouple wire were located on the steel frame, three on each stud at mid-height to measure the temperatures of the hot flange, web and the cold flange. Additional thermocouples were attached at the mid-height of the plasterboard to measure temperatures inside the wall cavity and on the fire exposed surface. To measure the temperature of the ambient surface of the wall assembly, five more thermocouples were attached to the unexposed surface of the plasterboard, one thermocouple at the center of the wall and one at the center of each quarter section of the wall, giving a total of 20 thermocouples.

Test Specimen 4 was lined on both sides by two layers of plasterboard (2 x 2). The base layer plasterboards were first attached to the three studs by 25 mm long self-drilling bugle head screws at 300 mm centers. The face layer plasterboards were then attached by 45 mm long self-drilling bugle head screws at 300 mm centers and penetrating the studs midway between the base layer screws. Test Specimen 4 was built with cavity filled with two layers of 50 mm thick glass fiber mats of original density 13.88 kg/m³ compressed to 90 mm thickness (cavity depth) giving the insulation a density of 15.42 kg/m³. The cavities of the studs and tracks were also packed with insulation to eliminate any air pockets.

Test Specimen 5 was built similar to Test Specimen 4, but with rock fiber of density 100 kg/m³ used as cavity insulation. Two 25 mm thick mats were placed in the cavity leaving a gap of 40 mm between the insulation and Plasterboard three. Test Specimen 6 was built similar to Specimens 4 and 5, but with cellulose fibre wet sprayed into the cavity until it was filled. The calculated density of cavity cellulose insulation was 125 kg/m³.

Further information about the validation can be found on the Data Sheets in Appendix D.



Fig. 27 – Experimental tests for the (a) glass fibre, (b) rock fibre and (c) cellulose fibre cavity insulation made by Kolarkar et al. [39]

Although the insulation do not entirely fill the cavities, as stated by the author, in the analysis made in this study it is considered to be completely filled both in the one dimensional and two dimensional analysis, without any air gap.

The materials properties considered for the simulations are in Appendix C. Steel properties were obtained from EN 1993-1-2 [45], gypsum plasterboard properties were obtained from Sultan, 1996 [38] and insulation properties varied for each material, being: rock fiber from TALAT [46] and glass fiber and cellulose fiber from Keerthan et al. [47], also mentioned by Kolarkar and Mahendran [39].

Results of the validation and fire resistance of the wall assemblies used by Kolarkar can be seen in Table 7.

Table 7 – Fire resistance values for Queensland University of Technology – 1.

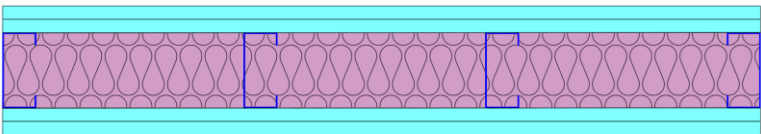
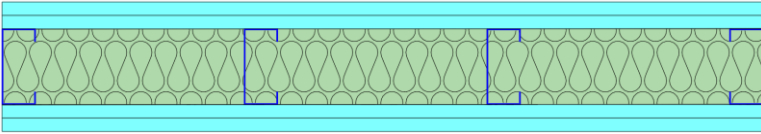
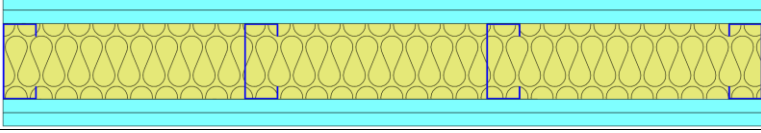
Spec.	Cavity Insulation	Fire Res. Exp. (I) (Ave) [min]	Fire Res. Num.I Simple Method 1 [min]	Fire Res. Num. Simple Method 2 [min]	Fire Res. Num Adv. (I) (Max) [min]	Fire Res. Num. Adv. (I) (Ave) [min]
4	Glass fiber	>200	153	151	152	152
5	Rock fiber	197	231	228	232	273
6	Cellulose fiber	>200	190	189	194	192

6.1.3. Queensland University of Technology – 2

In 2015, Rusthi et al. [40] made researches using a 3-D FE Model to validate the researches made by Kolarkar in 2010 [41]. In this study, both results of Kolarkar [41] and Rusthi [40] studies are going to be used to validate the numerical method proposed.

The details of the models is described in Table 8. The specimens used in this analysis are the 3, 4 and 5, with insulation material of Glass fibre, Rock fibre and Cellulose fibre, respectively.

Table 8 –Rusthi [40] studies considered in this research.

Model No.	Geometry	Insulation
3		Glass fibre
4		Rock fibre
5		Cellulose fibre

Gypsum

Steel

Glass Fibre

Rock Fibre

Cellulose Fibre

These are walls systems with two boards each side of 16 mm gypsum plasterboards and lipped channel studs (90 x 40 x 15 x1.15 mm) spaced at 600 mm.

The tests were conducted for 2.4 m x 2.1 m LSF walls exposed to standard fire time-temperatures curve on one side.



Fig. 28 – Experimental tests for the (a) glass fibre, (b) rock fibre and (c) cellulose fibre cavity insulation made by Kolarkar [41] and studied by Rusthi et al. [40]

The 3D FE models were developed in Abaqus/CAE with only two middle studs and gypsum plasterboards. The other studs were replaced with gypsum plasterboards, because according to the author, only the middle two studs are the critical studs in the tests. The model was rescaled to 0.6m height to reduce the analysis time. All the components were modelled using 8-node linear heat transfer brick elements (DC3D8). A mesh density of 50 mm on the x-y plane and 2 mm through thickness mesh of the model components was selected based on a sensitivity analysis of Models 1 and 2 and comparison of stud and plasterboards time-temperature profiles.

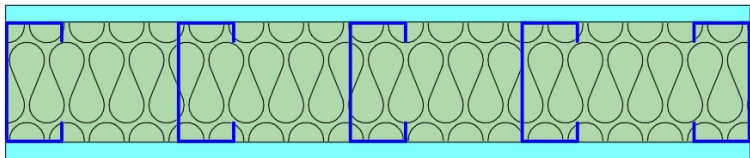
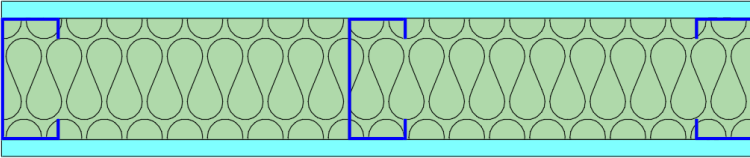
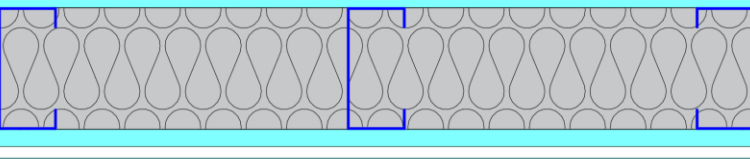
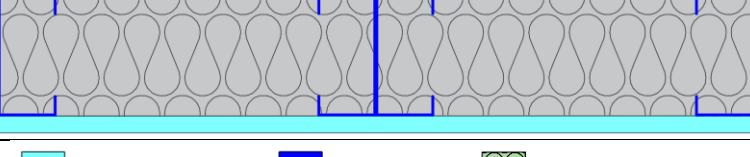
Table 9 – Fire resistance values for Queensland University of Technology – 2.

Spec.	Cavity Insulation	Fire Res. Exp. [min] (Ave)	Fire Res. FE Model [min] (Ave)	Fire Res. Num. Simple Method 1 [min]	Fire Res. Num. Simple Method 2 [min]	Fire Res. Num. Advanced (Max) [min]	Fire Res. Num. Advanced (Ave) [min]
3	Glass fibre	>110	>110	161	156	156	156
4	Rock fibre	>110	>110	244	284	243	289
5	Cellulose fibre	>110	>110	201	201	238	>240

6.1.4. Polytechnic Institute of Bragança

The presented study was made by Khetata et al. [42], [43] and Piloto [44] in the Laboratory of the Polytechnic Institute of Bragança. Specimens 3, 10, 15 and 16 were analyzed for this study and the overall size of the panel was 975 x 1000 mm walls exposed to standard fire time-temperatures curve on one side. The details of these models is presented in Table 10.

Table 10 – Khetata et al. [42], [43] and Piloto[44] studies considered in this research.

Spec. No.	Geometry	Cavity Insulation	Spacing between Studs
3		Rock fibre	190
10		Rock fibre	423
15		Super wool	423
16		Super wool	401.5

Gypsum
 Steel
 Rock Fibre
 Superwool

These panels have a geometry with one board each side of 12.5 mm gypsum plasterboards, with studs made of steel GD280 using the profile C90x43x15x1.5 and horizontal members (tracks) made of steel GD280 using the profile U93x43x1.5. The reference code gives the dimensions of the web, flange, lip and thickness of steep, respectively. The materials properties used for gypsum are those presented by Sultan [38], for steel are those presented by Eurocode 3 [45], for the rockfibre cavity insulation material are presented by TALAT [46] and for the superwool cavity insulation material, it is presented by the Morgan Datasheets [48], [49].



Fig. 29 – Experimental tests for Spec. 3, 10, 15 and 16, respectively, made by Khetata et al. [37], [42], [43] and Piloto [44].

One side of the wall is submitted to fire while the other side is assumed to remain at room temperature. The boundary conditions are in accordance to EN1991-1-2 [28], assuming heat transfer by radiation (emissivity of fire $\varepsilon_{fire} = 1$) and convection (convection coefficient $\alpha_{fire} = 25 [W/m^2K]$) in the exposed side and heat transfer by convection (convection coefficient $\alpha_{unex} = 9 [W/m^2K]$) to include the

radiation component) in the unexposed side. The temperature in the exposed side follows the standard BS 476 – Part 20 [30].

For the rock fibre cavity insulation, the results are presented in Table 11 and for the superwool cavity insulation, results are presented in Table 12.

Table 11 - Fire resistance values for Polytechnic Institute of Bragança for rock fibre.

Spec. No.	Fire Res. Exp. [min] (Max)	Fire Res. Exp. [min] (Ave)	Fire Res. IR [min] (Ave)	Fire Res. Num. Simple Method 1 [min]	Fire Res. Num. Simple Method 2 [min]	Fire Res. Num. Advanced [min] (Max)	Fire Res. Num. Advanced [min] (Ave)
3	88	99	90	90	74	76	102
10	79	94	99	78	74	77	97

Table 12 – Fire resistance values for Polytechnic Institute of Bragança for superwool.

Spec. No.	Fire Res. Exp. [min] (Max)	Fire Res. Exp. [min] (Ave)	Fire Res. IR [min] (Ave)	Fire Res. Num. Simple Method 1 [min]	Fire Res. Num. Simple Method 2 [min]	Fire Res. Num. Advanced [min] (Max)	Fire Res. Num. Advanced [min] (Ave)
15	95	115	115	92	84	85	118
16	86	100	104	92	84	85	106

7. Parametric Studies

This chapter presents some parametric analysis, following the same designations as the Specimen 10 of the Polytechnic Institute of Bragança studies.

Firstly, it was made a parametric analysis of the effect of the Cavity Insulation Material on the fire resistance, keeping every other variable still. After that, it was made a parametric analysis of the effect of the spacing between studs and lastly a parametric analysis of the effect of the web size in the fire resistance.

7.1. Parametric Analysis of the Cavity Insulation

The parametric analysis of the cavity insulation considers the variation of the material in the cavity insulation of the wall specimen and its densities.

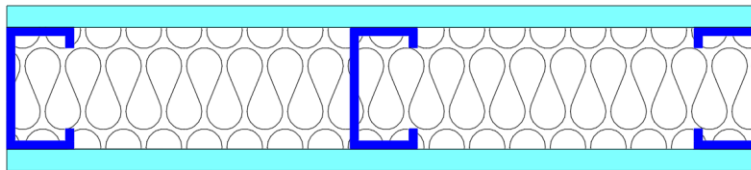


Fig. 30 – Configuration in scale for Spec. 10 used and the variation of the cavity insulation material.

This parametric analysis keeps every dimension fixed in the model according to Specimen 10, with a spacing between studs of 423 mm. The fire resistance was determined for all cases, taking into consideration the insulation criterion (I).

Table 13 – Fire resistance of the wall assemblies used for parametric analysis of the cavity insulation.

Case	Cavity Insulation	Density of Cavity Insulation [kg/m ³]	Fire Res. Simple Method 1 (I) [min]	Fire Res. Simple Method 2 (I) [min]	Fire Res. Advanced Method (I) [min]
1	Rock fibre	75	141	74	76
2	Rock fibre	100	155	78	80
3	Rock fibre	300	>240	106	103
4	Glass fibre	15.42	49	51	51
5	Cellulose fibre	125	75	66	70
6	Superwool	128	>240	84	85
7	Mineral wool	25	>240	76	78

Table 13 presents the results of this parametric analysis. Using method 1, for cases 1, 2, 4 and 5 the relative error is 85.5%, 93.7%, 3.9% and 7.1%, while using method 2, the relative error for every case is 2.6%, 2.5%, 2.9%, 0%, 5.7%, 1.17%, 2.5%, respectively.

7.2. Parametric Analysis of the Spacing Between Studs

This parametric analysis considers different spacing between studs to see their influence in the fire resistance according to the insulation criterion (I) of the LSF non-loadbearing wall. The geometry considered was the same as Specimen 10 from the Polytechnic Institute of Bragança studies and the cavity insulation material chosen was 75 kg/m³ density Rock Fibre.

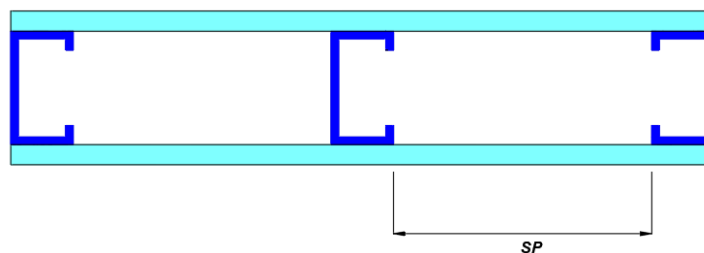


Fig. 31 – Configuration in scale for Spec. 10 used and the variation of the spacing between studs.

It is important to note that to make the spacing between studs larger but not change the configuration of the wall, it was needed to make the wall width also larger. That means that while the spacing between studs grows, also does the wall width.

Table 14 –Fire resistance of the wall assemblies used for parametric analysis of the spacing between studs.

Case	Spacing between studs [mm]	Fire Resistance Simplified Method 1 (I) [min]	Fire Resistance Simplified Method 2 (I) [min]	Advanced Method Fire Resistance (I) [min]
8	400	141	73	76
9	500	141	73	76
10	600	141	68	77
11	700	141	66	77
12	800	141	65	77

Table 14 presents the results of the parametric studies. The relative error for cases 8 and 9 using method 1 is 85.5%, while for cases 10, 11 and 12 the error is 83.1%. Using method 2, the error for cases 8 and 9 is 3.9%, and for cases 10, 11 and 12, it is 11.6%, 14.2% and 15.5%, respectively.

7.3. Parametric Analysis of the Cavity Spacing

This study considers the change in the cavity spacing and, consequently, the web size to analyze the fire resistance according to the insulation criterion (I) in a non-loadbearing LSF wall system.

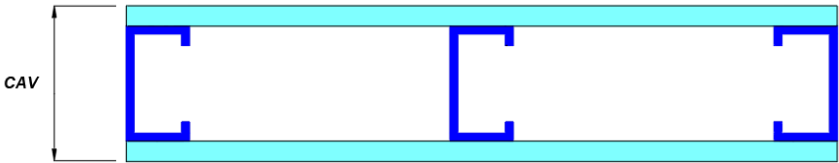


Fig. 32 – Configuration in scale for Spec. 10 used and the variation of the cavity spacing.

The analysis uses the same geometry as Specimen 10 of the Polytechnic Institute of Bragança studies, with a spacing between studs of 423 mm and cavity insulation material as Rock fibre with a density of 75kg/m³.

Table 15 – Characteristics and fire resistance of the wall assemblies used for parametric analysis of the web size.

Case	Web size [mm]	Fire Res. Simple Method 1 (I) [min]	Fire Res. Simple Method 2 (I) [min]	Fire Res. Advanced Method (I) [min]
13	45	78	48	55
14	90	141	73	76
15	120	201	95	93
16	150	>240	123	112
17	240	>240	>240	190

Table 15 presents the fire resistance of both the simplified and advanced method for fire resistance using the insulation criterion (I).

For cases 13, 14 and 15, the relative error between results for the method one are 41.8%, 85.5%, 116.1%, respectively, while for method 2, the relative error are 12.7%, 3.9%, 2.1%, respectively and 9.8% for case 16.

8. Comparison of Results

This section of the study presents the results and comparison of each analysis and both methods proposed for the simple calculation method.

8.1. University of Manchester

In Fig. 33, it is shown the configuration and discrete points of analysis that were gathered by the experimental and numerical data for the results from Feng et al. [15]. The numbers and red points symbolize the placement of the thermocouples.

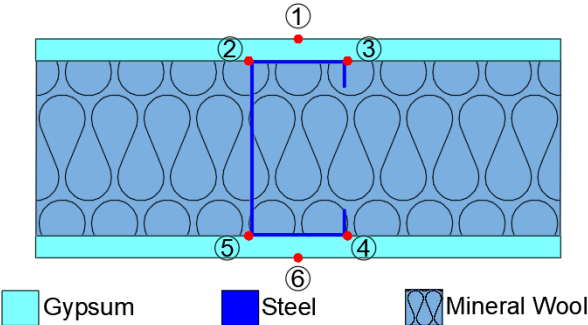


Fig. 33 – Configuration and discrete points of analysis for the University of Manchester

Fig. 34 presents the experimental results in each distinct point, as shown in the graph by “EXP”, the Finite Element model made by Feng et al [15], represented by “FE”, the results from the advanced calculation method made in this study, represented by “ANSYS”, and both of the simple calculation methods proposed, represented by “M1” and “M2”.

Both the advanced and simple calculation methods did not consider the exact same points as the experimental and finite element analysis made by Feng et al. [15], but actually considered a point between P2 and P3 and between P4 and P5. For that reason, in the graph there is two curves considered P2_P3 and P4_P5 which represents the temperature in the middle of those respective flanges.

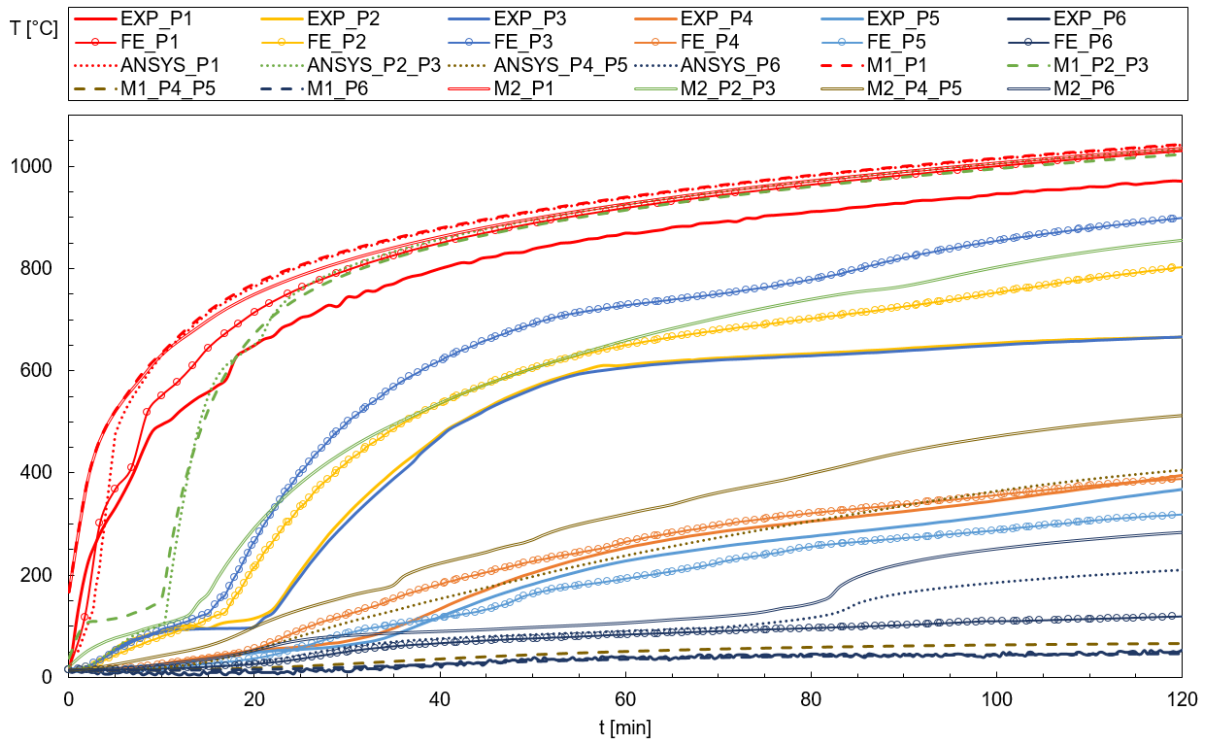


Fig. 34 – Graph of experimental and numerical results for the University of Manchester.

Fig. 35 shows the insulation criterion (I) and curves for the unexposed surface, for every study also presented in Fig. 34. Since this study only considers a wall of dimensions 300 x 300 mm, every temperature is considered the maximum temperature for the unexposed wall. The relative error for the fire resistance according to the insulation criterion (I) of both the simple calculation methods and also the advanced method, when compared to the experimental and the advanced calculation methods are presented in Table 16.

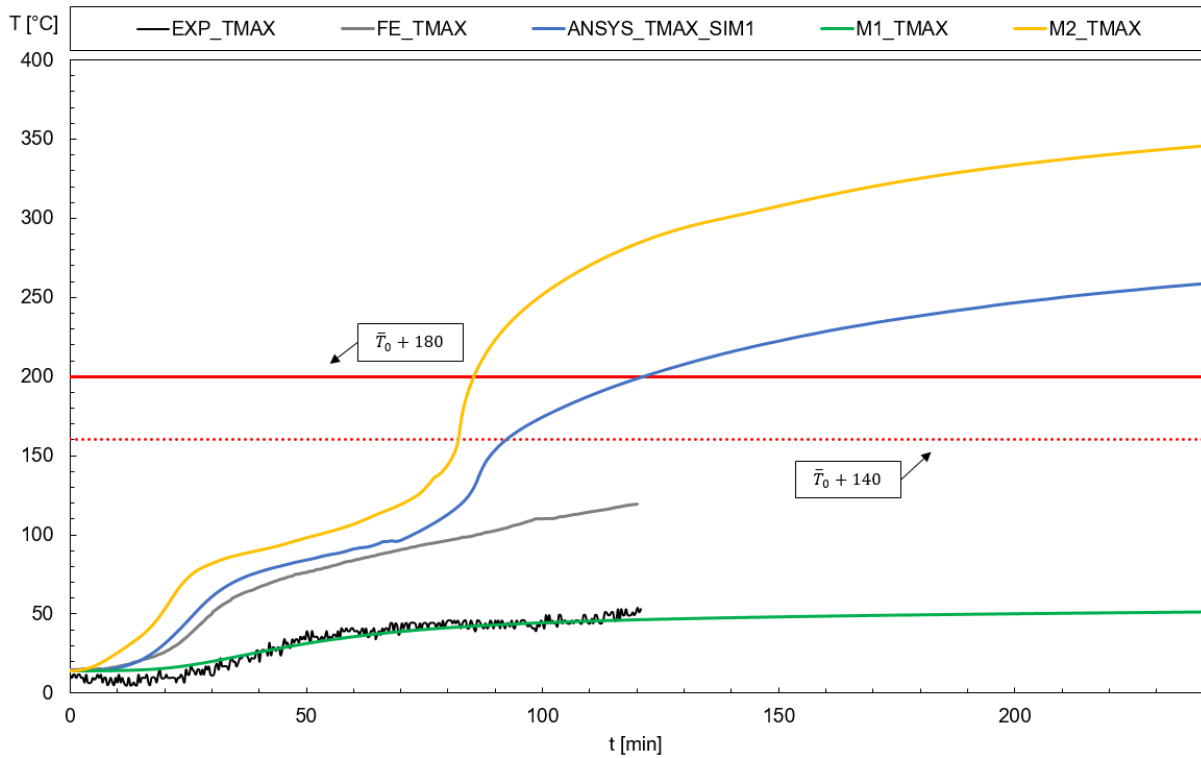


Fig. 35 – Graph of the unexposed wall temperature compared to the insulation criterion (I) for University of Manchester.

Table 16 – Relative error of results by University of Manchester.

	Relative Error Simple Method 1 [%]	Relative Error Simple Method 2 [%]	Relative Error Advanced Method [%]
Exp.	–	–	–
Adv.	–	20	–

8.2. Queensland University of Technology – 1

This study presents the experimental results in each discrete point, for the three different configurations used by Queensland University of Technology – 1, where the difference between each configuration is solely the cavity insulation material. Since the wall configuration and placement of thermocouples are the same for the three specimens analysed, Fig. 36 is a representation of the configuration of the wall and the discrete points used by Kolarkar et al. [39]. The numbers and red points symbolize the placement of the thermocouples.

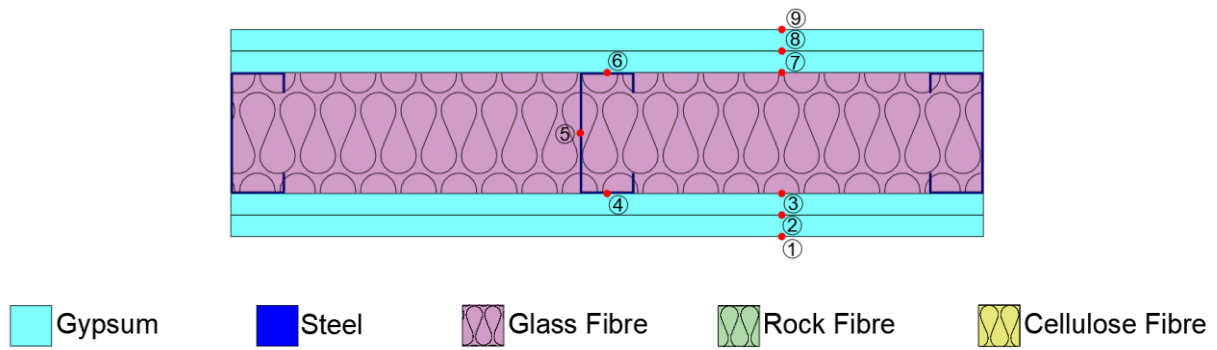


Fig. 36 – Configuration and discrete points of analysis for the Queensland University of Technology – 1.

The graphs for the results of experimental and numerical data for Spec. 4, which is the configuration with glass fibre cavity insulation material, are shown in Fig. 37, followed by the comparison of the curves for the unexposed wall and insulation criterion (I) in Fig. 38. In sequence, Fig. 39 shows the experimental and numerical results for Spec. 5, with rock fibre cavity insulation material, and Fig. 40 shows the comparison of the curves for the unexposed wall and insulation criterion (I). Lastly, Figs. Fig. 41 and Fig. 42 shows the same results for the Spec. 6, with cellulose fibre cavity insulation material.

It was decided to show only the points that were considered more important for the analysis, which in this case are P1, P4, P5, P6 and P9. The names used for the legend of the graph are the same as the ones explained in the University of Manchester.

The graph for the insulation criterion (I) shows the average temperature for the experimental and advanced calculation methods, which is represented by the dotted lines, and the maximum temperature for the advanced and simplified calculation methods, which is represented by the solid lines.

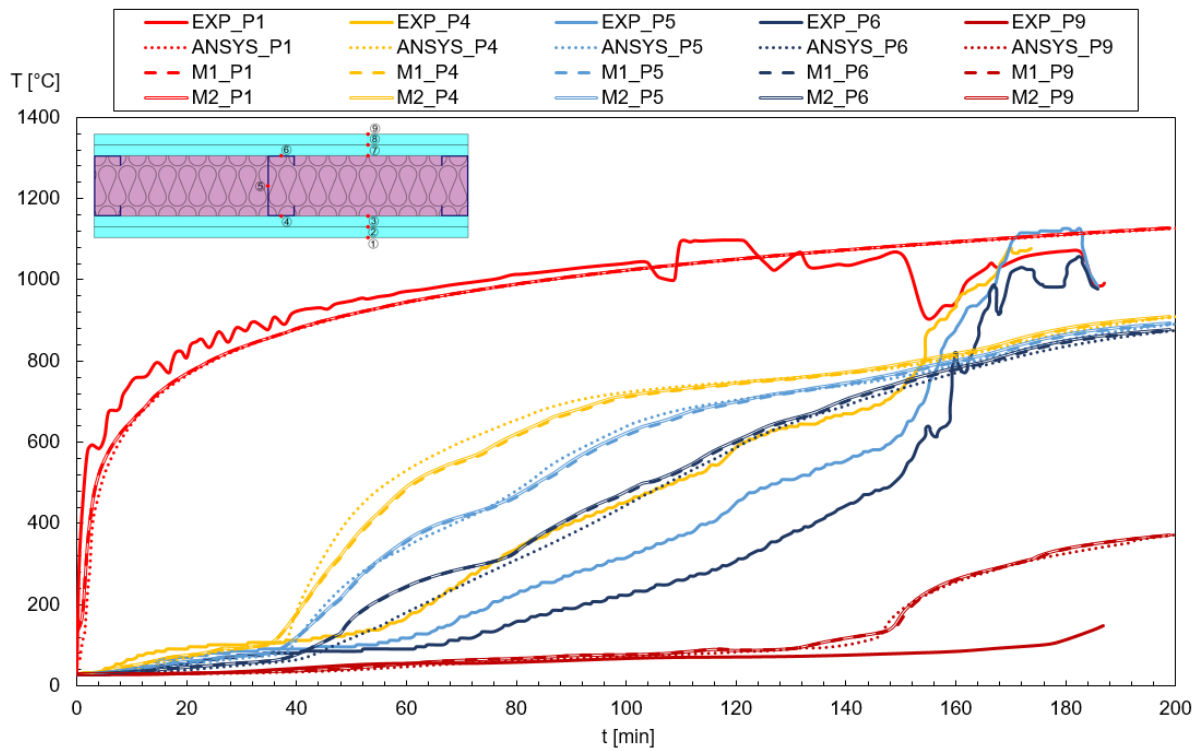


Fig. 37 – Graph of experimental and numerical results for Spec. 4 of Queensland University of Technology – 1.

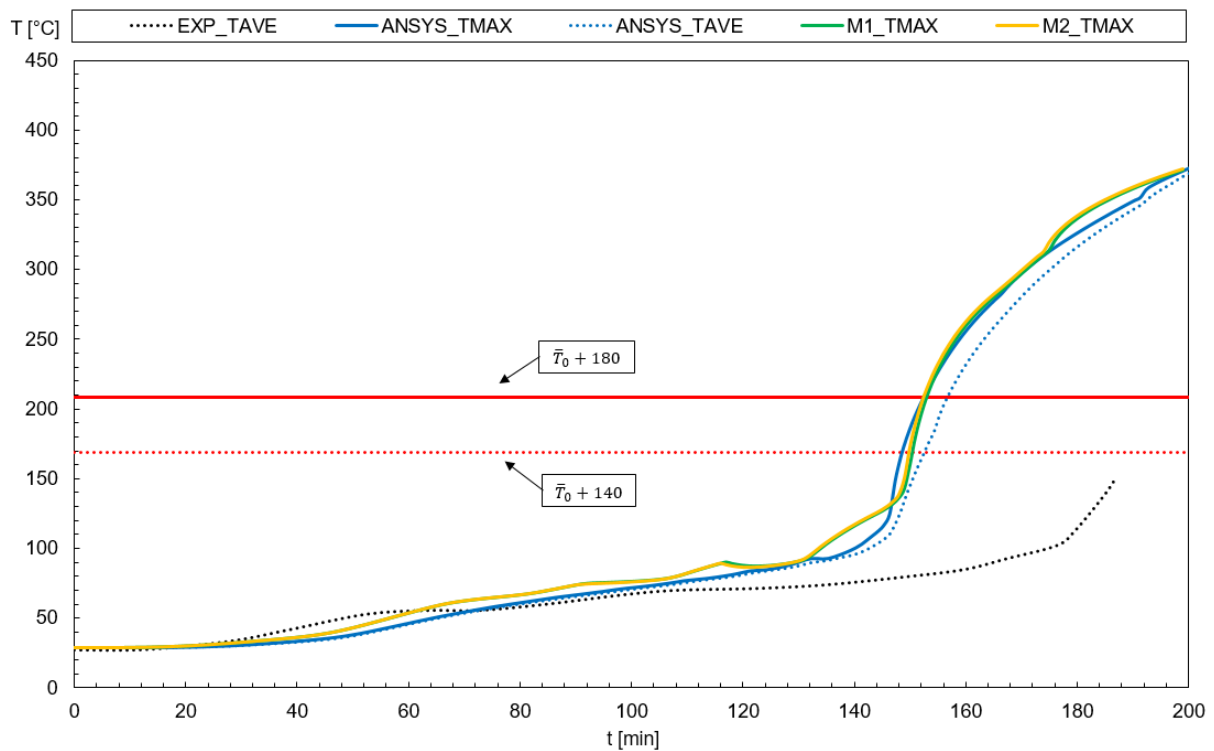


Fig. 38 – Graph of the unexposed wall temperature compared to the insulation criterion (I) for Spec. 4 of Queensland University of Technology – 1.

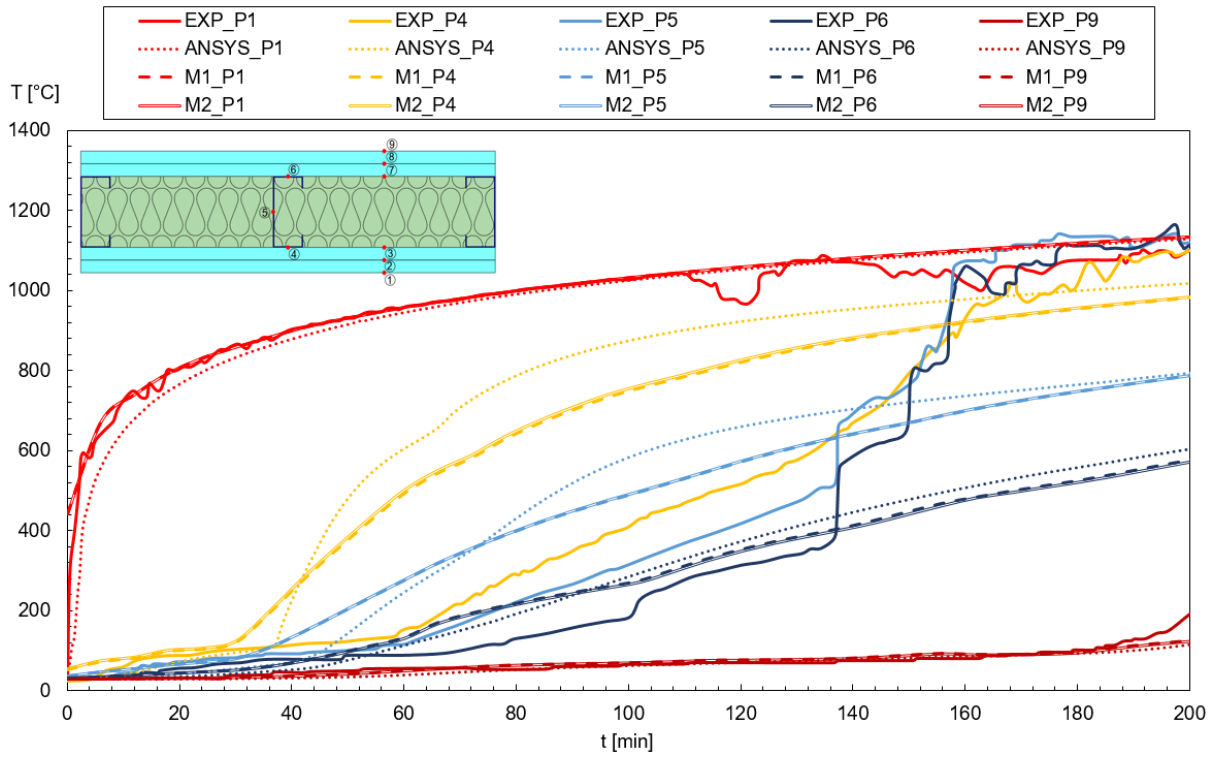


Fig. 39 – Graph of experimental and numerical results for Spec. 5 of Queensland University of Technology – 1.

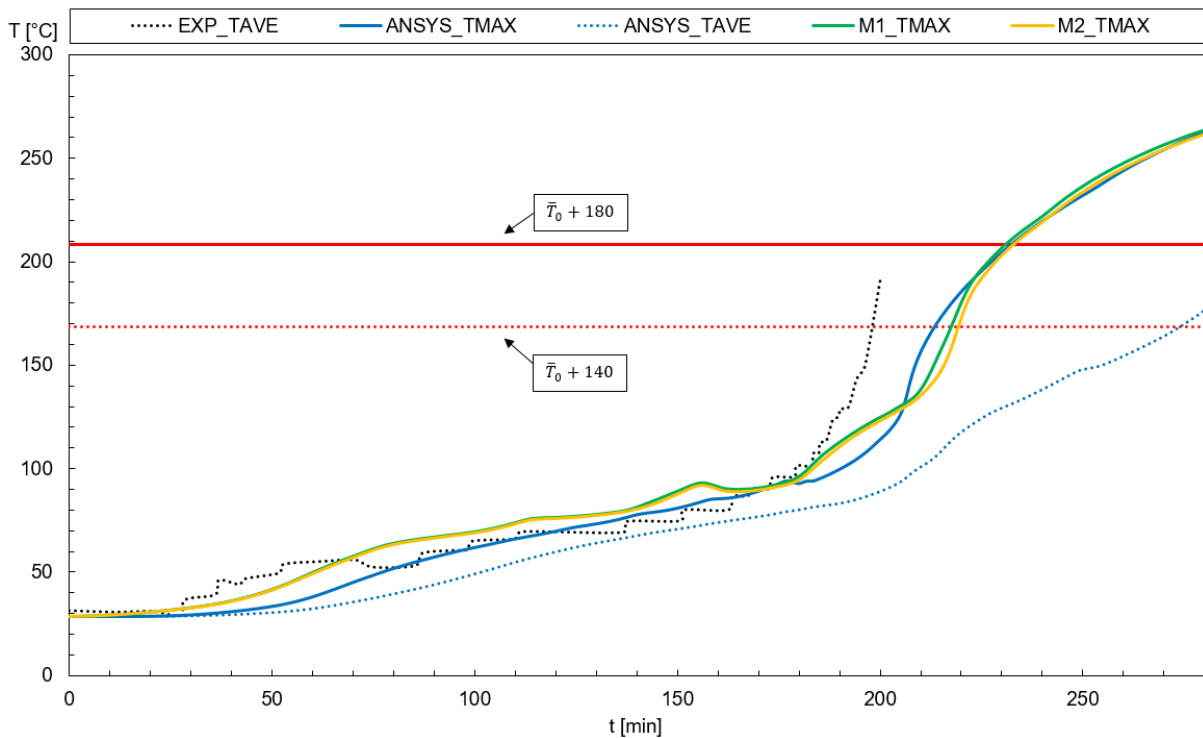


Fig. 40 – Graph of the unexposed wall temperature compared to the insulation criterion (I) for Spec. 5 of Queensland University of Technology – 1.

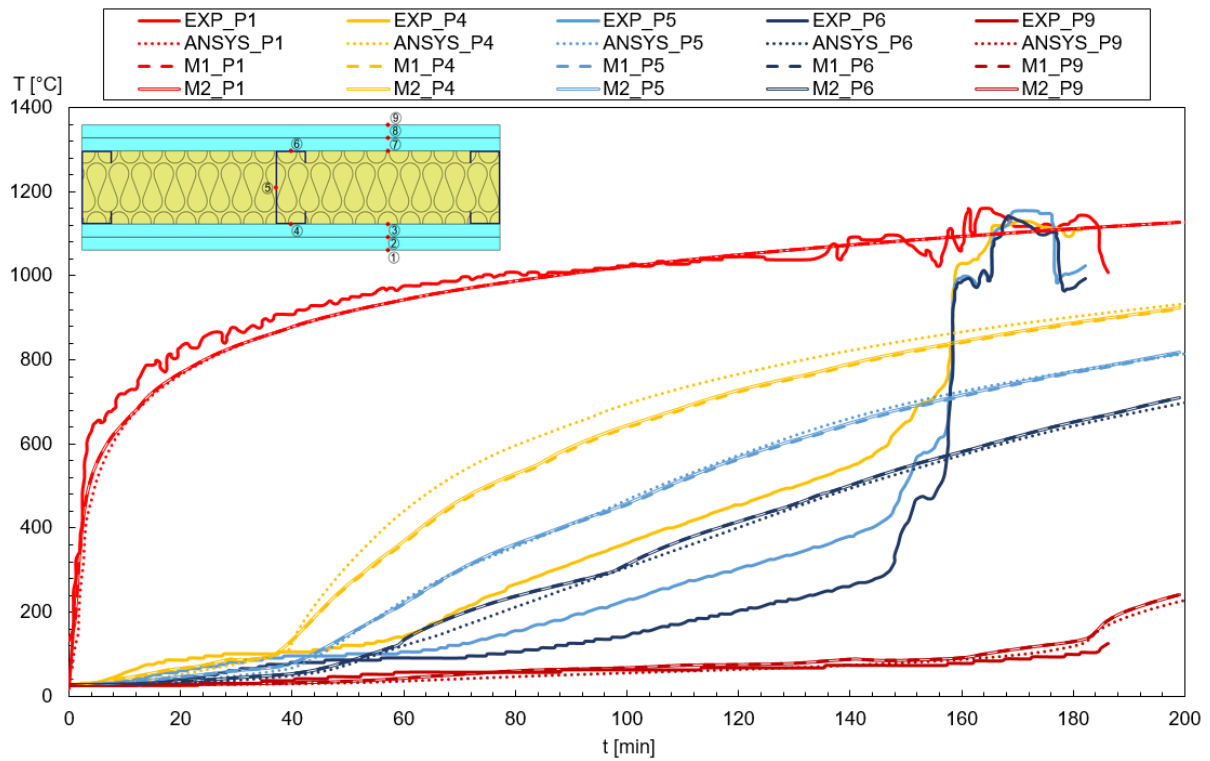


Fig. 41 – Graph of experimental and numerical results for Spec. 6 of Queensland University of Technology – 1.

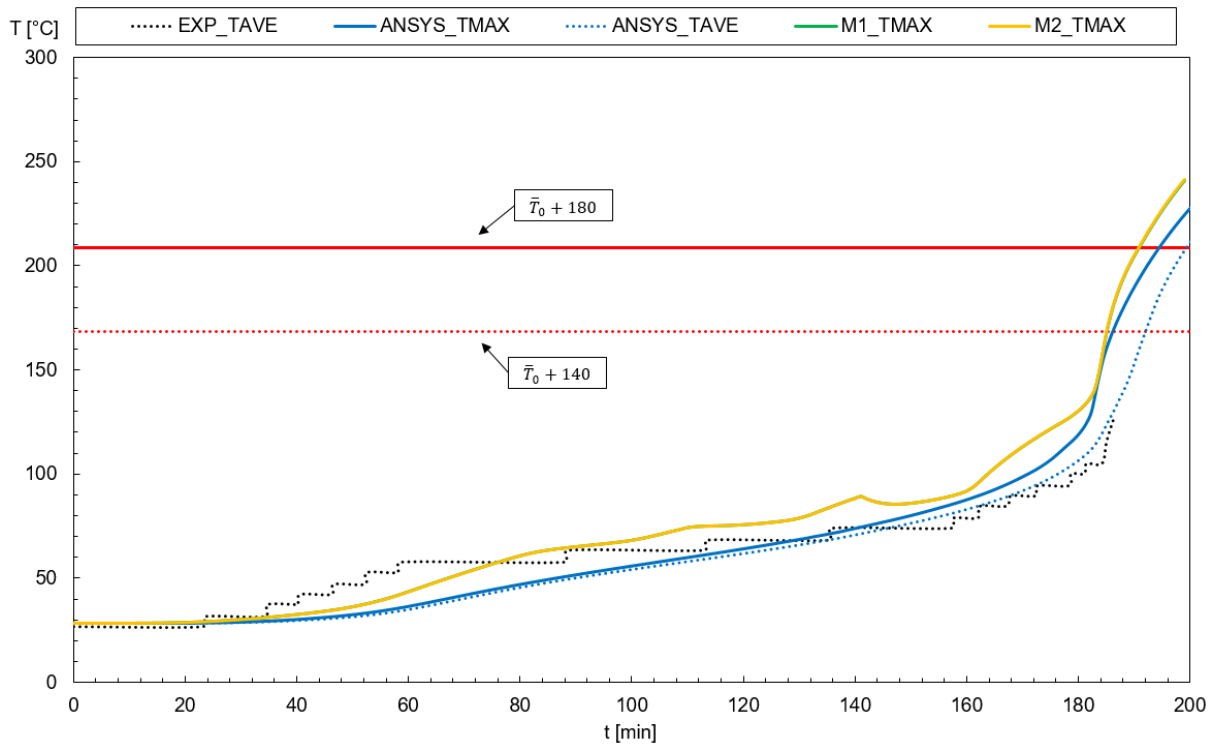


Fig. 42 – Graph of the unexposed wall temperature compared to the insulation criterion (I) for Spec. 6 of Queensland University of Technology – 1.

Table 17 shows the relative error for both of the simplified methods and the advanced method, when compared to the experimental and advanced calculation results. When the curve of reference, which is either the experimental or advanced, does not meet the insulation criterion (I), the relative error cannot be calculated.

Table 17 – Relative error of results by Queensland University of Technology – 1.

	Cavity Insulation	Relative Error Simple Method 1 [%]	Relative Error Simple Method 2 [%]	Relative Error Advanced Method [%]
Exp.	Glass fibre	–	–	–
Exp.	Rock fibre	17.25	15.73	38.58%
Exp.	Cellulose fibre	–	–	–
Adv.	Glass fibre	0.65	0.65	–
Adv.	Rock fibre	0.43	1.73	–
Adv.	Cellulose fibre	2.06	2.58	–

8.3. Queensland University of Technology – 2

The second configuration from Queensland University of Technology is presented by Rusthi et al. [40], where it was made an FE analysis of the experimental research made by Kolarkar [41]. Likewise the Queensland University of Technology – 1, it uses the same wall configuration with changes in the cavity insulation material, using glass fibre for Spec. 3, rock fibre for Spec. 4 and cellulose fibre for Spec. 5. The wall configuration in this study is presented in Fig. 43, where the numbers and red dots represent the thermocouples placements.

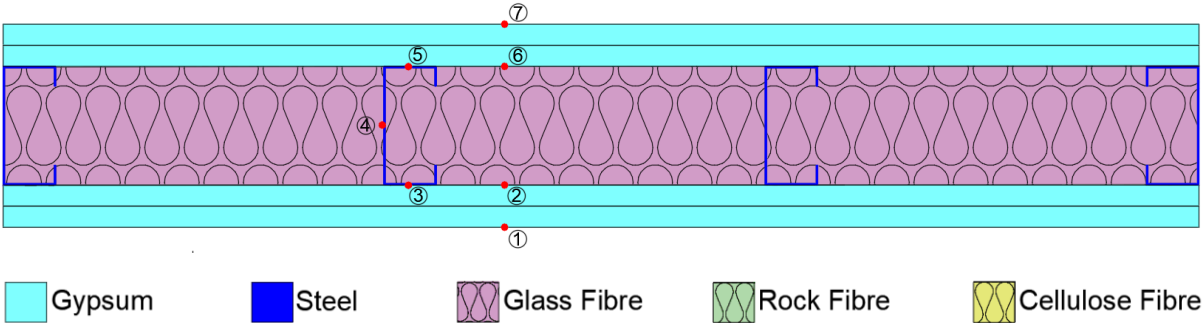


Fig. 43 - Configuration and discrete points of analysis for the Queensland University of Technology – 2.

The graphs for the results of experimental and numerical data for Spec. 3 are shown in Fig. 44 and the comparison of the curves for the unexposed wall and insulation criterion (I) are in Fig. 45. For Spec. 4, the results of experimental and numerical data are in Fig. 46, and Fig. 47 shows the comparison of the curves for the unexposed wall and insulation criterion (I). For Spec. 5, Figs Fig. 48 and Fig. 49 show its results.

The points decided to account for in this analysis are the ones for P1, P3, P4, P5 and P7. The results of the Finite Element model made by Rusthi et al. [40] are represented in the graphs by “FE”. Both experimental e finite element model are considered as average temperatures for the unexposed surface of the wall.

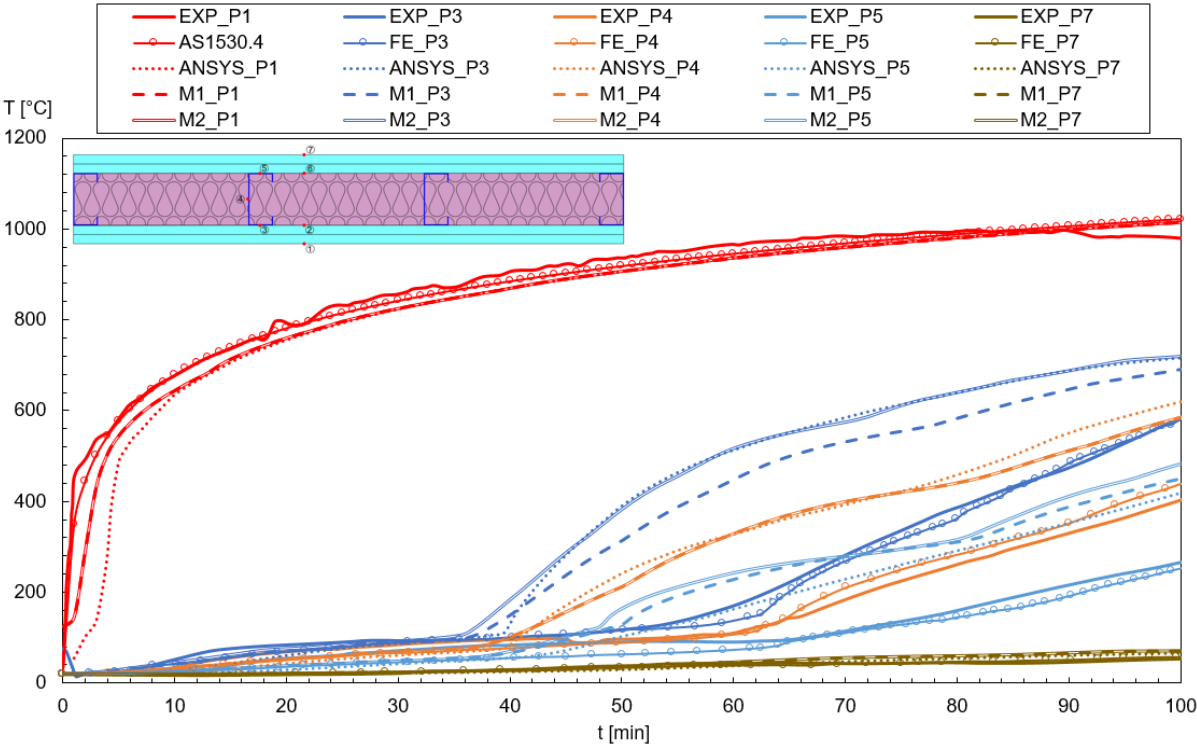


Fig. 44 – Graph of experimental and numerical results for Spec. 3 of Queensland University of Technology – 2.

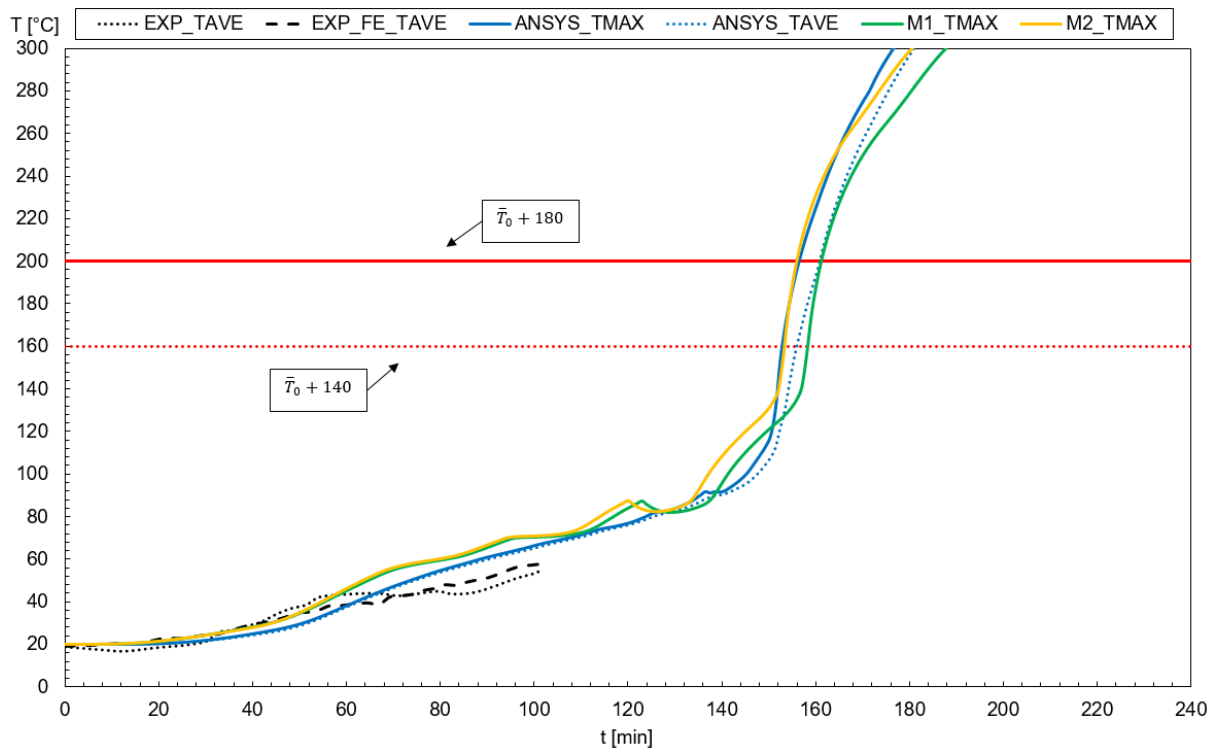


Fig. 45 – Graph of the unexposed wall temperature compared to the insulation criterion (I) for Spec. 3 of Queensland University of Technology – 2.

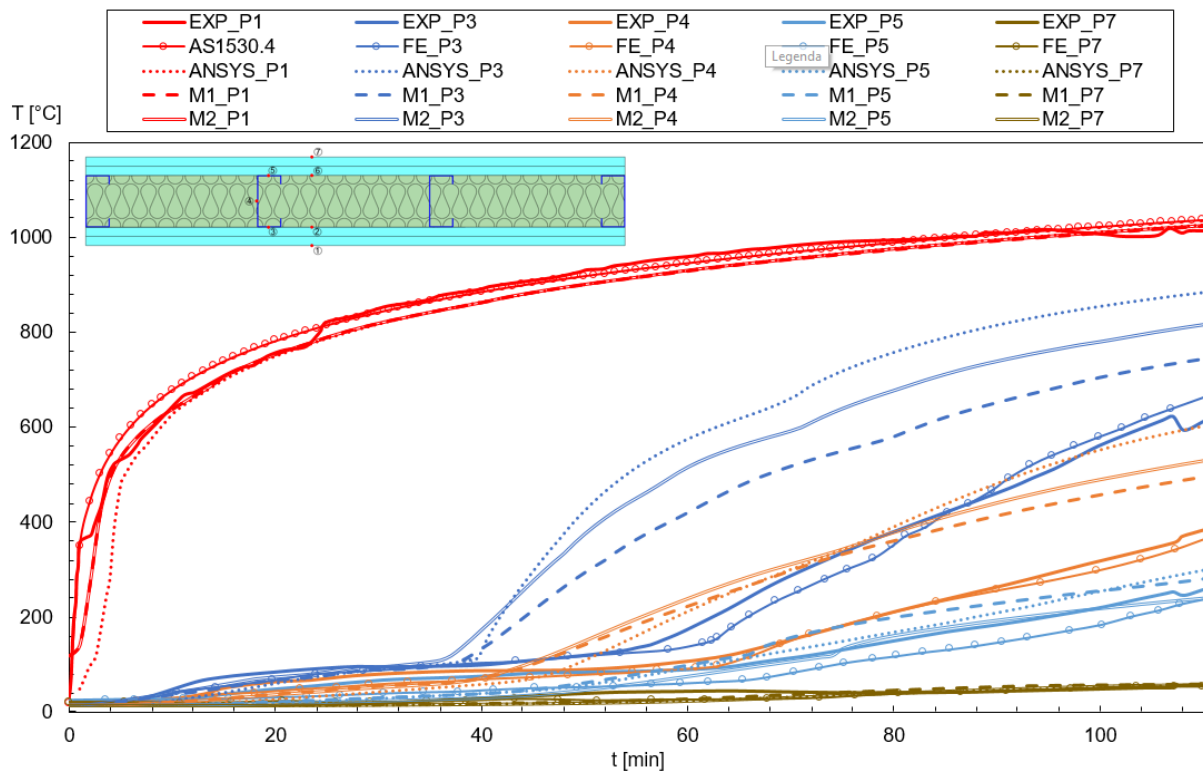


Fig. 46 – Graph of experimental and numerical results for Spec. 4 of Queensland University of Technology – 2.

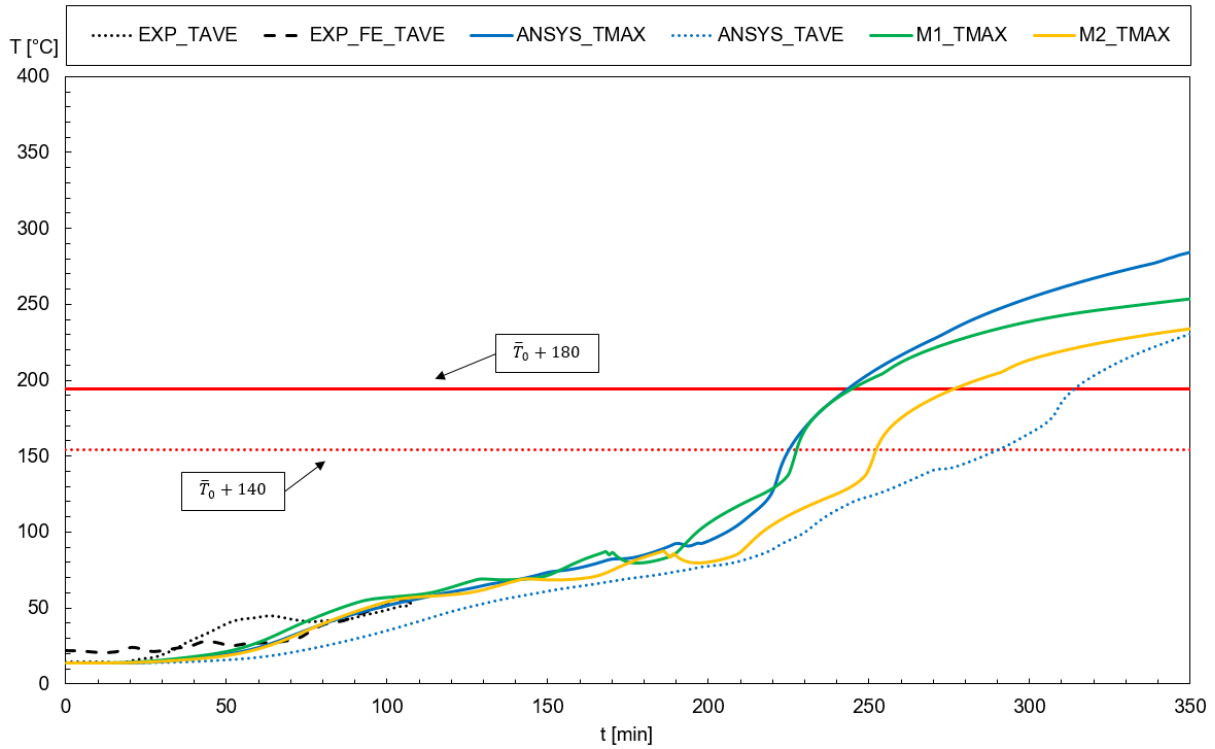


Fig. 47 – Graph of the unexposed wall temperature compared to the insulation criterion (I) for Spec. 4 of Queensland University of Technology – 2.

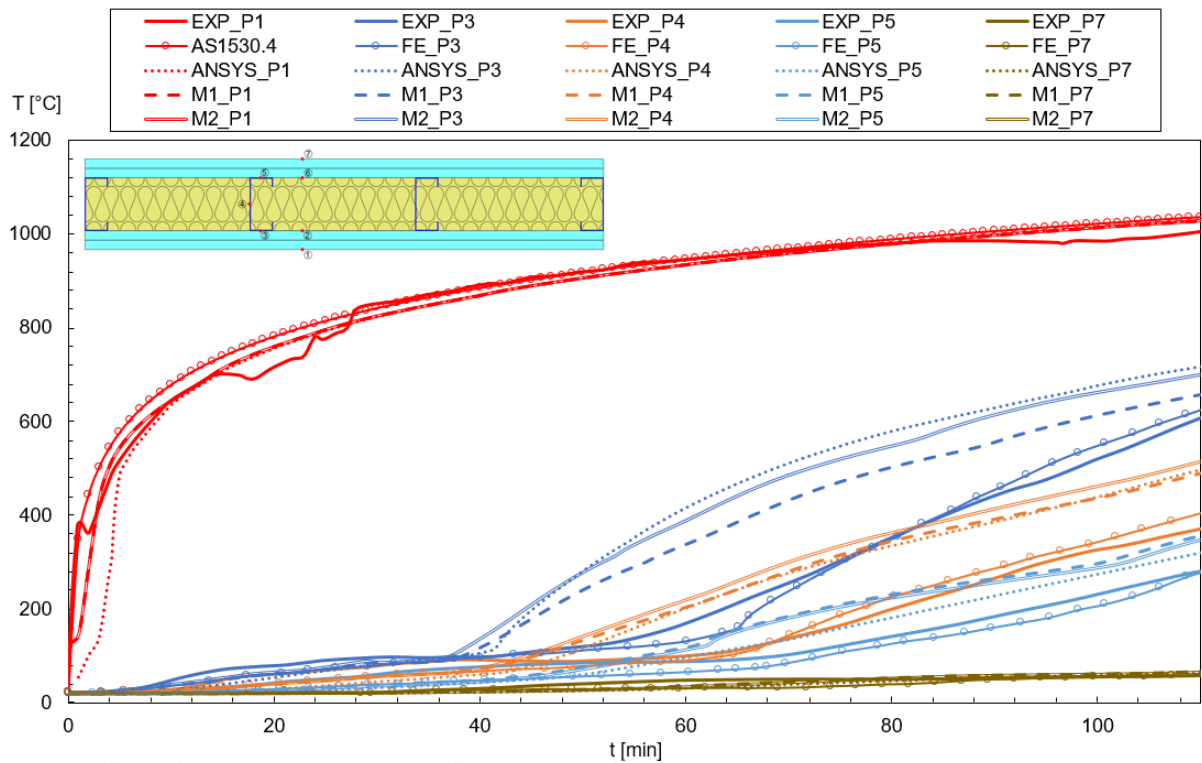


Fig. 48 – Graph of experimental and numerical results for Spec. 5 of Queensland University of Technology – 2.

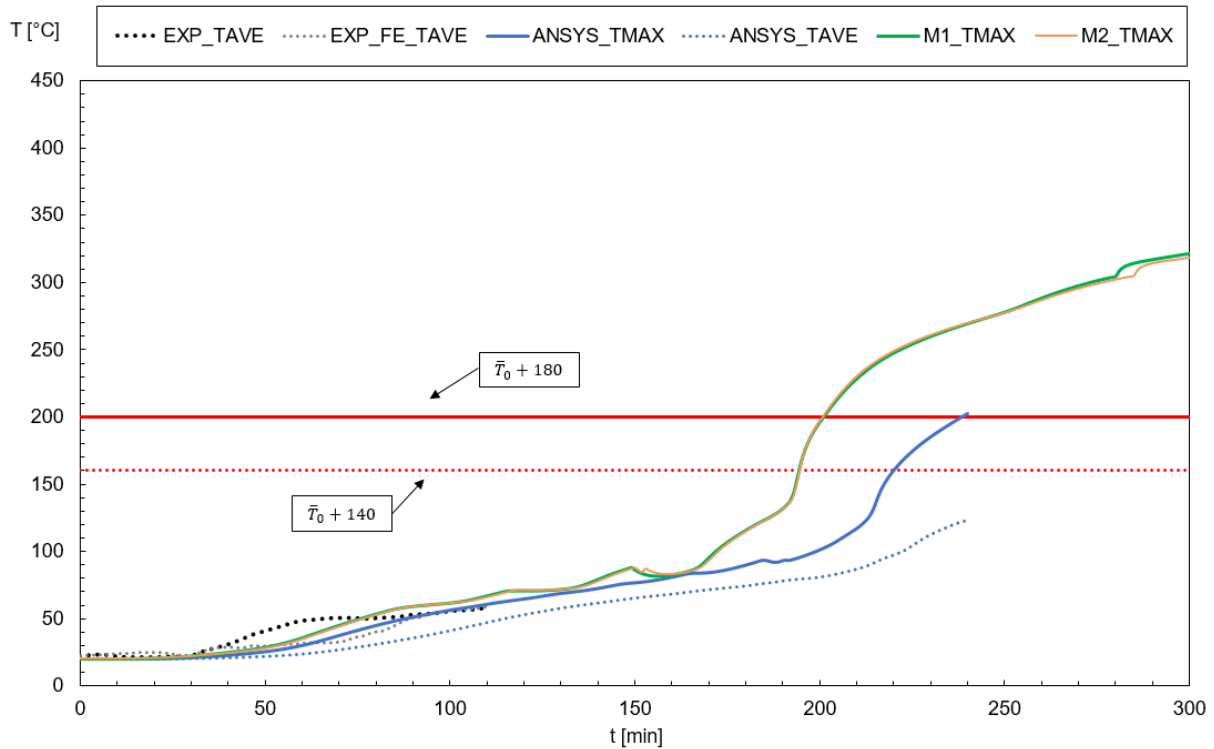


Fig. 49 – Graph of the unexposed wall temperature compared to the insulation criterion (I) for Spec. 5 of Queensland University of Technology – 2.

The relative error is presented in Table 18 for both the simple calculation methods proposed and the advanced calculation method, when compared to the experimental and advanced calculation results. The experimental or finite element model do not meet the insulation criterion (I).

Table 18 - Relative Error of results by Queensland University of Technology – 2.

	Cavity Insulation	Relative Error Simple Method 1 [%]	Relative Error Simple Method 2 [%]	Relative Error Advanced Method [%]
Exp.	Glass fibre	–	–	–
Exp.	Rock fibre	–	–	–
Exp.	Cellulose fibre	–	–	–
Adv.	Glass fibre	3.2	0	–
Adv.	Rock fibre	0.41	16.8	–
Adv.	Cellulose fibre	15.55%	15.55%	–

8.4. Polytechnic Institute of Bragança

For the Polytechnic Institute of Bragança, there are four different wall configurations with the same placement of thermocouples. For that reason, Fig. 50 shows only the

configuration for Spec. 3 and is used as reference for the thermocouple placement of the other configurations.

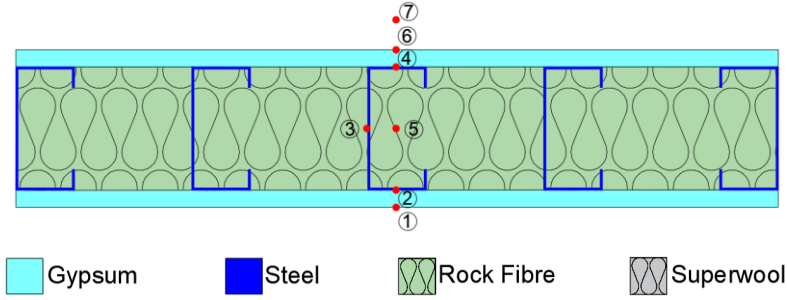


Fig. 50 – Configuration and discrete points of analysis for the Polytechnic Institute of Bragança.

For this analysis, besides the experimental, advanced and simple calculation methods, there is also the Infra-Red (IR), which is data collected from the unexposed wall by an Infra-Red. There is sufficient data to be able to point out maximum and average temperature of the unexposed wall for the experimental and numerical simulations, but the IR data is only considered to be the average because there may be errors in the collection of this data.

The results of Spec. 3 are shown in Figs. Fig. 51 and Fig. 52, for Spec. 10, in Figs. Fig. 53 and Fig. 54. Figs Fig. 55 and Fig. 56 show the results for Spec. 15 and Figs Fig. 57 and Fig. 58, for Spec. 16.

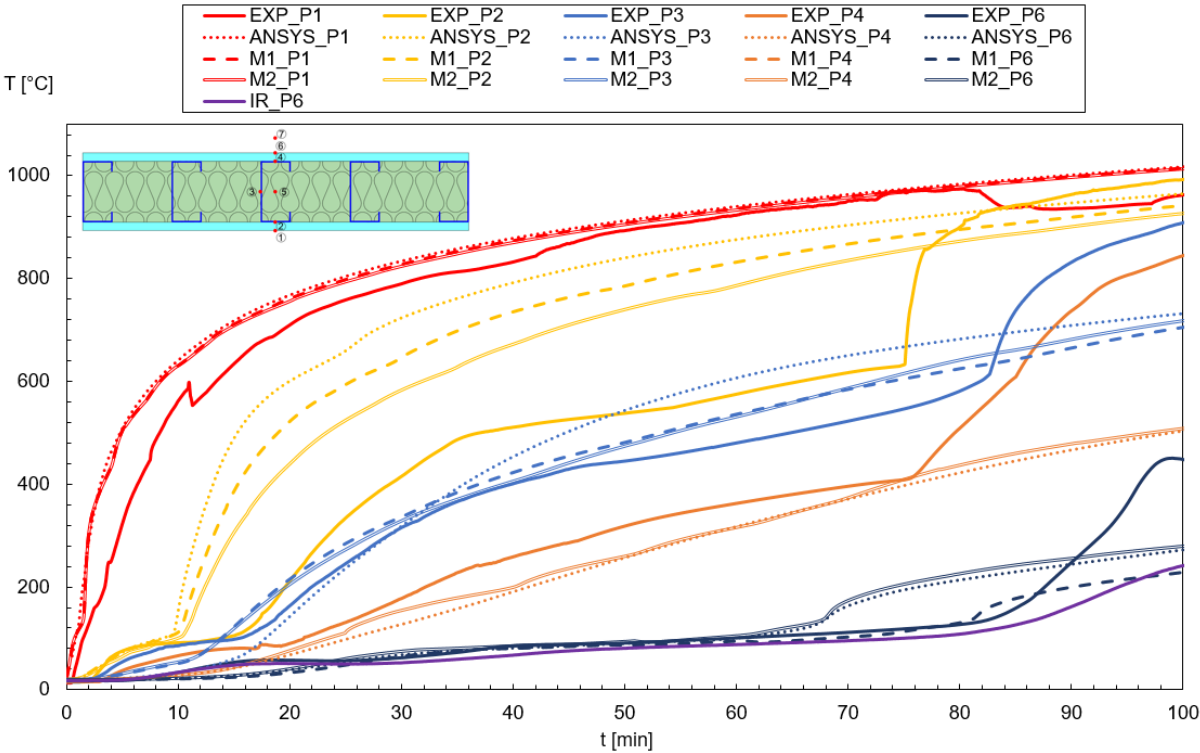


Fig. 51 – Graph of experimental and numerical results for Spec. 3 of Polytechnic Institute of Bragança.

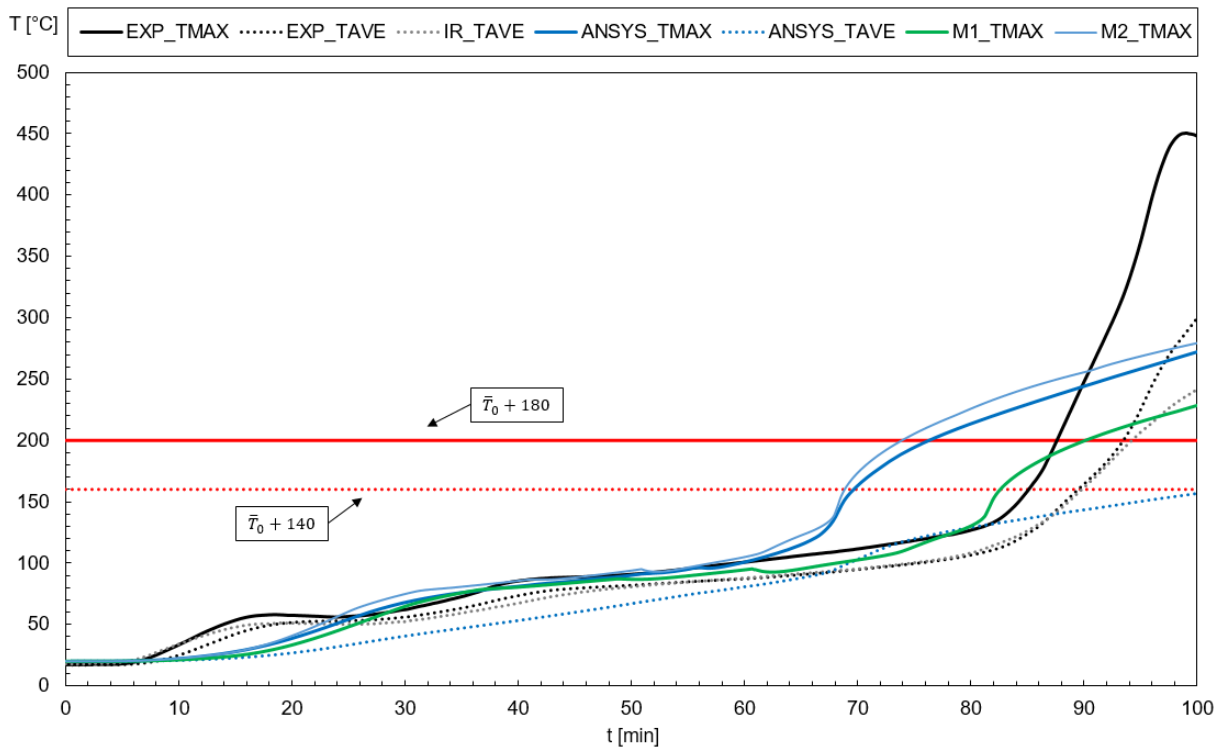


Fig. 52 – Graph of the unexposed wall temperature compared to the insulation criterion (I) for Spec. 3 of Polytechnic Institute of Bragança.

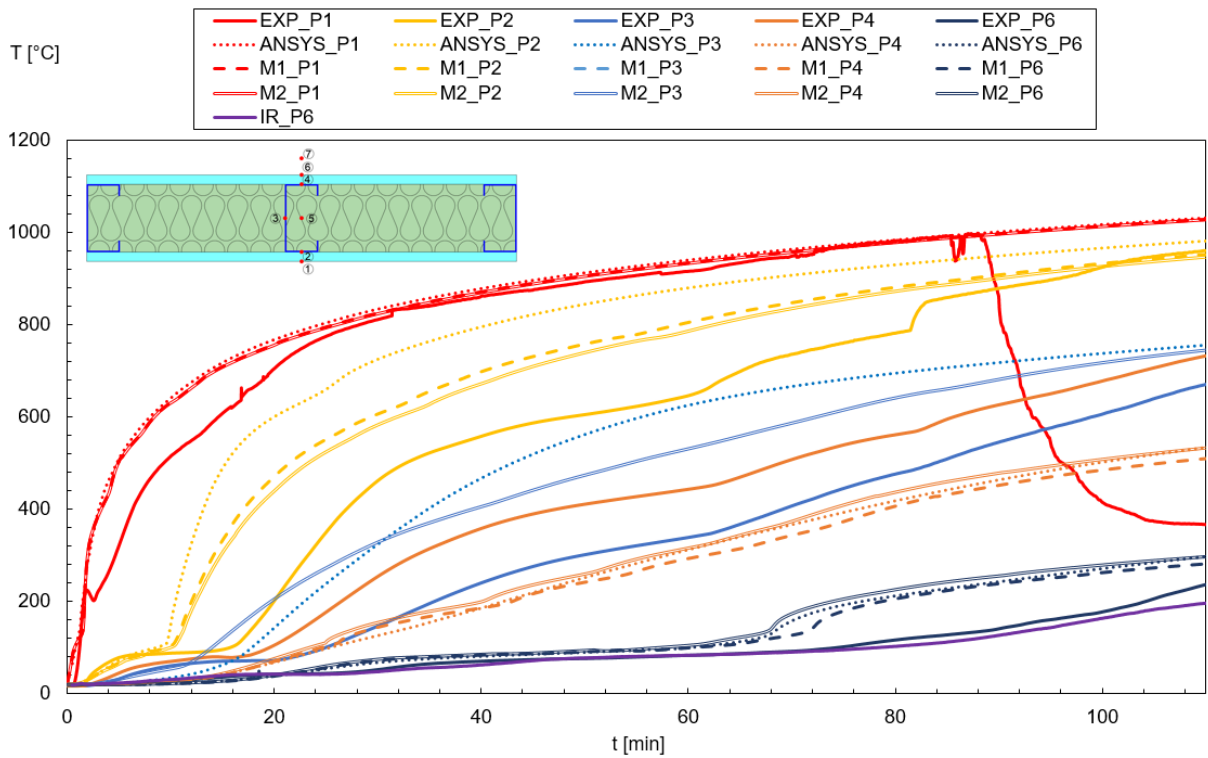


Fig. 53 – Graph of experimental and numerical results for Spec. 10 of Polytechnic Institute of Bragança.

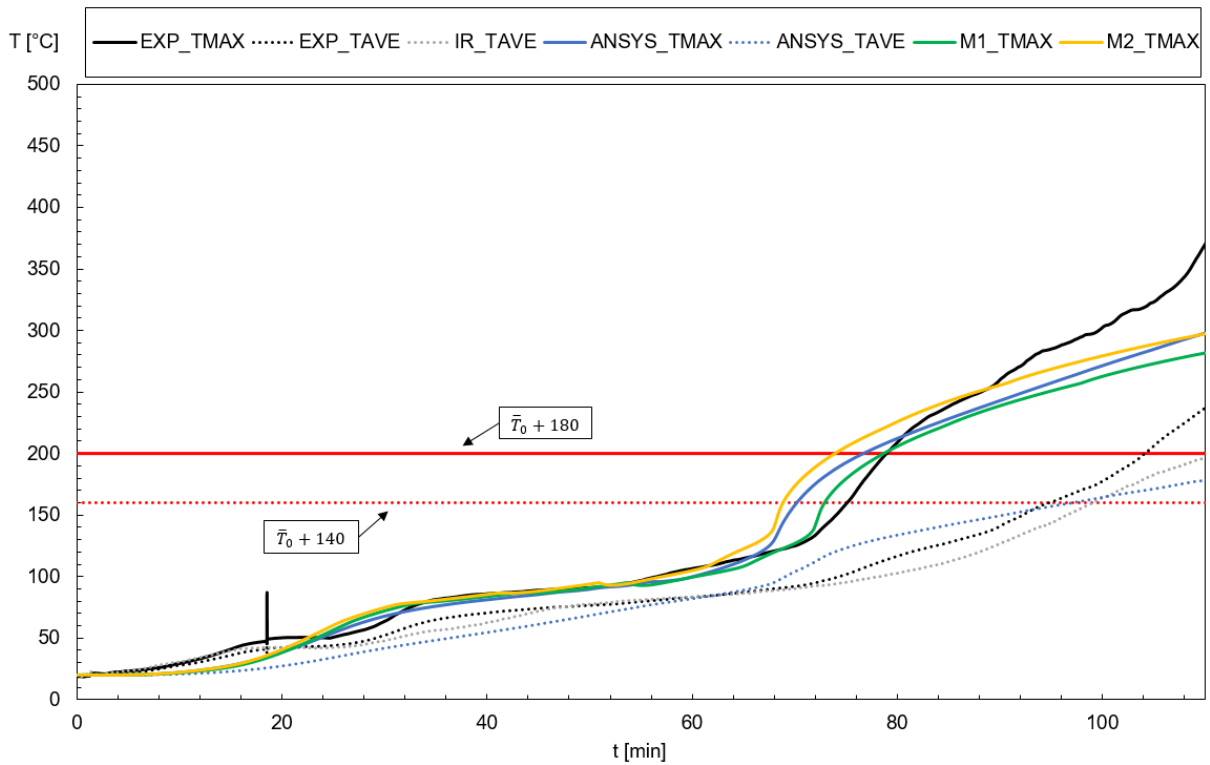


Fig. 54 – Graph of the unexposed wall temperature compared to the insulation criterion (I) for Spec. 10 of Polytechnic Institute of Bragança.

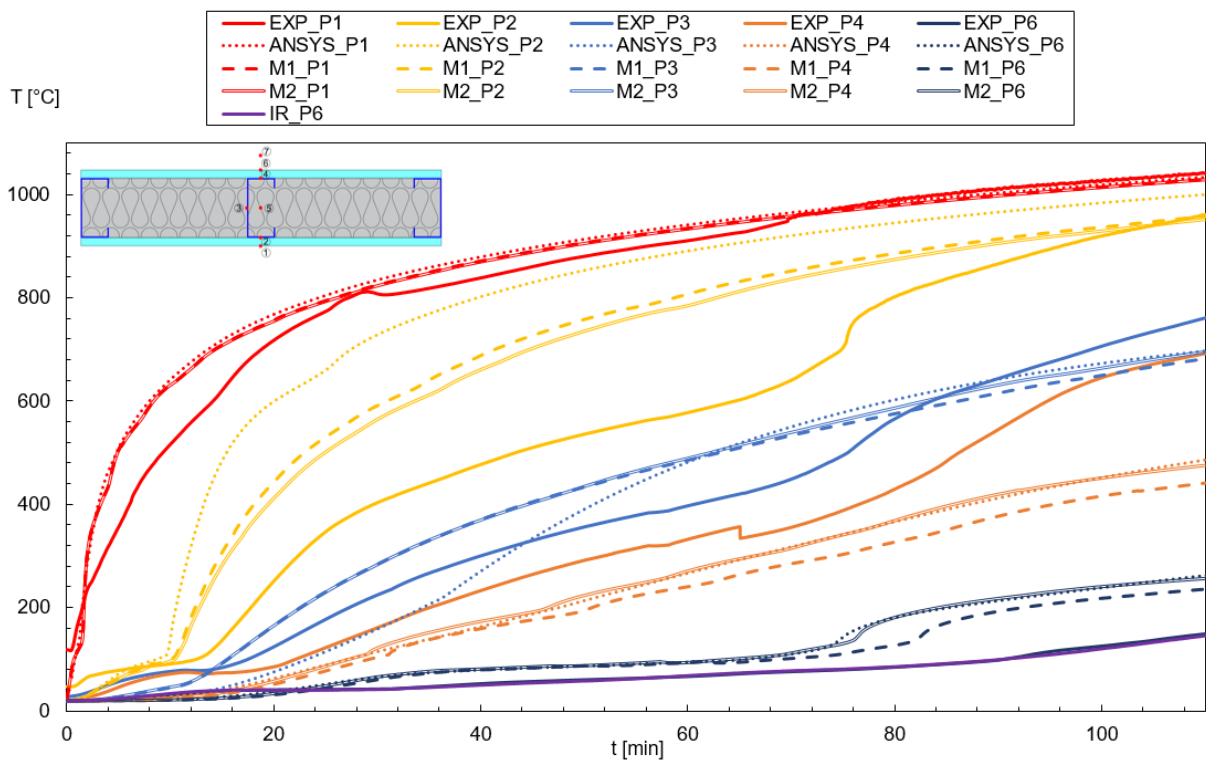


Fig. 55 – Graph of experimental and numerical results for Spec. 15 of Polytechnic Institute of Bragança.

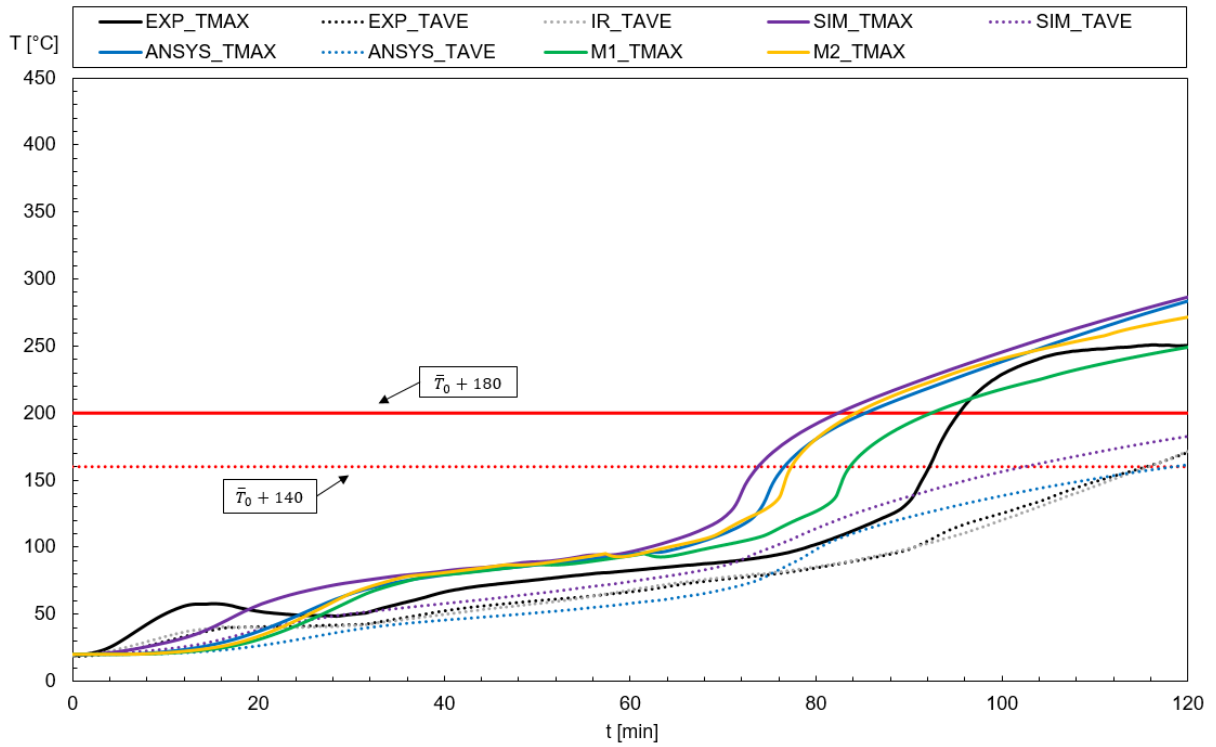


Fig. 56 – Graph of the unexposed wall temperature compared to the insulation criterion (I) for Spec. 15 of Polytechnic Institute of Bragança.

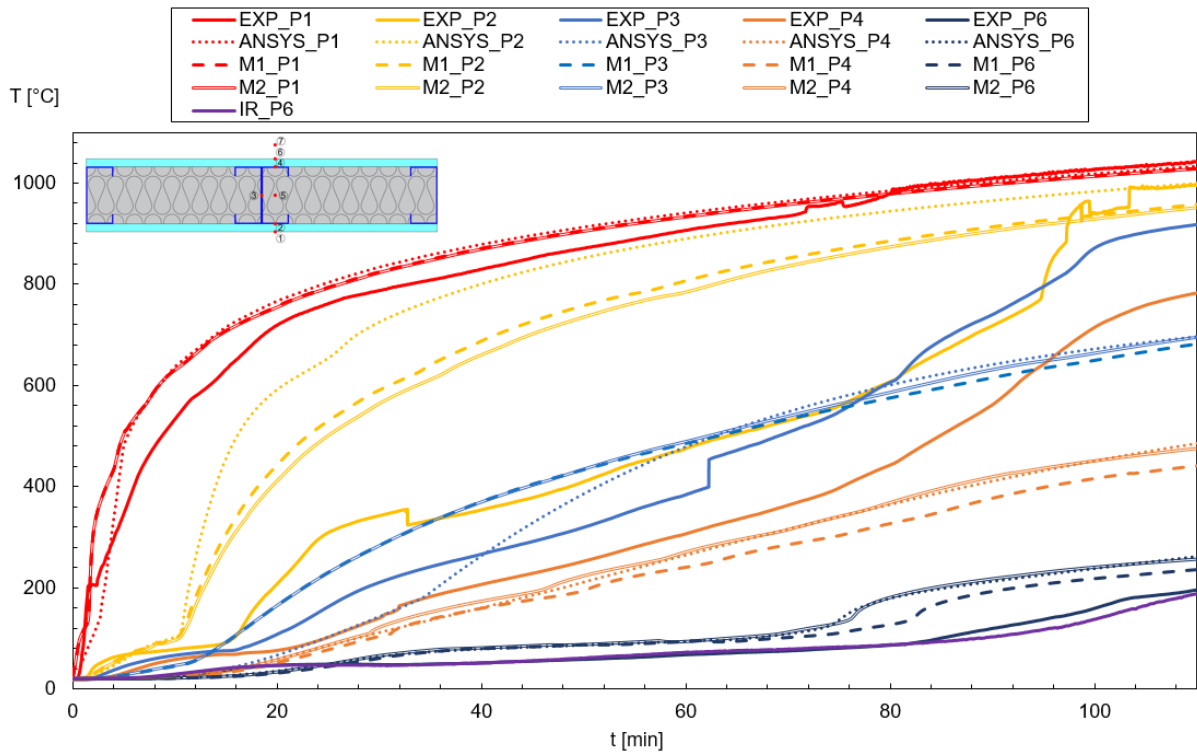


Fig. 57 – Graph of experimental and numerical results for Spec. 16 of Polytechnic Institute of Bragança.

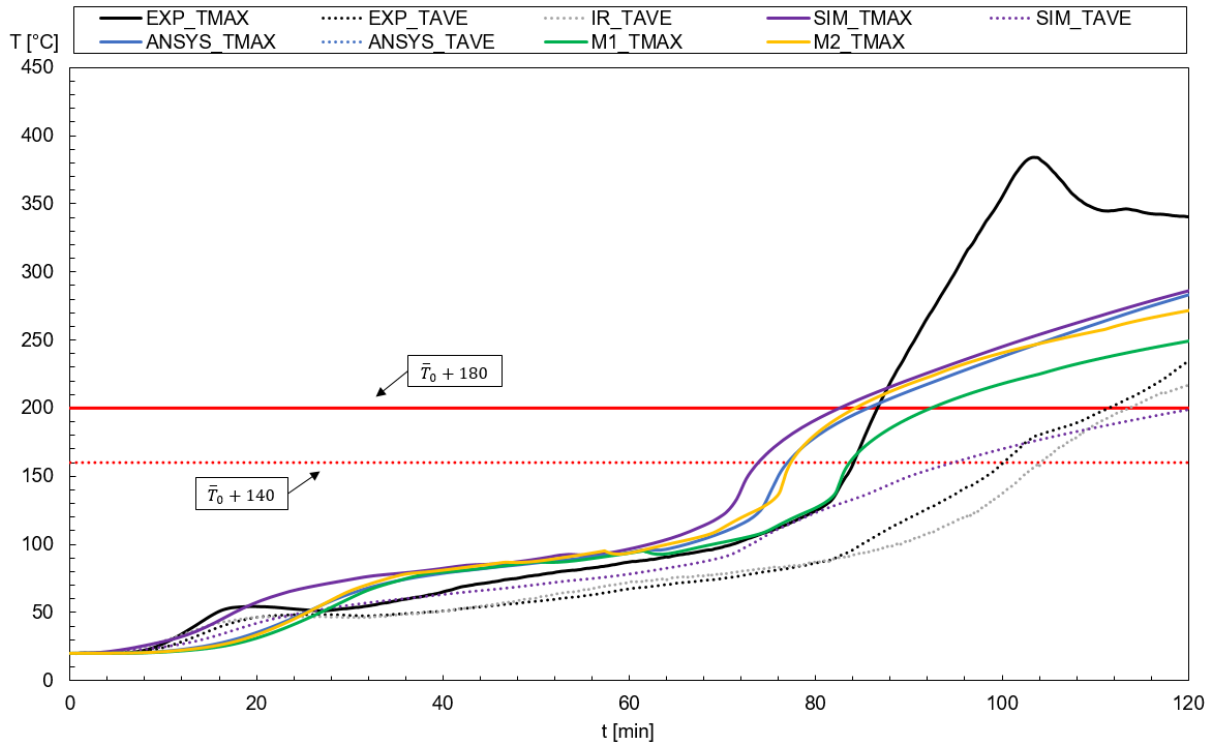


Fig. 58 – Graph of the unexposed wall temperature compared to the insulation criterion (I) for Spec. 16 of Polytechnic Institute of Bragança.

Table 19 shows the relative error of the advanced calculation and methods 1 and 2 when compared to the experimental, IR and advanced calculation values. Since the only results for IR are from the average temperature of the unexposed surface of the wall, it cannot be compared to the simple methods, since those represent the maximum temperature of the unexposed surface of the wall and the error would be greater due to that.

Table 19 – Relative Error of results by Polytechnic Institute of Bragança.

	Spec.	Rel. Error Simple Method 1 [%]	Rel. Error Simple Method 2 [%]	Rel. Error Advanced Method (Ave) [%]
Exp.	3	2.27	15.9	3.03
Exp.	10	1.26	6.32	3.19
Exp.	15	3.15	11.5	2.6
Exp.	16	6.98	2.3	6
IR	3	–	–	13.3
IR	10	–	–	2.02

IR	15	–	–	2.6
IR	16	–	–	1.92
Adv.	3	18.42	2.6	–
Adv.	10	1.29	3.90	–
Adv.	15	8.2	1.2	–
Adv.	16	8.2	1.2	–

8.5. Parametric Studies

For the cavity insulation study, the results for the relative error between both simple calculation methods and the advanced calculation method in the fire resistance time are presented in Table 20. Values that show a dash (–) is because they did not meet the insulation criterion (I) for fire resistance and therefore the relative error cannot be calculated.

Table 20 – Relative error for the cavity insulation material study.

Case.	Rel. Error Simple Method 1 [%]	Rel. Error Simple Method 2 [%]
1	85.5	2.60
2	93.7	2.50
3	–	2.90
4	3.90	0
5	7.10	5.70
6	–	1.17
7	–	2.50

Table 21 presents the relative error for the study in which the spacing between studs was analysed and both of the simple calculation methods proposed were compared to the advanced calculation method.

Table 21 – Relative error for the spacing between studs study.

Case	Rel. Error Simple Method 1 [%]	Rel. Error Simple Method 2 [%]
8	85.5	3.90
9	85.5	3.90
10	83.1	11.60
11	83.1	14.20
12	83.1	15.50

Lastly, Table 22 shows the relative error for both of the simple calculation methods proposed when compared to the advanced calculation method, for the study of the influence of the cavity spacing in the fire resistance time.

Table 22 – Relative error for the cavity spacing study.

Case	Rel. Error Simple Method 1 [%]	Rel. Error Simple Method 2 [%]
13	41.80	12.70
14	85.50	3.90
15	116.10	2.10
16	–	9.80
17	–	–

9. Conclusions and Future Work

This chapter will present both the conclusions of the study made in this work and ideas for future works related to this topic.

9.1. Conclusions

This study had the main objective of proposing a new equation for the effective width considered when analysing the non-loadbearing LSF wall panel in an one-dimensional heat transfer.

In order to achieve this objective, it was necessary to use the minimum and maximum width possible for each configuration and test which width would provide a better approximation compared to either the experimental tests or the advanced method analysis. After finding the best width possible for each case, the cellulose fibre properties were found to be inconsistent with the results, since the best width for each case with the cellulose fibre properties presented in Rusthi [40] and Keerthan [47] would be either the minimum or maximum values possible. Due to this reason, the cellulose fibre studies were disconsidered of the full analysis to find an effective width, along with Specimen 16 of the Polytechnic Institute of Bragança because of its configuration, which is not considered by the equations of heat transfer used in this study.

After proposing two different methods for calculating the effective width, it was time for the validation of these values to see if the equation actually presented a considerable result. The equations were used to predict the effective width (WL) of every wall panel that was analyzed in this study.

The largest error for the Fire Resistance according to the insulation criterion (I) value for method 1 was an error of 18.42% for spec 03 of Polytechnic Institute of Bragança, when comparing to the results of the advanced calculation analysis, while for method 2, the largest error was of 16.8% for the rock fibre cavity insulation of the Queensland University of Technology – 2, when comparing to the results of the advanced calculation analysis.

For the parametric studies, the largest error for method 1 was of 116.1% for case 15, with a web size of 120 mm, while for method 2, it was of 15.5% for case 12 with a spacing between studs of 800 mm.

From the observation of this study, it is clear that the method 1 had a very large error when used in the parametric studies, since it was proposed using results from the experimental tests and the parametric studies used a comparison with the advanced calculation analysis alone. On the other hand, method 2 presented relative error not too high compared to every single analysis, which makes it the most interesting method in this study.

9.2. Future Work

From this presented study, it is possible to understand the need in analysing a few other concepts that were not approached, as follows:

- Study various other configurations both in small scale physical tests and simulation approach, specially for different sizes of spacing between studs and wall width, since the parametric studies of the spacing between studs showed that the fire resistance of those walls did not change if the wall width grew accordingly, which isn't the case for the studies used for validation, since most walls are close to each other in width size;
- Study different materials in the cavity insulation, and propose a different equation for each material for a more controlled outcome;
- Study different panels configurations, e.g. sandwich sheathing wall (gypsum-composite-gypsum configuration);
- Study the effect on changing spacing between studs along with the materials of both cavity insulation and sheathing insulation (as in the sandwich configuration).

10. References

- [1] P. Santos, "Energy Efficiency of Lightweight Steel-Framed Buildings," *Energy Effic. Build.*, no. September, 2017.
- [2] E.L.S.C., "European Lightweight Steel-framed Construction." Arcelor, Belgium, 2004.
- [3] E. Barbour, J. Goodrow, J. Kosny, and J. E. Christian, "Thermal performance of steel-framed walls. Final report," 1994.
- [4] J. Kosny and D. W. Yarbrough, *CRC Handbook of Thermal Engineering / edited by Raj P. Chhabra.*, 2nd ed. 2017.
- [5] A. Amundarain, J. L. Torero, A. Usmani, and A. M. Al-remal, "Light Steel Framing: Improving the Integral Design," *Current*, no. October, pp. 1–8, 2014.
- [6] S. Gunalan, "Structural Behaviour and Design of Cold-formed Steel Wall Systems Under Fire Conditions," no. December, p. 604, 2011.
- [7] N. Soares, P. Santos, and J. J. Costa, "Energy efficiency and thermal performance of lightweight steel-framed (LSF) construction: a review," pp. 1–52, 2017.
- [8] S. Wanniarachchi, "Flexural Behaviour and Design of Cold- formed Steel Beams with Rectangular Hollow Flanges," Queensland University of Technology, 2005.
- [9] A. Chajes, S. J. Britvec, and G. Winter, "Effects of Cold-Straining on Structural Sheet Steels," *J. Struct. Div.*, vol. 89, pp. 1–32, 1963.
- [10] K. J. Schwartz and T. T. Lie, "Investigating the unexposed surface temperature criteria of standard ASTM E119," *Fire Technol.*, vol. 21, no. 3, pp. 169–180, 1985.
- [11] J. R. Mehaffey, P. Cuerrier, and G. Carisse, "A model for predicting heat transfer through gypsum-board/wood-stud walls exposed to fire," *Fire Mater.*, vol. 18, no. 5, pp. 297–305, 1994.
- [12] A. McGowan and A. O. Desjarlais, "A Comparison of Thermal Bridging Calculation Methods," *Therm. Envel. VI*, pp. 241–246, 1995.
- [13] M. A. Sultan and G. D. Loughheed, "The effect of insulation on the fire resistance of small-scale gypsum board wall," in *Proceedings of the Third International Conference on Fire and Materials*, 1994, pp. 11–20.
- [14] M. A. Sultan, "Effect of insulation in the wall cavity on the fire resistance rating

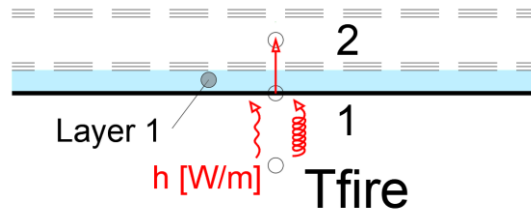
- of full-scale asymmetrical (1x2) gypsum board protected wall assemblies,” *Proc. Int. Conf. Fire Res. Eng.*, no. January 2010, pp. 545–550, 1995.
- [15] M. Feng, Y. C. Wang, and J. M. Davies, “Thermal performance of cold-formed thin-walled steel panel systems in fire,” *Fire Saf. J.*, vol. 38, no. 4, pp. 365–394, 2003.
- [16] J. Kosny and D. W. Yarbrough, “Effects of Framing on the Thermal Performance of Wood and Steel-Framed Walls,” in *Proceedings of the Fifteenth Symposium on Improving Building Systems in Hot and Humid Climates*, 2006.
- [17] P. N. Kolarkar and M. Mahendran, “Thermal Performance of Plasterboard Lined Steel Stud Walls,” in *19th International Specialty Conference : Recent Research and Developments in Cold-Formed Steel Structures*, 2008, pp. 517–530.
- [18] Y. A. Cengel, *Heat Transfer: A Practical Approach*, 2nd editio. Mcgraw-Hill (Tx), 2002.
- [19] R. and A.-C. E. American Society of Heating, *ASHRAE Fundamentals Handbook (SI)*. American Society of Heating, Refrigerating and Air-Conditioning Engineers, 2001, 2001.
- [20] W. Strzepek, “Thermal Resistances of Metal Frame Wall Constructions Incorporating Various Combinations of Insulating Materials,” *Insul. Mater. Test. Appl.*, vol. ed. D. McE, pp. 362–377, 1990.
- [21] ISO 6946, “Building components and building elements: Thermal resistance and thermal transmittance – Calculation method,” 2015.
- [22] P. V. Real, *Incêndio em estruturas metálicas: Cálculo estrutural*, Orion. 2003.
- [23] F. P. Incropera, T. L. Bergman, A. S. Lavine, and D. P. DeWitt, *Fundamentals of Heat and Mass Transfer*, 6th editio., vol. 13. 2008.
- [24] Y. A. Çengel, *Heat transfer: A practical approach*, 2nd Editio. New York : McGraw-Hill, 2004, 2004.
- [25] Q. V. Truong, T. H. Pham, and T. B. Chu, “Failure of building structural members during the cooling phase of a fire,” *Lect. Notes Mech. Eng.*, vol. PartF3, pp. 65–77, 2018.
- [26] L. A. de S. F. Silva, “Fire Resistance Of Non-Loadbearing LSF Walls,” no. February, p. 88, 2018.
- [27] C. N. Costa and V. P. Silva, “Revisão histórica das curvas padronizadas de incêndio,” *Nutau - USP*, no. 2, 2006.
- [28] E. 1991-1-2, “Eurocode 1: Actions on structures - Part 1-2: General actios -

- actions on structures exposed to fire,” *Brussels Eur. Comm. Stand.*, 2002.
- [29] ISO 834-1, “Fire-Resistance Tests - Elements of Building Construction - Part 1: General Requirements,” *Tech. Comm. ISO/TC 92*, no. September, 1999.
- [30] B. 476 Part 20, “Fire tests on building materials and structures - Part 20: Method for determination of the fire resistance of elements of construction (general principles).” 1987.
- [31] AS 1530.4, “Methods for Fire Tests on Buildings Materials, Components and Structures, Part. 4: Fire Resistance Tests of Elements of Building Construction,” *Stand. Aust.*, 2005.
- [32] E. 1363-1, “Fire Resistance Tests - part 1: General Requirements,” *Eur. Comm. Stand.*, no. July, p. 52, 2012.
- [33] E. 1364-1, “Fire Resistance Tests for Non-load Bearing Elements. Part 1: Walls,” *Eur. Comm. Stand.*, no. July, p. 66, 2015.
- [34] M. Feng, Y. C. Wang, and J. M. Davies, “Axial strength of cold-formed thin-walled steel channels under non-uniform temperatures in fire,” *Fire Saf. J.*, vol. 38, no. 8, pp. 679–707, 2003.
- [35] A. Shahbazian and Y. C. Wang, “Calculating the global buckling resistance of thin-walled steel members with uniform and non-uniform elevated temperatures under axial compression,” *Thin-Walled Struct.*, vol. 49, no. 11, pp. 1415–1428, 2011.
- [36] A. Shahbazian and Y. C. Wang, “A simplified approach for calculating temperatures in axially loaded cold-formed thin-walled steel studs in wall panel assemblies exposed to fire from one side,” *Thin-Walled Struct.*, vol. 64, pp. 60–72, 2013.
- [37] P. A. G. Piloto, M. S. Khetata, and A. B. R. Gavilán, “Fire Performance of Non-Loadbearing Light Steel Framing Walls – Numerical and Simple Calculation Methods,” *MATTER Int. J. Sci. Technol.*, vol. 3, no. 3, pp. 13–23, 2017.
- [38] M. A. Sultan, “A model for predicting heat transfer through noninsulated unloaded steel-stud gypsum board wall assemblies exposed to fire,” *Fire Technol.*, vol. 32, no. 3, pp. 239–257, 1996.
- [39] P. Kolarkar and M. Mahendran, “Experimental studies of non-load bearing steel wall systems under fire conditions,” *Fire Saf. J.*, vol. 53, pp. 85–104, 2012.
- [40] M. Rusthi, P. Keerthan, A. Ariyanayagam, and M. Mahendran, “Numerical studies of gypsum plasterboard and MgO board lined LSF walls exposed to fire,”

- no. Kolarkar 2010, pp. 1077–1084, 2016.
- [41] P. N. Kolarkar, “Structural and Thermal Performance of Cold-formed Steel Stud Wall Systems Under Fire Conditions,” Queensland University of Technology, 2010.
- [42] S. M. Khetata, P. A. G. Piloto, and A. B. R. Gavilán, “Non-loadbearing light steel framing walls under fire,” in *5th Iberian-Latin-American Congress on Fire Safety - CILASCI 5*, 2019, pp. 169–185.
- [43] S. M. Khetata, P. A. G. Piloto, and A. B. R. Gavilán, “Fire Resistance of Composite Non-loadbearing Light Steel Framing Walls,” *Submitt. to J. Fire Sci.*, 2019.
- [44] P. A. G. Piloto, “Light Steel Framed Walls made with Composite Panels Under Fire Conditions,” in *Proceedings of the 6th Conference on Urban Fire Safety and 1st Civil Protection Conference*, 2018, pp. 103–123.
- [45] E. 1993-1-2, “Eurocode 3: Design of Steel Structures. Part 1-2: General Rules - Structural Fire Design,” *Eur. Comm. Stand.*, vol. 1, no. April, 2005.
- [46] S. Lundberg, H. A. Structures, and Karmoy, “Material Aspects of Fire Design,” *TALAT Lect. 2502*, no. November, pp. 1–21, 1997.
- [47] P. Keerthan and M. Mahendran, “Thermal Performance of Composite Panels Under Fire Conditions Using Numerical Studies: Plasterboards, Rockwool, Glass Fibre and Cellulose Insulations,” *Fire Technol.*, vol. 49, no. 2, pp. 329–356, 2013.
- [48] T. Ceramics, “Data sheet: Superwool blanket,” *Morgan Adv. Mater.*, pp. 3–5, 2016.
- [49] T. Ceramics, “Data sheet: Superwool Plus,” *Morgan Adv. Mater.*, pp. 29–34, 2016.

A. Appendix – Detailed Heat Balance Equations

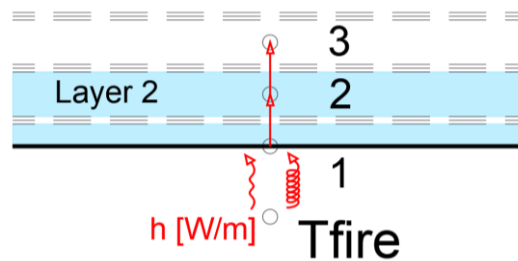
• Layer 1



$$\dot{Q}_1 - \dot{Q}_{COND1,2} = \dot{Q}_{CAP1}$$

$$\alpha[T_{fire} - T_1]WL + \varepsilon_f \varepsilon_G \sigma [T_{fire}^4 - T_1^4]WL - \frac{\lambda_G}{\left(\frac{TG}{4}\right)} [T_1 - T_2]WL = \rho_G C p_G WL \left(\frac{TG}{8}\right) \frac{[T_1 - T_1^{i-1}]}{\Delta t}$$

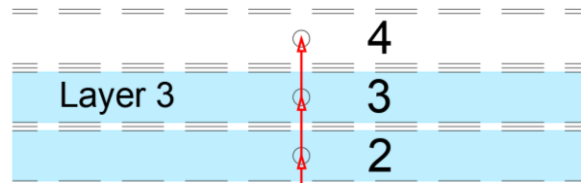
• Layer 2



$$\dot{Q}_{COND1,2} - \dot{Q}_{COND2,3} = \dot{Q}_{CAP2}$$

$$\frac{\lambda_G}{\left(\frac{TG}{4}\right)} [T_1 - T_2]WL - \frac{\lambda_G}{\left(\frac{TG}{4}\right)} [T_2 - T_3]WL = \rho_G C p_G WL \left(\frac{TG}{4}\right) \frac{[T_2 - T_2^{i-1}]}{\Delta t}$$

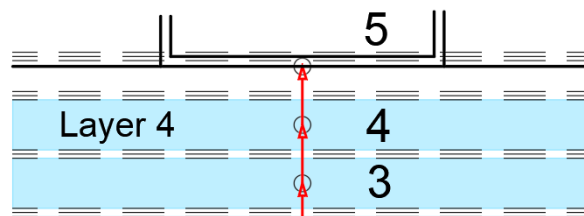
- Layer 3



$$\dot{Q}_{COND2,3} - \dot{Q}_{COND3,4} = \dot{Q}_{CAP3}$$

$$\left(\frac{\lambda_G}{4}\right) [T_2 - T_3] WL - \left(\frac{\lambda_G}{4}\right) [T_3 - T_4] WL = \rho_G C p_G WL \left(\frac{TG}{4}\right) \frac{[T_3 - T_3^{i-1}]}{\Delta t}$$

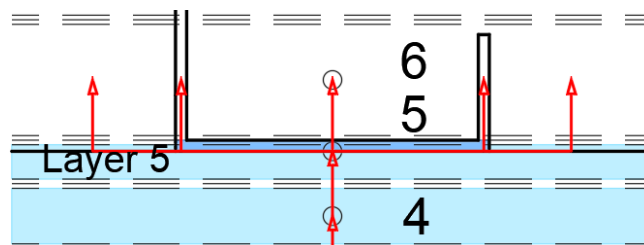
- Layer 4



$$\dot{Q}_{COND3,4} - \dot{Q}_{COND4,5} = \dot{Q}_{CAP4}$$

$$\left(\frac{\lambda_G}{4}\right) [T_3 - T_4] WL - \left(\frac{\lambda_G}{4}\right) [T_4 - T_5] WL = \rho_G C p_G WL \left(\frac{TG}{4}\right) \frac{[T_4 - T_4^{i-1}]}{\Delta t}$$

- Layer 5



$$\dot{Q}_{COND4,5} - \dot{Q}_{COND5,6} = \dot{Q}_{CAP5}$$

$$\frac{\lambda_G}{\left(\frac{TG}{4}\right)} [T_4 - T_5] WL - \frac{T_5 - T_6}{R_{COND5,6}} = \frac{T_5 - T_5^{i-1}}{R_{CAP5}}$$

$$R_{COND5,6} = \frac{1}{\frac{1}{R_{i-1}_{5,6}} + \frac{1}{R_{s-1}_{5,6}} + \frac{1}{R_{s-2}_{5,6} + R_{i-2}_{5,6}} + \frac{1}{R_{s-3}_{5,6}} + \frac{1}{R_{i-3}_{5,6}}}$$

$$R_{CAP5} = R_G + \frac{1}{\frac{1}{R_{i-1}_5} + \frac{1}{R_{s-1}_5} + \frac{1}{R_{i-2}_5}}$$

R for conduction

$$R_{i-1}_{5,6} = \frac{\text{thick}}{\text{cond} \cdot \text{width}} = \frac{TS + \frac{BL - TS}{2}}{\lambda_i \cdot TI}$$

$$R_{s-1}_{5,6} = \frac{TS + \frac{BL - TS}{2}}{\lambda_s \cdot TS}$$

$$R_{s-2}_{5,6} = \frac{TS}{\lambda_s (BF - 2TS)}$$

$$R_{i-2}_{5,6} = \frac{\frac{BL - TS}{2}}{\lambda_i (BF - 2TS)}$$

$$R_{s-3}_{5,6} = \frac{TS + \left(\frac{BL - TS}{2}\right)}{\lambda_s \cdot TS}$$

$$R_{i-3}_{5,6} = \frac{TS + \frac{BL - TS}{2}}{\lambda_i \cdot BI}$$

R for capacity

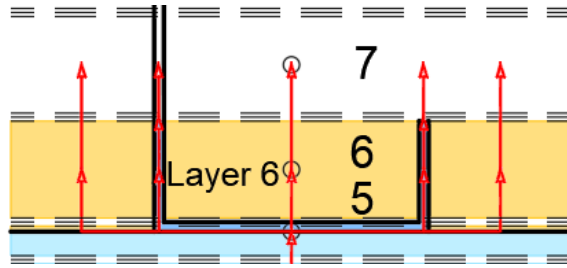
$$R_G = \frac{\Delta t}{\rho_G C p_G \left(\frac{TG}{8}\right) WL}$$

$$R_{i-1}_5 = \frac{\Delta t}{\rho_i C p_i TS \cdot TI}$$

$$R_{s-1}_5 = \frac{\Delta t}{\rho_s C p_s TS \cdot BF}$$

$$R_{i-2}_5 = \frac{\Delta t}{\rho_i C p_i TS \cdot BI}$$

- Layer 6



$$\dot{Q}_{COND5,6} - \dot{Q}_{COND6,7} = \dot{Q}_{CAP6}$$

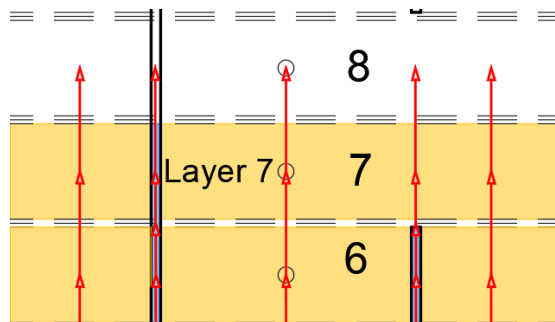
$$\frac{T_5 - T_6}{R_{COND5,6}} - \frac{T_6 - T_7}{R_{COND6,7}} = \frac{T_6 - T_6^{i-1}}{R_{CAP6}}$$

$$R_{COND6,7} = \frac{1}{\frac{1}{R_{i-1,6,7}} + \frac{1}{R_{s-1,6,7}} + \frac{1}{R_{i-2,6,7}} + \frac{1}{R_{s-2,6,7} + R_{i-3,6,7}} + \frac{1}{R_{i-4,6,7}}}$$

$$R_{CAP6} = \frac{1}{\frac{1}{R_{i-1,6}} + \frac{1}{R_{s-1,6}} + \frac{1}{R_{i-2,6}} + \frac{1}{R_{s-2,6}} + \frac{1}{R_{i-3,6}}}$$

R for conduction	R for capacity
$R_{i-1,6,7} = \frac{\frac{BW - 2BL}{4} + \frac{BL - TS}{2}}{\lambda_i \cdot TI} = \frac{\frac{BW}{4} - \frac{TS}{2}}{\lambda_i \cdot TI}$	$R_{i-1,6} = \frac{\Delta t}{\rho_i C p_i (BL - TS) \cdot TI}$
$R_{s-1,6,7} = \frac{\frac{BW}{4} - \frac{TS}{2}}{\lambda_s \cdot TS}$	$R_{s-1,6} = \frac{\Delta t}{\rho_s C p_s (BL - TS) \cdot TS}$
$R_{i-2,6,7} = \frac{\frac{BW}{4} - \frac{TS}{2}}{\lambda_i \cdot TS}$	$R_{i-2,6} = \frac{\Delta t}{\rho_i C p_i (BL - TS)(BF - 2TS)}$
$R_{s-2,6,7} = \frac{\frac{BL - TS}{2}}{\lambda_s \cdot TS}$	$R_{s-2,6} = \frac{\Delta t}{\rho_s C p_s (BL - TS) \cdot TS}$
$R_{i-3,6,7} = \frac{BW - 2BL}{4 \lambda_i \cdot TS}$	$R_{i-3,6} = \frac{\Delta t}{\rho_i C p_i (BL - TS) \cdot BI}$
$R_{i-4,6,7} = \frac{\frac{BW}{4} - \frac{TS}{2}}{\lambda_i \cdot BI}$	

- **Layer 7**



$$\dot{Q}_{COND6,7} - \dot{Q}_{COND7,8} = \dot{Q}_{CAP7}$$

$$\frac{T_6 - T_7}{R_{COND6,7}} - \frac{T_7 - T_8}{R_{COND7,8}} = \frac{T_7 - T_7^{i-1}}{R_{CAP7}}$$

$$R_{COND6,7} = \frac{1}{\frac{1}{R_{i-1}_{7,8}} + \frac{1}{R_{s-1}_{7,8}} + \frac{1}{R_{i-2}_{7,8}} + \frac{1}{R_{i-3}_{7,8}} + \frac{1}{R_{i-4}_{7,8}}}$$

$$R_{CAP7} = \frac{1}{\frac{1}{R_{i-1}_7} + \frac{1}{R_{s-1}_7} + \frac{1}{R_{i-2}_7} + \frac{1}{R_{i-3}_7} + \frac{1}{R_{i-4}_7}}$$

R for conduction

$$R_{i-1}_{7,8} = \frac{BW - 2BL}{\lambda_i \cdot TI}$$

$$R_{s-1}_{7,8} = \frac{BW - 2BL}{\lambda_s \cdot TS}$$

$$R_{i-2}_{7,8} = \frac{BW - 2BL}{\lambda_i (BF - 2TS)}$$

$$R_{i-3}_{7,8} = \frac{BW - 2BL}{\lambda_i \cdot TS}$$

$$R_{i-4}_{7,8} = \frac{BW - 2BL}{\lambda_i \cdot BI}$$

R for capacity

$$R_{i-1}_7 = \frac{\Delta t}{\rho_i C p_i \left(\frac{BW - 2BL}{2} \right) TI}$$

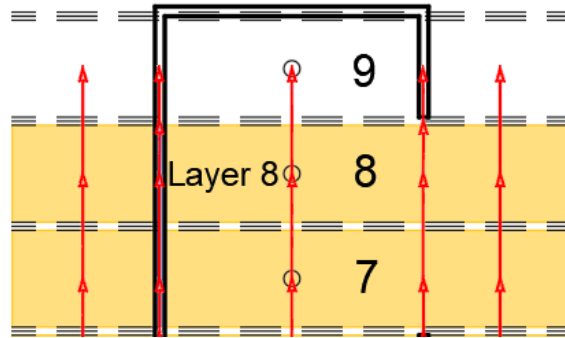
$$R_{s-1}_7 = \frac{\Delta t}{\rho_s C p_s \left(\frac{BQ - 2BL}{2} \right) TS}$$

$$R_{i-2}_7 = \frac{\Delta t}{\rho_i C p_i \left(\frac{BW - 2BL}{2} \right) (BF - 2TS)}$$

$$R_{i-3}_7 = \frac{\Delta t}{\rho_i C p_i \left(\frac{BW - 2BL}{2} \right) TS}$$

$$R_{i-4}_7 = \frac{\Delta t}{\rho_i C p_i \left(\frac{BW - 2BL}{2} \right) BI}$$

- Layer 8



$$\dot{Q}_{COND7,8} - \dot{Q}_{COND8,9} = \dot{Q}_{CAP8}$$

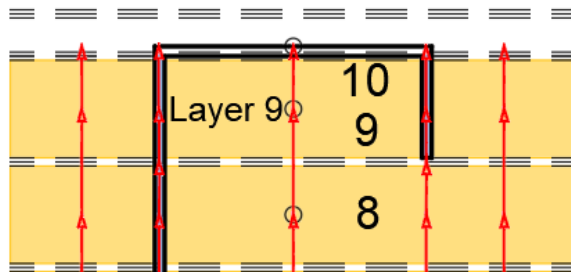
$$\frac{T_7 - T_8}{R_{COND7,8}} - \frac{T_8 - T_9}{R_{COND8,9}} = \frac{T_8 - T_8^{i-1}}{R_{CAP8}}$$

$$R_{COND8,9} = \frac{1}{\frac{1}{R_{i-1}_{8,9}} + \frac{1}{R_{s-1}_{8,9}} + \frac{1}{R_{i-2}_{8,9}} + \frac{1}{R_{i-3}_{8,9} + R_{s-2}_{8,9}} + \frac{1}{R_{i-4}_{8,9}}}$$

$$R_{CAP8} = \frac{1}{\frac{1}{R_{i-1}_8} + \frac{1}{R_{s-1}_8} + \frac{1}{R_{i-2}_8} + \frac{1}{R_{i-3}_8} + \frac{1}{R_{i-4}_8}}$$

R for conduction	R for capacity
$R_{i-1,8,9} = \frac{\left(\frac{BW - 2BL}{4}\right) + \frac{BL - TS}{2}}{\lambda_i \cdot TI} = \frac{\frac{BW}{4} - \frac{TS}{2}}{\lambda_i \cdot TI}$	$R_{i-1,8} = \frac{\Delta t}{\rho_i C p_i \left(\frac{BW - 2BL}{2}\right) TI}$
$R_{s-1,8,9} = \frac{\frac{BW}{4} - \frac{TS}{2}}{\lambda_s \cdot TS}$	$R_{s-1,8} = \frac{\Delta t}{\rho_s C p_s \left(\frac{BW - 2BL}{2}\right) TS}$
$R_{i-2,8,9} = \frac{\frac{BW}{4} - \frac{TS}{2}}{\lambda_i (BF - 2TS)}$	$R_{i-2,8} = \frac{\Delta t}{\rho_i C p_i \left(\frac{BW - 2BL}{2}\right) (BF - 2TS)}$
$R_{i-3,8,9} = \frac{BW - 2BL}{4 \lambda_i \cdot TS}$	$R_{i-3,8} = \frac{\Delta t}{\rho_i C p_i \left(\frac{BW - 2BL}{2}\right) TS}$
$R_{s-2,8,9} = \frac{BL - TS}{\lambda_s \cdot TS}$	$R_{i-4,8} = \frac{\Delta t}{\rho_i C p_i \left(\frac{BW - 2BL}{2}\right) BI}$
$R_{i-4,8,9} = \frac{\frac{BW}{4} - \frac{TS}{2}}{\lambda_i \cdot BI}$	

- Layer 9**



$$\dot{Q}_{COND8,9} - \dot{Q}_{COND9,10} = \dot{Q}_{CAP9}$$

$$\frac{T_8 - T_9}{R_{COND8,9}} - \frac{T_9 - T_{10}}{R_{COND9,10}} = \frac{T_9 - T_9^{i-1}}{R_{CAP9}}$$

$$R_{COND9,10} = \frac{1}{\frac{1}{R_{i-1}_{9,10}} + \frac{1}{R_{s-1}_{9,10}} + \frac{1}{R_{i-2}_{9,10} + R_{s-2}_{9,10}} + \frac{1}{R_{s-3}_{9,10}} + \frac{1}{R_{i-3}_{9,10}}}$$

$$R_{CAP9} = \frac{1}{\frac{1}{R_{i-1}_9} + \frac{1}{R_{s-1}_9} + \frac{1}{R_{i-2}_9} + \frac{1}{R_{s-2}_9} + \frac{1}{R_{i-3}_9}}$$

R for conduction

$$R_{i-1}_{9,10} = \frac{\frac{BL - TS}{2} + TS}{\lambda_i \cdot TI} = \frac{\frac{BL}{2} + \frac{TS}{2}}{\lambda_i \cdot TI}$$

$$R_{s-1}_{9,10} = \frac{\frac{BL}{2} + \frac{TS}{2}}{\lambda_s \cdot TS}$$

$$R_{i-2}_{9,10} = \frac{\frac{BL - TS}{2}}{\lambda_i (BF - 2TS)}$$

$$R_{s-2}_{9,10} = \frac{TS}{\lambda_s (BF - 2TS)}$$

$$R_{s-3}_{9,10} = \frac{\frac{BL}{2} + \frac{TS}{2}}{\lambda_s \cdot TS}$$

$$R_{i-3}_{9,10} = \frac{\frac{BL}{2} + \frac{TS}{2}}{\lambda_i \cdot BI}$$

R for capacity

$$R_{i-1}_9 = \frac{\Delta t}{\rho_i C p_i (BL - TS) TI}$$

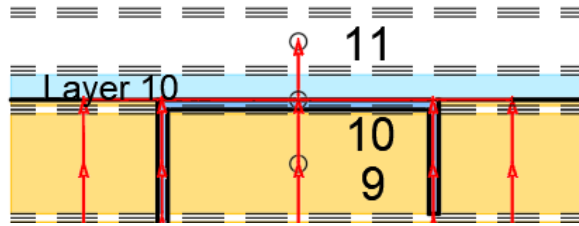
$$R_{s-1}_9 = \frac{\Delta t}{\rho_s C p_s (BL - TS) TS}$$

$$R_{i-2}_9 = \frac{\Delta t}{\rho_i C p_i (BL - TS) (BF - 2TS)}$$

$$R_{s-2}_9 = \frac{\Delta t}{\rho_s C p_s (BL - TS) TS}$$

$$R_{i-3}_9 = \frac{\Delta t}{\rho_i C p_i (BL - TS) BI}$$

- Layer 10



$$\dot{Q}_{COND9,10} - \dot{Q}_{COND10,11} = \dot{Q}_{CAP10}$$

$$\frac{T_9 - T_{10}}{R_{COND9,10}} - \frac{\lambda_G}{\left(\frac{TG}{4}\right)} [T_{10} - T_{11}] WL = \frac{T_{10} - T_{10}^{i-1}}{R_{CAP10}}$$

$$R_{CAP10} = R_{G2} + \frac{1}{\frac{1}{R_{i-1,10}} + \frac{1}{R_{s-1,10}} + \frac{1}{R_{i-2,10}}}$$

R for capacity

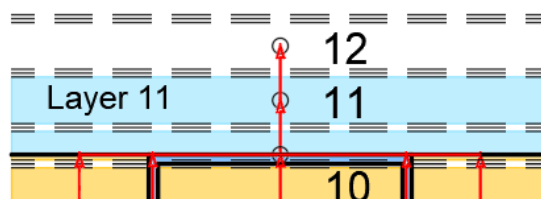
$$R_{G2} = \frac{\Delta t}{\rho_G C p_G \left(\frac{TG}{8}\right) WL}$$

$$R_{i-1,10} = \frac{\Delta t}{\rho_i C p_i TS \cdot TI}$$

$$R_{s-1,10} = \frac{\Delta t}{\rho_s C p_s TS \cdot BF}$$

$$R_{i-2,10} = \frac{\Delta t}{\rho_i C p_i TS \cdot BI}$$

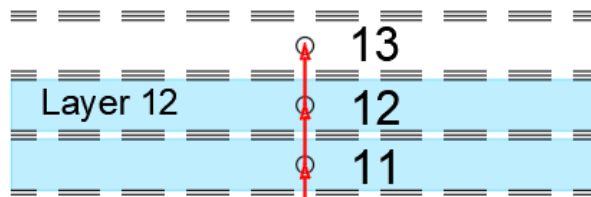
- Layer 11



$$\dot{Q}_{COND10,11} - \dot{Q}_{COND11,12} = \dot{Q}_{CAP11}$$

$$\frac{\lambda_G}{\left(\frac{TG}{4}\right)} [T_{10} - T_{11}] \cdot WL - \frac{\lambda_G}{\left(\frac{TG}{4}\right)} [T_{11} - T_{12}] \cdot WL = \rho_G C p_G \left(\frac{TG}{4}\right) \frac{[T_{11} - T_{11}^{i-1}]}{\Delta t} \cdot WL$$

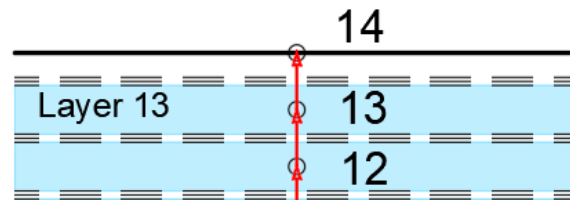
- **Layer 12**



$$\dot{Q}_{COND11,12} - \dot{Q}_{COND12,13} = \dot{Q}_{CAP12}$$

$$\frac{\lambda_G}{\left(\frac{TG}{4}\right)} [T_{11} - T_{12}] \cdot WL - \frac{\lambda_G}{\left(\frac{TG}{4}\right)} [T_{12} - T_{13}] \cdot WL = \rho_G C p_G \left(\frac{TG}{4}\right) \frac{[T_{12} - T_{12}^{i-1}]}{\Delta t} \cdot WL$$

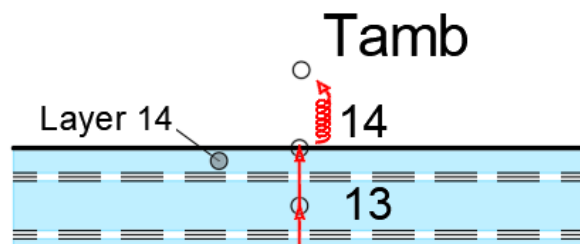
- **Layer 13**



$$\dot{Q}_{COND12,13} - \dot{Q}_{COND13,14} = \dot{Q}_{CAP13}$$

$$\frac{\lambda_G}{\left(\frac{TG}{4}\right)} [T_{12} - T_{13}] \cdot WL - \frac{\lambda_G}{\left(\frac{TG}{4}\right)} [T_{13} - T_{14}] \cdot WL = \rho_G C p_G \left(\frac{TG}{4}\right) \frac{[T_{13} - T_{13}^{i-1}]}{\Delta t} \cdot WL$$

- Layer 14



$$\dot{Q}_{COND13,14} - \dot{Q}_{CONV} = \dot{Q}_{CAP14}$$

$$\frac{\lambda_G}{\left(\frac{TG}{4}\right)} [T_{13} - T_{14}] \cdot WL - \alpha [T_{14} - T_{amb}] \cdot WL = \rho_G C p_G \left(\frac{TG}{8}\right) \frac{[T_{14} - T_{14}^{i-1}]}{\Delta t}$$

B. Appendix – Matrix of Heat Transfer

Matrix of Heat Transfer for the finite-difference method															
	T ₁	T ₂	T ₃	T ₄	T ₅	T ₆	T ₇	T ₈	T ₉	T ₁₀	T ₁₁	T ₁₂	T ₁₃	T ₁₄	LOAD
EQ1	k_{11}	k_{12}	0	0	0	0	0	0	0	0	0	0	0	0	F_1
EQ2	k_{21}	k_{22}	k_{23}	0	0	0	0	0	0	0	0	0	0	0	F_2
EQ3	0	k_{32}	k_{33}	k_{34}	0	0	0	0	0	0	0	0	0	0	F_3
EQ4	0	0	k_{43}	k_{44}	k_{45}	0	0	0	0	0	0	0	0	0	F_4
EQ5	0	0	0	k_{54}	k_{55}	k_{56}	0	0	0	0	0	0	0	0	F_5
EQ6	0	0	0	0	k_{65}	k_{66}	k_{67}	0	0	0	0	0	0	0	F_6
EQ7	0	0	0	0	0	k_{76}	k_{77}	k_{78}	0	0	0	0	0	0	F_7
EQ8	0	0	0	0	0	0	k_{87}	k_{88}	k_{89}	0	0	0	0	0	F_8
EQ9	0	0	0	0	0	0	0	k_{98}	k_{99}	k_{910}	0	0	0	0	F_9
EQ10	0	0	0	0	0	0	0	0	k_{109}	k_{1010}	k_{1011}	0	0	0	F_{10}
EQ11	0	0	0	0	0	0	0	0	0	k_{1110}	k_{1111}	k_{1112}	0	0	F_{11}
EQ12	0	0	0	0	0	0	0	0	0	0	k_{1211}	k_{1212}	k_{1213}	0	F_{12}
EQ13	0	0	0	0	0	0	0	0	0	0	0	k_{1312}	k_{1313}	k_{1314}	F_{13}
EQ14	0	0	0	0	0	0	0	0	0	0	0	0	k_{1413}	k_{1414}	F_{14}

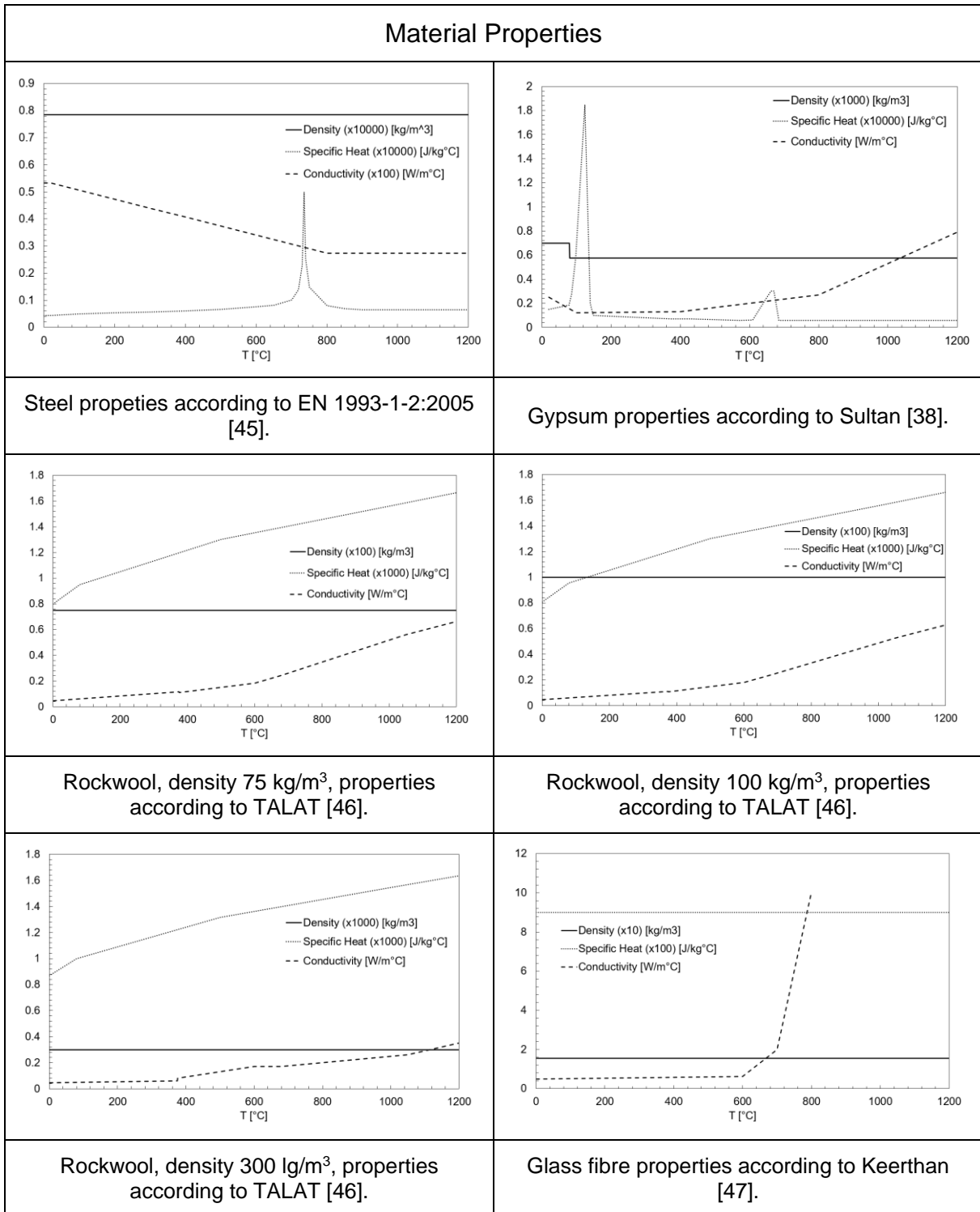
Where:

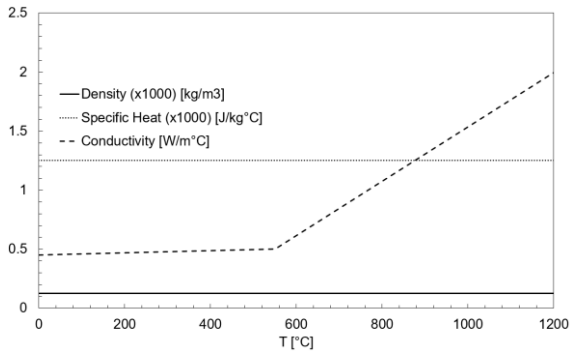
$k_{11} = -[\alpha_r + \alpha_c]WL - \frac{\lambda_g}{\left(\frac{\tau_g}{4}\right)}WL - \frac{\rho_g c p_g}{\Delta t}WL \left(\frac{\tau_g}{8}\right)$ $k_{12} = + \frac{\lambda_g}{\left(\frac{\tau_g}{4}\right)}WL$	$k_{21} = \frac{WL\lambda_g}{\left(\frac{\tau_g}{4}\right)}$ $k_{22} = - \frac{WL\lambda_g}{\left(\frac{\tau_g}{4}\right)} - \frac{\lambda_g WL}{\left(\frac{\tau_g}{4}\right)} - \rho_g c p_g WL \left(\frac{\tau_g}{4}\right) \frac{1}{\Delta t}$ $k_{23} = + \frac{\lambda_g WL}{\left(\frac{\tau_g}{4}\right)}$
--	---

$k_{32} = + \frac{WL\lambda_G}{\left(\frac{TG}{4}\right)}$ $k_{33} = - \frac{WL\lambda_G}{\left(\frac{TG}{4}\right)} - \frac{\lambda_G WL}{\left(\frac{TG}{4}\right)} - \rho_G c p_G WL \left(\frac{TG}{4}\right) \frac{1}{\Delta t}$ $k_{34} = + \frac{\lambda_G WL}{\left(\frac{TG}{4}\right)}$	$k_{43} = + \frac{WL\lambda_G}{\left(\frac{TG}{4}\right)}$ $k_{44} = - \frac{WL\lambda_G}{\left(\frac{TG}{4}\right)} - \frac{\lambda_G WL}{\left(\frac{TG}{4}\right)} - \rho_G c p_G WL \left(\frac{TG}{4}\right) \frac{1}{\Delta t}$ $k_{45} = + \frac{\lambda_G WL}{\left(\frac{TG}{4}\right)}$
$k_{54} = + \frac{WL\lambda_G}{\left(\frac{TG}{4}\right)}$ $k_{55} = - \frac{WL\lambda_G}{\left(\frac{TG}{4}\right)} - \frac{1}{R_{COND5,6}} - \frac{1}{R_{CAP5}}$ $k_{56} = + \frac{1}{R_{COND5,6}}$	$k_{65} = + \frac{1}{R_{COND5,6}}$ $k_{66} = - \frac{1}{R_{COND5,6}} - \frac{1}{R_{COND6,7}} - \frac{1}{R_{CAP6}}$ $k_{67} = + \frac{1}{R_{COND6,7}}$
$k_{76} = + \frac{1}{R_{COND6,7}}$ $k_{77} = - \frac{1}{R_{COND6,7}} - \frac{1}{R_{COND7,8}} - \frac{1}{R_{CAP7}}$ $k_{78} = + \frac{1}{R_{COND7,8}}$	$k_{87} = + \frac{1}{R_{COND7,8}}$ $k_{88} = - \frac{1}{R_{COND7,8}} - \frac{1}{R_{COND8,9}} - \frac{1}{R_{CAP8}}$ $k_{89} = + \frac{1}{R_{COND8,9}}$
$k_{98} = + \frac{1}{R_{COND8,9}}$ $k_{99} = - \frac{1}{R_{COND8,9}} - \frac{1}{R_{COND9,10}} - \frac{1}{R_{CAP9}}$ $k_{910} = + \frac{1}{R_{COND9,10}}$	$k_{109} = + \frac{1}{R_{COND9,10}}$ $k_{1010} = - \frac{1}{R_{COND9,10}} - \frac{\lambda_G WL}{\left(\frac{TG}{4}\right)} - \frac{1}{R_{CAP10}}$ $k_{1011} = + \frac{\lambda_G WL}{\left(\frac{TG}{4}\right)}$
$k_{1110} = + \frac{\lambda_G WL}{\left(\frac{TG}{4}\right)}$ $k_{1111} = - \frac{\lambda_G WL}{\left(\frac{TG}{4}\right)} - \frac{\lambda_G WL}{\left(\frac{TG}{4}\right)} - \rho_G c p_G WL \left(\frac{TG}{4}\right) \frac{1}{\Delta t}$ $k_{1112} = + \frac{\lambda_G WL}{\left(\frac{TG}{4}\right)}$	$k_{1211} = + \frac{\lambda_G WL}{\left(\frac{TG}{4}\right)}$ $k_{1212} = - \frac{\lambda_G WL}{\left(\frac{TG}{4}\right)} - \frac{\lambda_G WL}{\left(\frac{TG}{4}\right)} - \rho_G c p_G WL \left(\frac{TG}{4}\right) \frac{1}{\Delta t}$ $k_{1213} = + \frac{\lambda_G WL}{\left(\frac{TG}{4}\right)}$

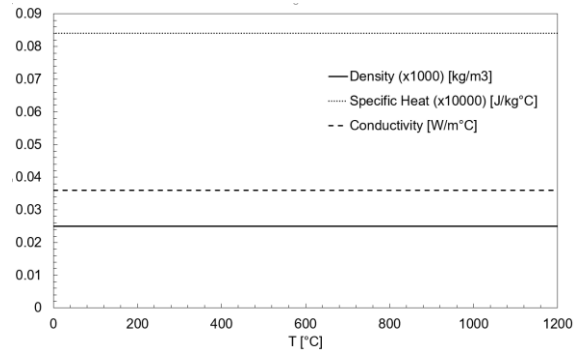
$k_{1312} = + \frac{\lambda_G WL}{\left(\frac{T_G}{4}\right)}$ $k_{1313} = - \frac{\lambda_G WL}{\left(\frac{T_G}{4}\right)} - \frac{\lambda_G WL}{\left(\frac{T_G}{4}\right)} - \rho_G Cp_G WL \left(\frac{T_G}{4}\right) \frac{1}{\Delta t}$ $k_{1314} = + \frac{\lambda_G WL}{\left(\frac{T_G}{4}\right)}$	$k_{1413} = + \frac{\lambda_G WL}{\left(\frac{T_G}{4}\right)}$ $k_{1414} = - \frac{\lambda_G WL}{\left(\frac{T_G}{4}\right)} - \alpha_c WL - \rho_G Cp_G WL \left(\frac{T_G}{8}\right) \frac{1}{\Delta t}$
LOAD:	
$F_1 = -[\alpha_R + \alpha_c] T_{fire} WL - \rho_G Cp_G WL \left(\frac{T_G}{8}\right) \frac{1}{\Delta t} T_1^{i-1}$ $F_2 = -\rho_G Cp_G WL \left(\frac{T_G}{4}\right) \frac{1}{\Delta t} T_2^{i-1}$ $F_3 = -\rho_G Cp_G WL \left(\frac{T_G}{4}\right) \frac{1}{\Delta t} T_3^{i-1}$ $F_4 = -\rho_G Cp_G WL \left(\frac{T_G}{4}\right) \frac{1}{\Delta t} T_4^{i-1}$ $F_5 = -\frac{1}{R_{CAP5}} T_5^{i-1}$ $F_6 = -\frac{1}{R_{CAP6}} T_6^{i-1}$ $F_7 = -\frac{1}{R_{CAP7}} T_7^{i-1}$	$F_8 = -\frac{1}{R_{CAP8}} T_8^{i-1}$ $F_9 = -\frac{1}{R_{CAP9}} T_9^{i-1}$ $F_{10} = -\frac{1}{R_{CAP10}} T_{10}^{i-1}$ $F_{11} = -\rho_G Cp_G WL \left(\frac{T_G}{4}\right) \frac{1}{\Delta t} T_{11}^{i-1}$ $F_{12} = -\rho_G Cp_G WL \left(\frac{T_G}{4}\right) \frac{1}{\Delta t} T_{12}^{i-1}$ $F_{13} = -\rho_G Cp_G WL \left(\frac{T_G}{4}\right) \frac{1}{\Delta t} T_{13}^{i-1}$ $F_{14} = -\alpha_c T_{amb} WL - \rho_G Cp_G WL \left(\frac{T_G}{8}\right) \frac{1}{\Delta t} T_{14}^{i-1}$
$\alpha_R = \varepsilon_f \varepsilon_G \sigma (T_{fire} + T_1)(T_{fire}^2 + T_1^2)$	

C. Appendix – Material Properties

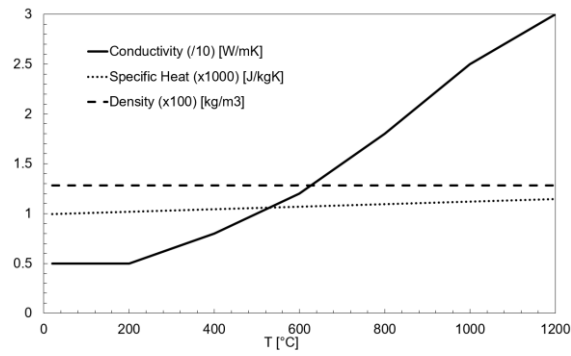




Cellulose fibre properties according to Keerthan [47].



Mineral wool properties according to Feng et al. [15].

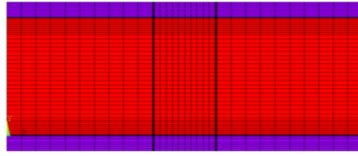


Superwool properties according to Morgan DataSheet [48], [49].

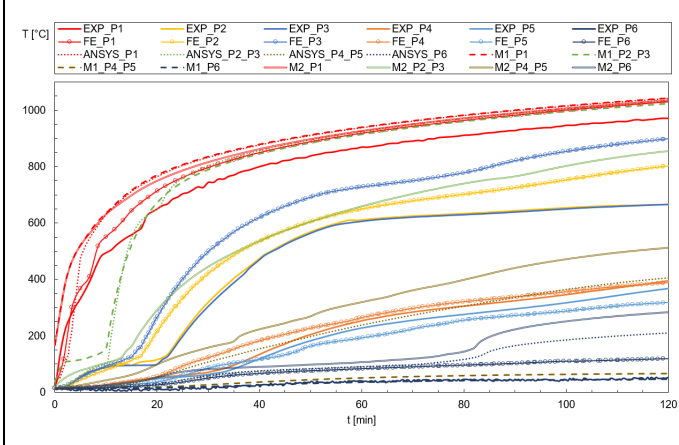
D. Appendix – Data Sheets

Description		
Author: Feng, M.; Wang, Y. C.; Davies, J. M. [15]	Test no.: Tlip12-a3	Insulation: Isowool 1000
Local: University of Manchester, UK.	Year: 2002	Gypsum board: 12.5 mm
<p>Observations:</p> <ul style="list-style-type: none"> - Dimensions in millimeters; - Steel properties from Eurocode 3: Part 2 was used; - Images on the left are from the experimental test and the mesh from the ABAQUS program used by the author for the finite element analysis; - FE in the graph represents the results of the finite element analysis made by the author. 		

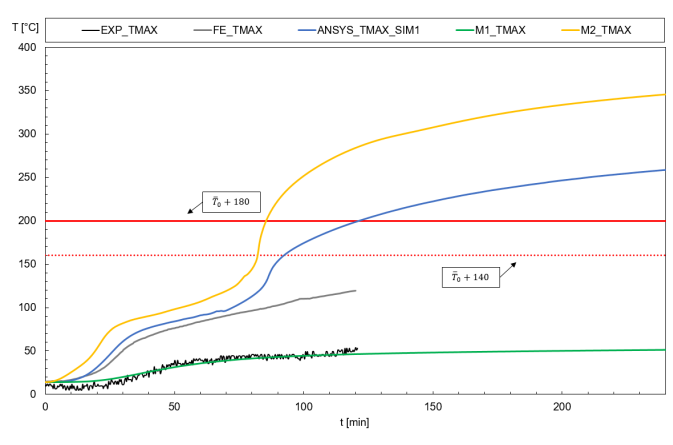
SIM.	WL [mm]		Matlab Fire resistance (min)		Ansys Fire resistance (min)	
	1	M1: 246.7	M2: 45	M1: >1200	M2: 84	Ave: 768



Mesh from Ansys

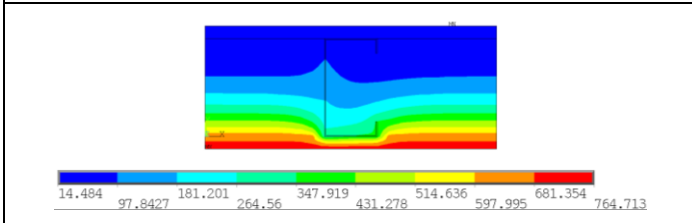


Comparison between all results

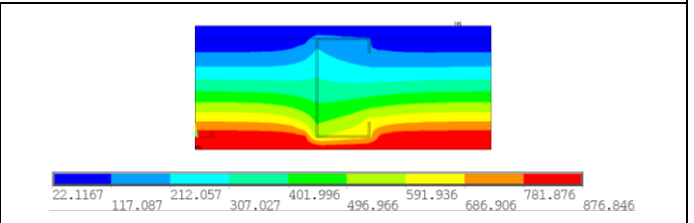


Unexposed curves with insulation criterion (I)

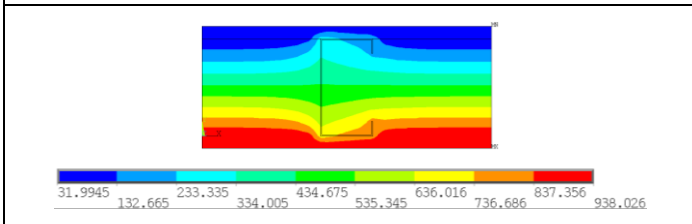
Ansys results through time



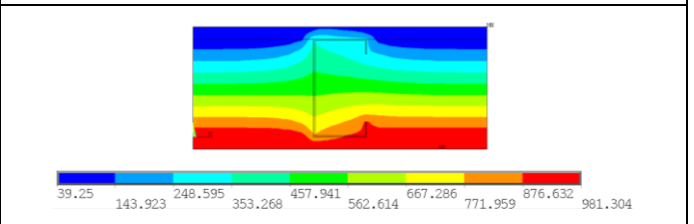
t = 20 min



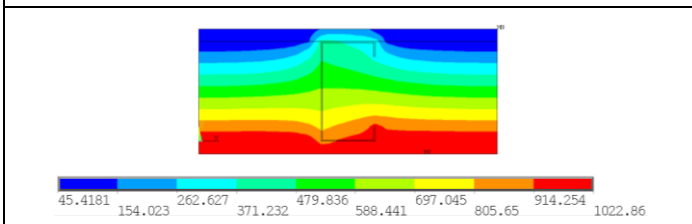
t = 40 min



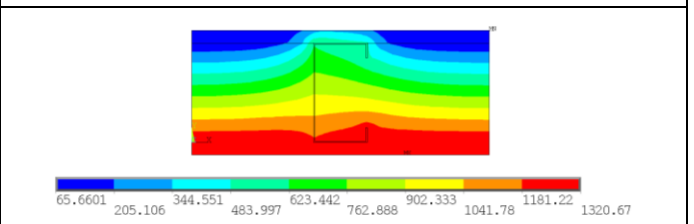
t = 60 min



t = 80 min



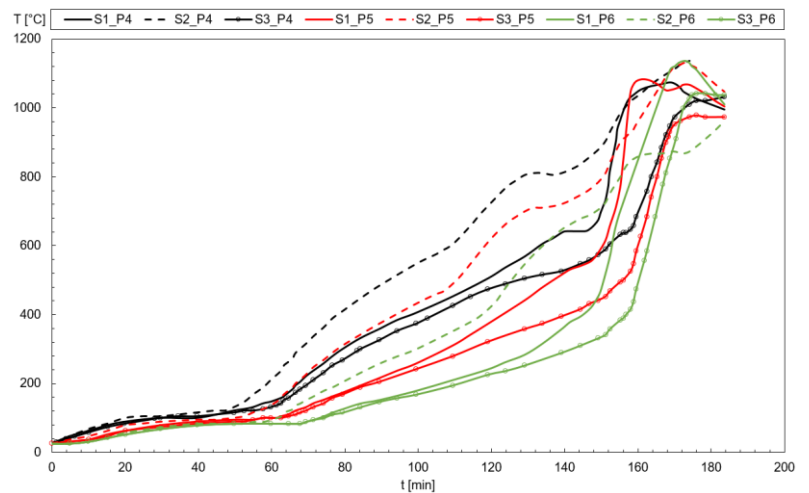
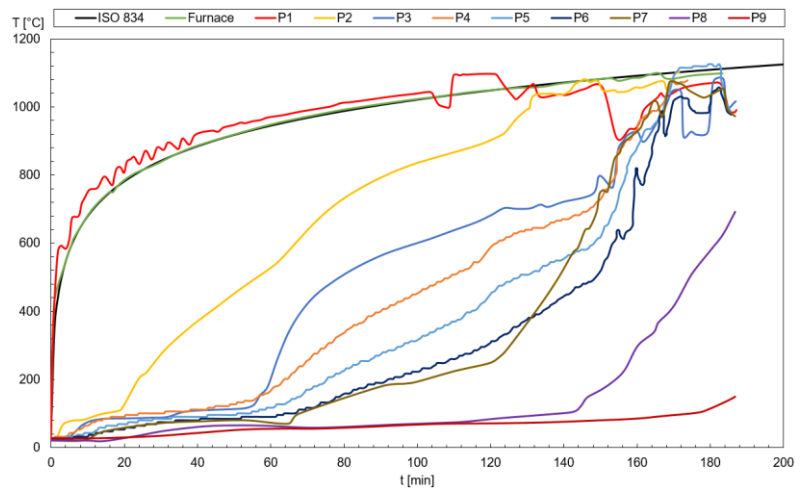
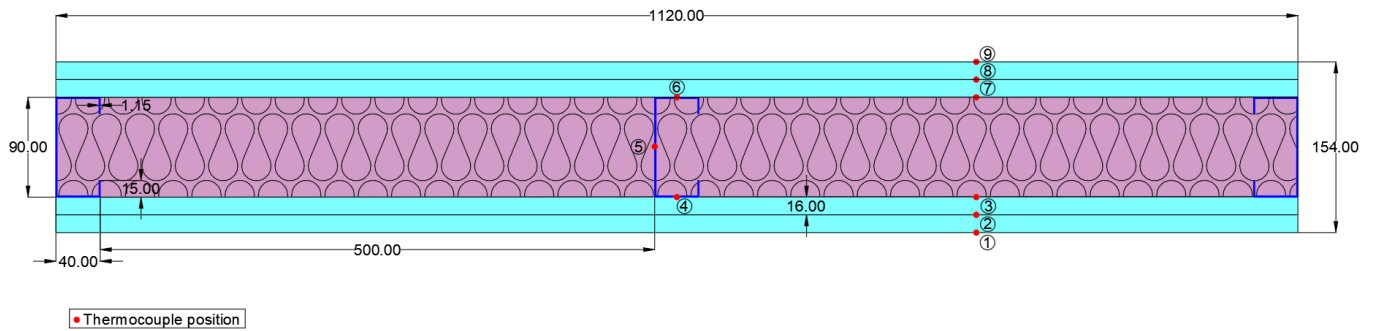
t = 105 min (TMAX)



t = 768 min (TAVE)

Description

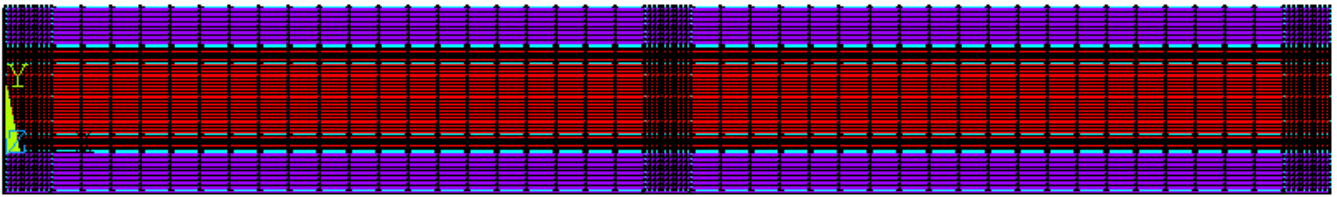
Author: Kolarkar, P.; Mahendran, M. [39]	Test no.: 4	Insulation: Glassfibre 15.42 kg/m ³
Local: Queensland University of Technology, AUS	Year: 2011	Gypsum board: 2 x 16 mm



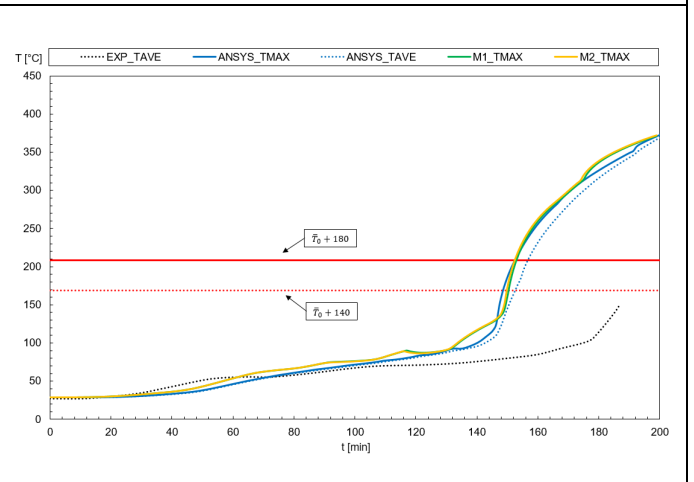
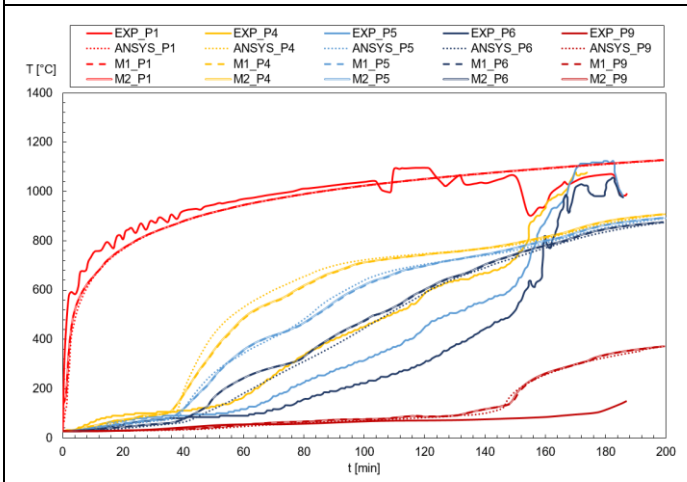
Observations:

- Dimensions in millimeters;
- Steel properties from Eurocode 3: Part 2 was used;
- The second graph represents temperatures in each stud.

SIM.	WL		Matlab Fire resistance (min)		Ansys Fire resistance (min)	
	1	M1: 159.06	M2: 168	M1: 153	M2: 151	Ave: 152



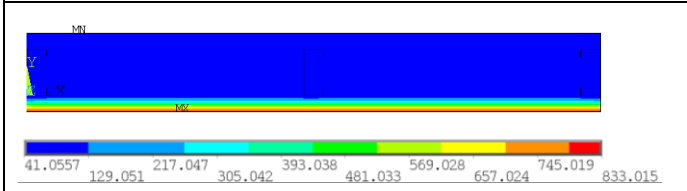
Mesh from Ansys



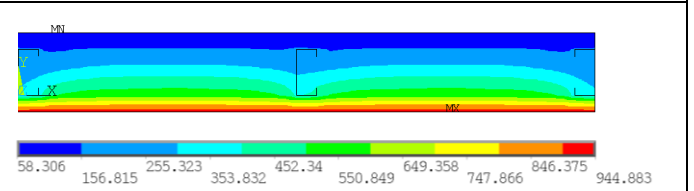
Comparison between all results

Unexposed curves with insulation criterion (I)

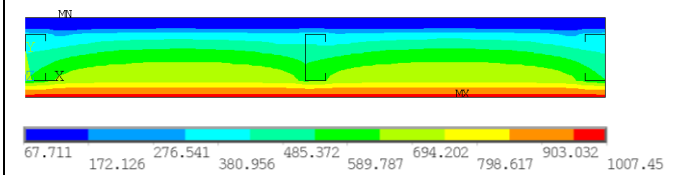
Ansys results through time



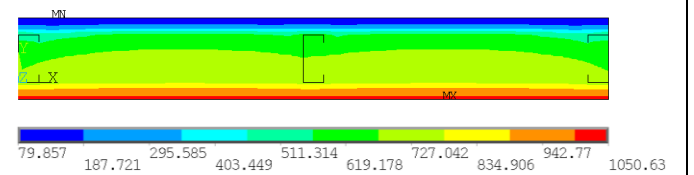
t = 30 min



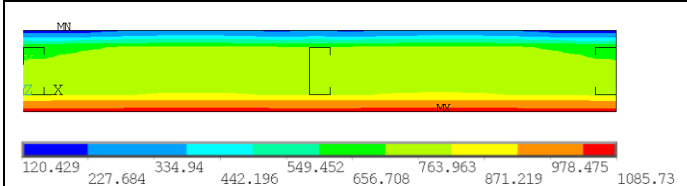
t = 60 min



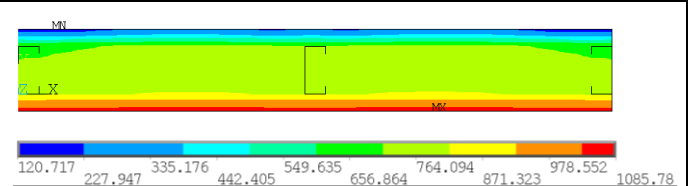
t = 90 min



t = 120 min



t = 152 min (TMAX)



t = 152 min (TAVE)

Description

Author: Kolarkar, P.; Mahendran, M. [39]

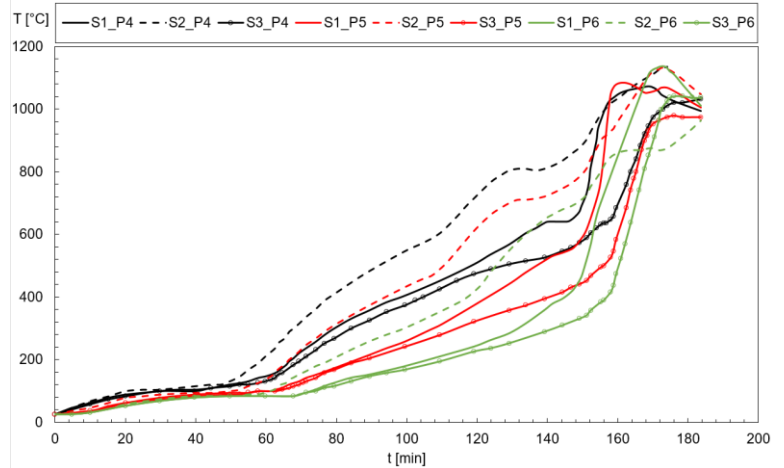
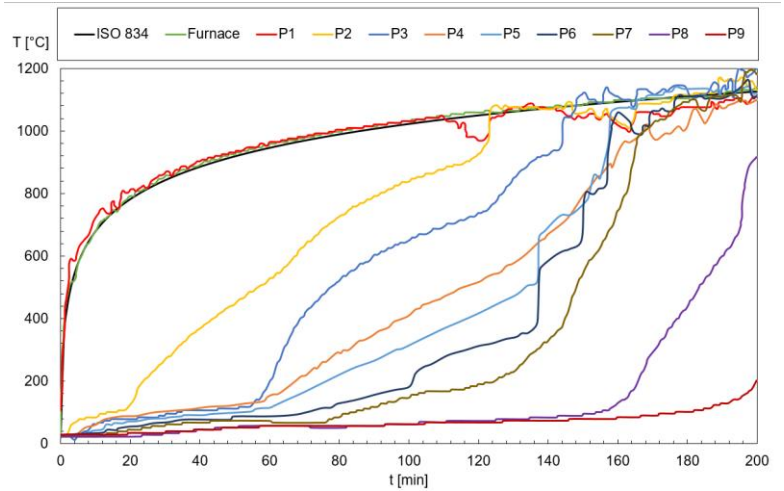
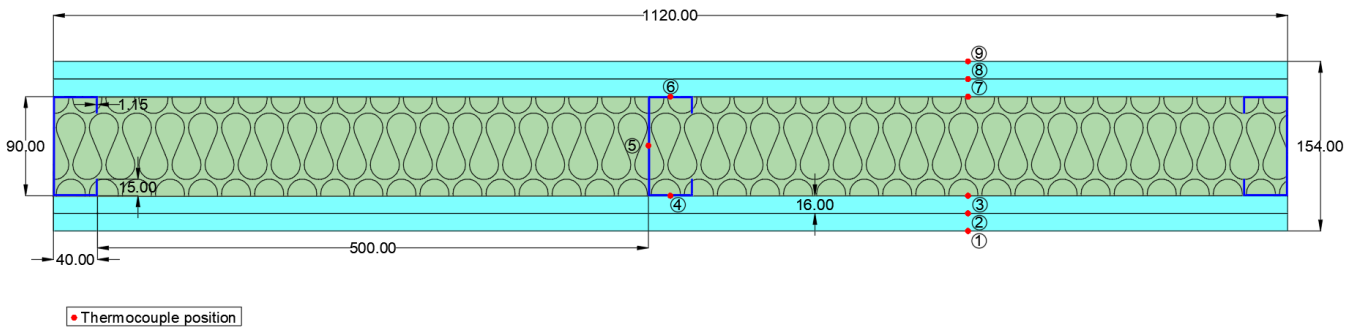
Test no.: 5

Insulation: Rockwool 100kg/m³

Local: Queensland University of Technology, AUS

Year: 2011

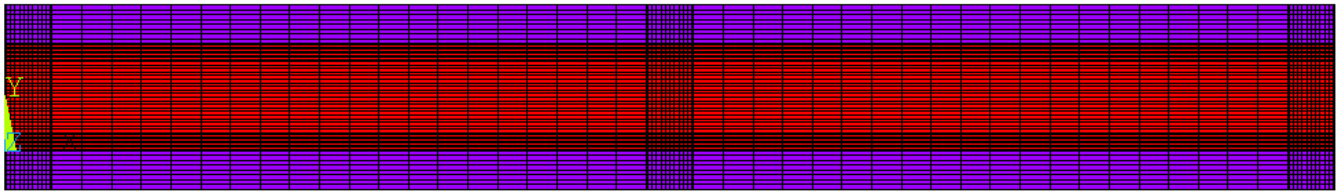
Gypsum board: 2 x 16 mm



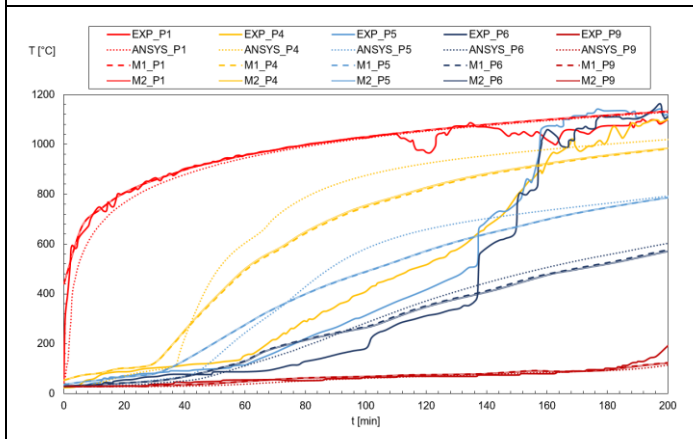
Observations:

- Dimensions in millimeters;
- Steel properties from Eurocode 3: Part 2 was used;
- The second graph represents temperatures in each stud, left to right.

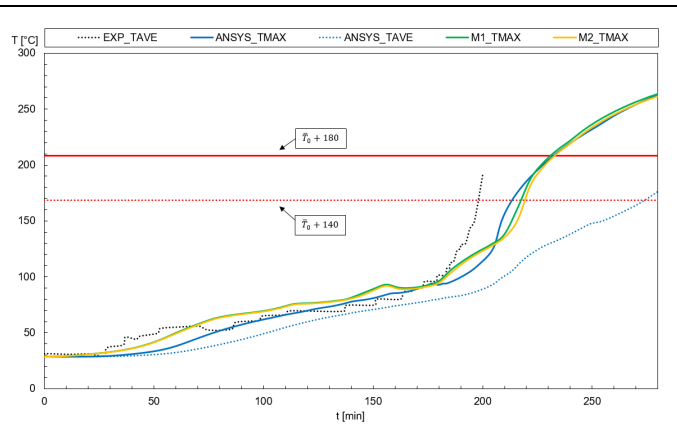
SIM. 1	WL [mm]		Matlab Fire resistance (min)		Ansys Fire resistance (min)	
	M1: 159.06	M2: 168	M1: 231	M2: 228	Ave: 273	Max: 232



Mesh from Ansys

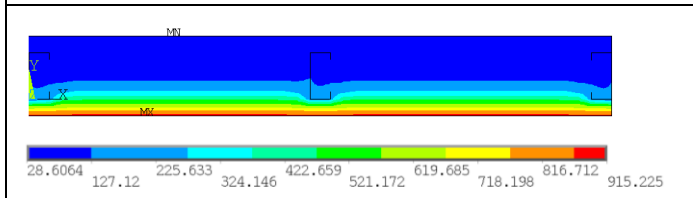


Comparison between all results

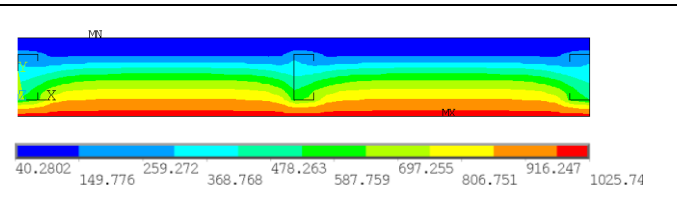


Unexposed curves with insulation criterion (I)

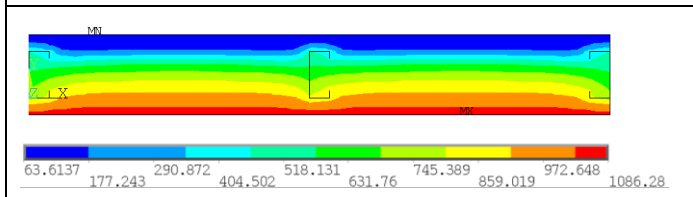
Ansys results through time



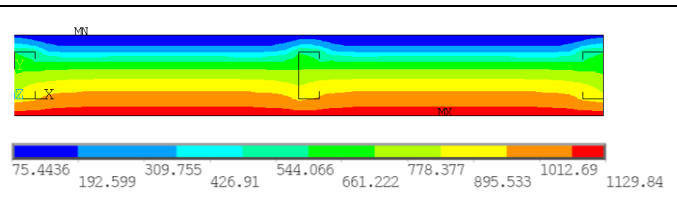
t = 50 min



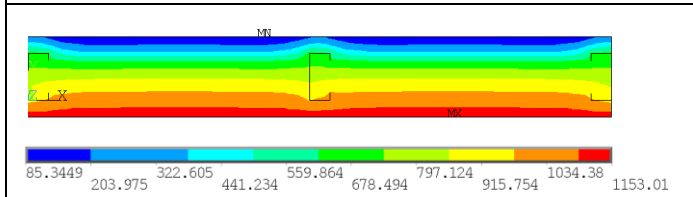
t = 100 min



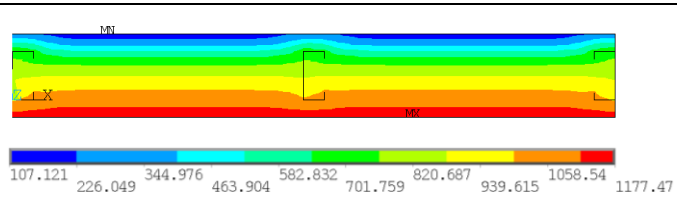
t = 150 min



t = 200 min



t = 232 min (TMAX)



t = 274 min (TAVE)

Description

Author: Kolarkar, P.; Mahendran, M. [39]

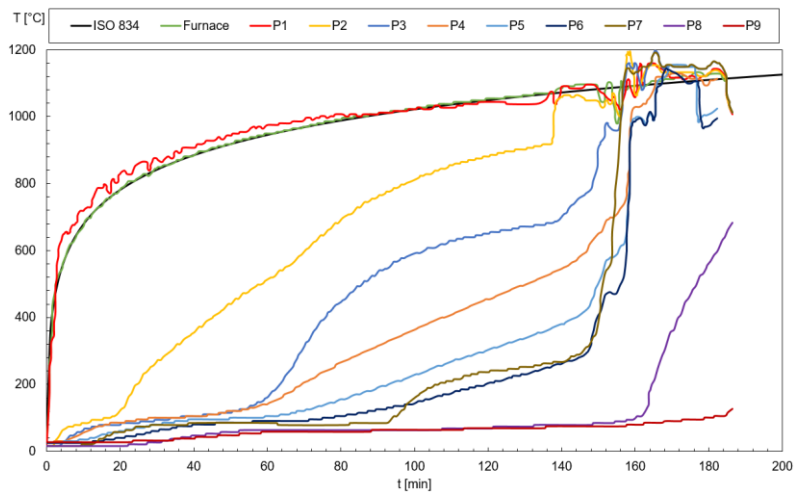
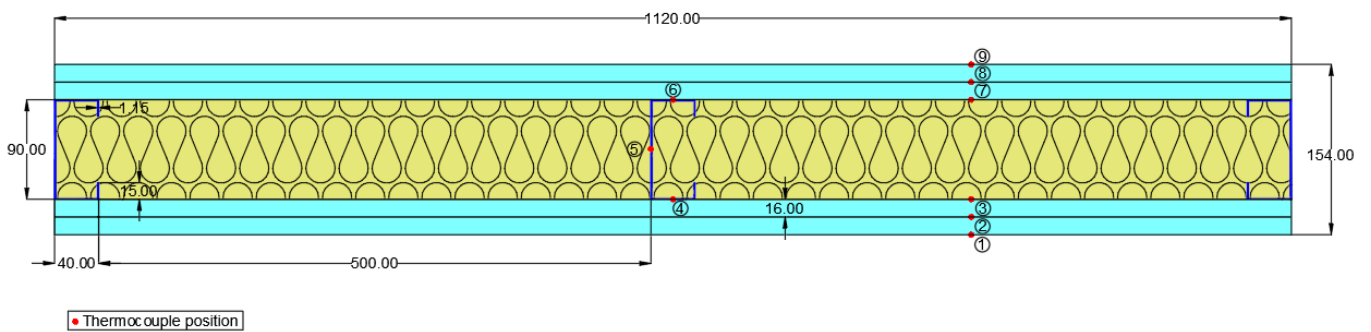
Test no.: 6

Insulation: Cellulose fibre 125kg/m³

Local: Queensland University of Technology, AUS

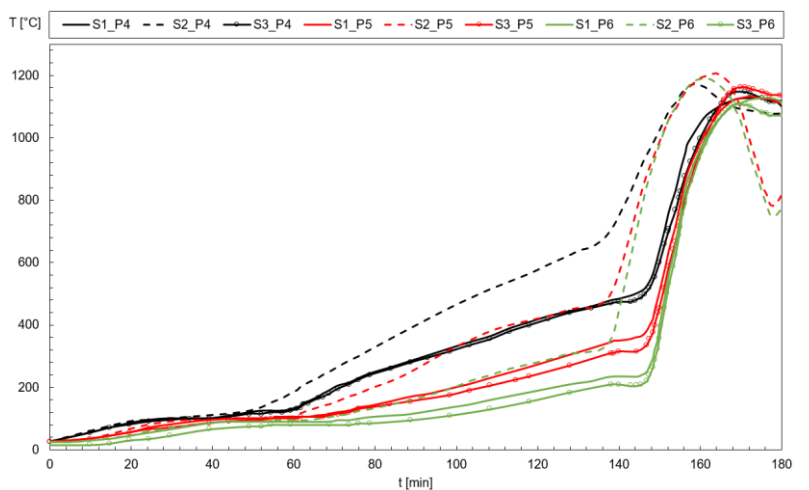
Year: 2011

Gypsum board: 2 x 16 mm

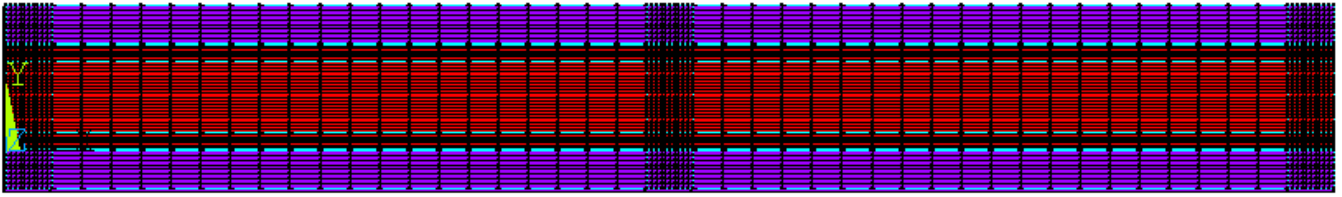


Observations:

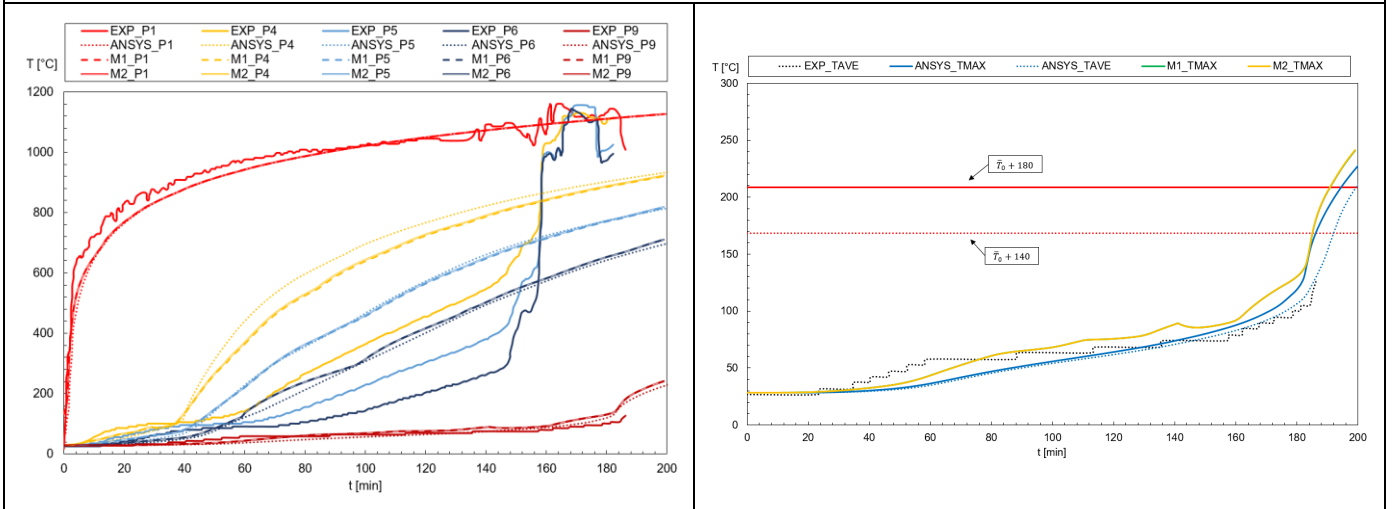
- Dimensions in millimeters;
- Steel properties from Eurocode 3: Part 2 was used;
- The second graph represents temperatures in each stud, left to right.



SIM. 1	WL [mm]		Matlab Fire resistance (min)		Ansys Fire resistance (min)	
	M1:159.06	M2: 168	M1: 190	M2: 189	Ave: 192	Max: 194



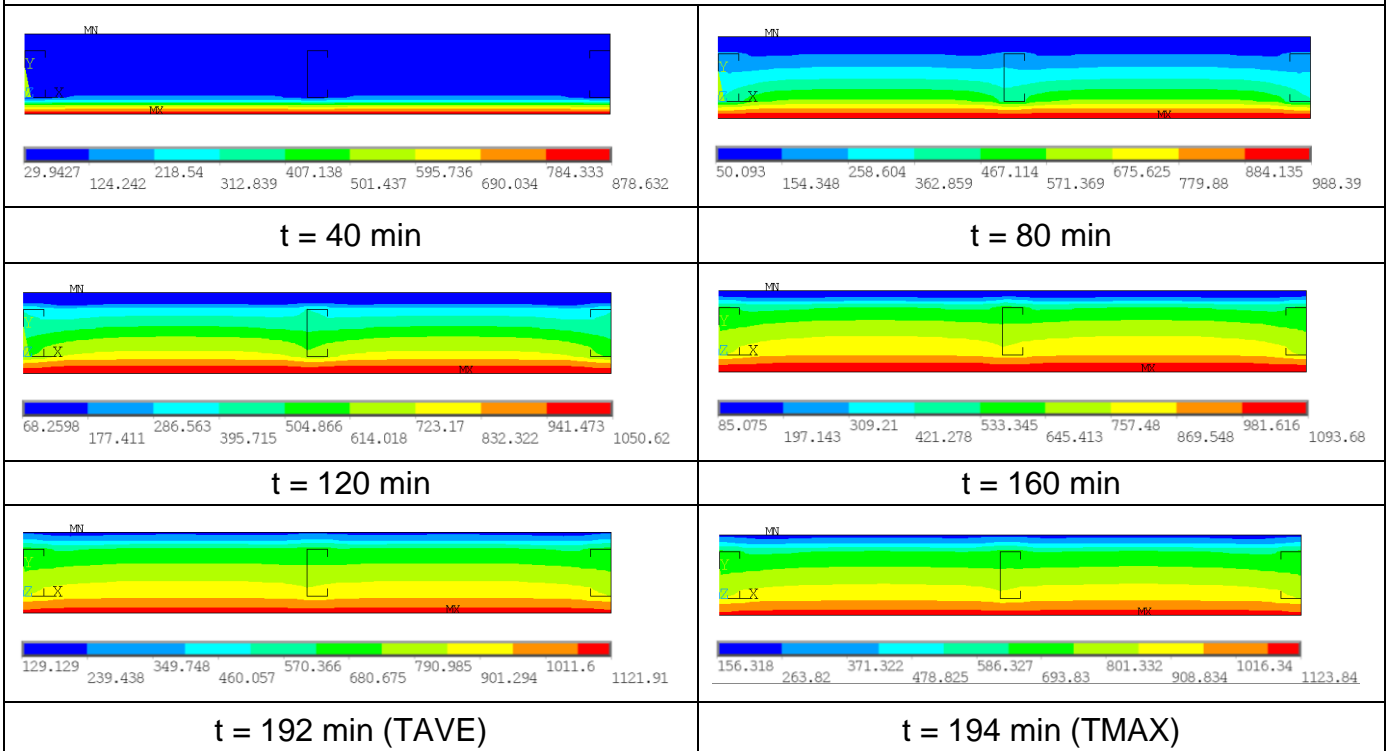
Mesh from Ansys



Comparison between all results

Unexposed curves with insulation criterion (I)

Ansys results through time



Description

Author: Rusthi, M.; Keerthan, P.; Ariyanayagam, A.; Mahendran, M. [40]

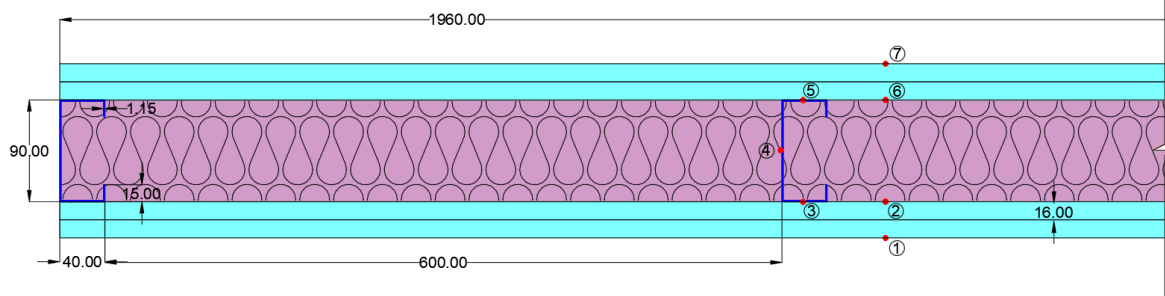
Test no.: 3

Insulation: Glass fibre 15.42kg/m³

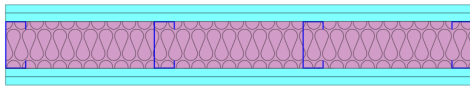
Local: Queensland University of Technology, AUS

Year: 2015

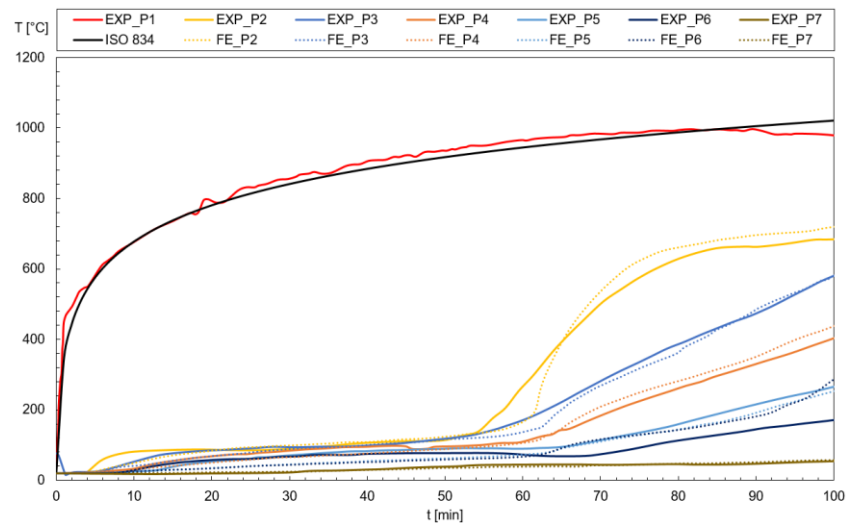
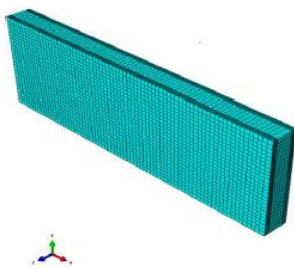
Gypsum board: 2 x 16 mm



• Thermocouple position



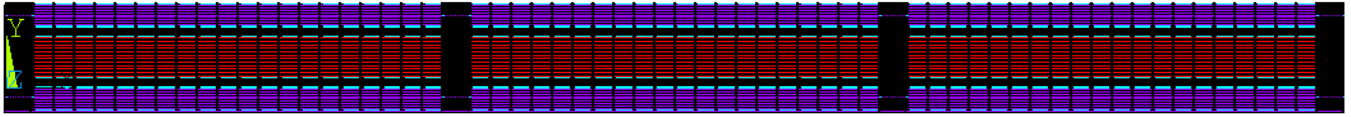
*scale drawing of the entire wall



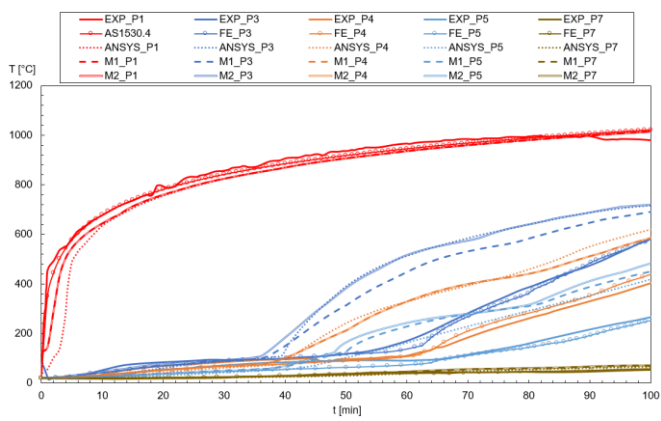
Observations:

- Dimensions in millimeters;
- Steel properties from Eurocode 3: Part 2 was used;
- Images on the left are from the experimental test and the mesh from the ABAQUS program used by the author for the finite element analysis;
- FE in the graph represents the results of the finite element analysis made by the author.

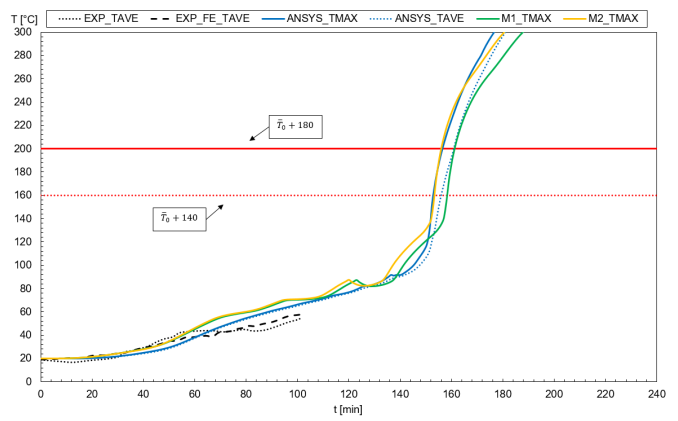
SIM. 1	WL [mm]		Matlab Fire resistance (min)		Ansys Fire resistance (min)	
	M1: 140.24	M2: 294	M1: 244	M2: 156	Ave: 289	Max: 243



Mesh from Ansys

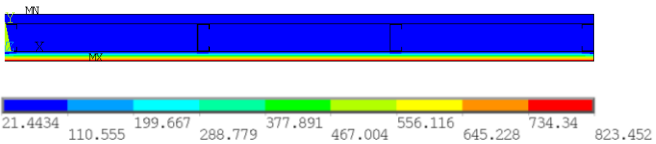


Comparison between all results

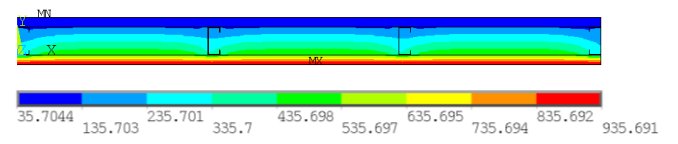


Unexposed curves with insulation criterion (I)

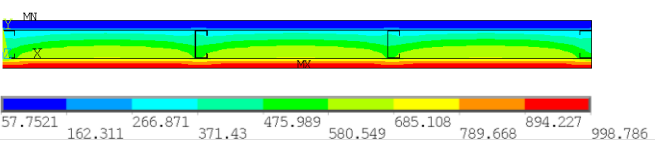
Ansys results through time



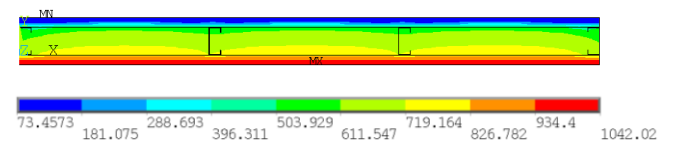
t = 30 min



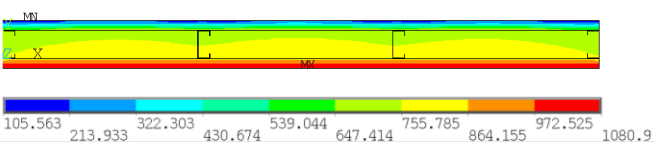
t = 60 min



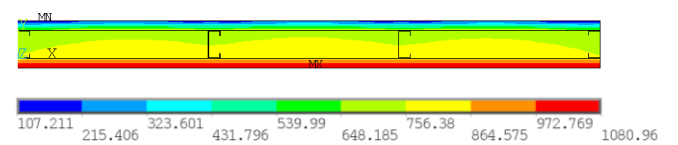
t = 90 min



t = 120 min



t = 156 min (TAVE)



t = 156 min (TMAX)

Description

Author: Rusthi, M.; Keerthan, P.; Ariyanayagam, A.; Mahendran, M. [40]

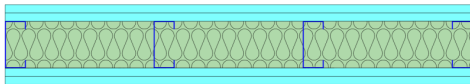
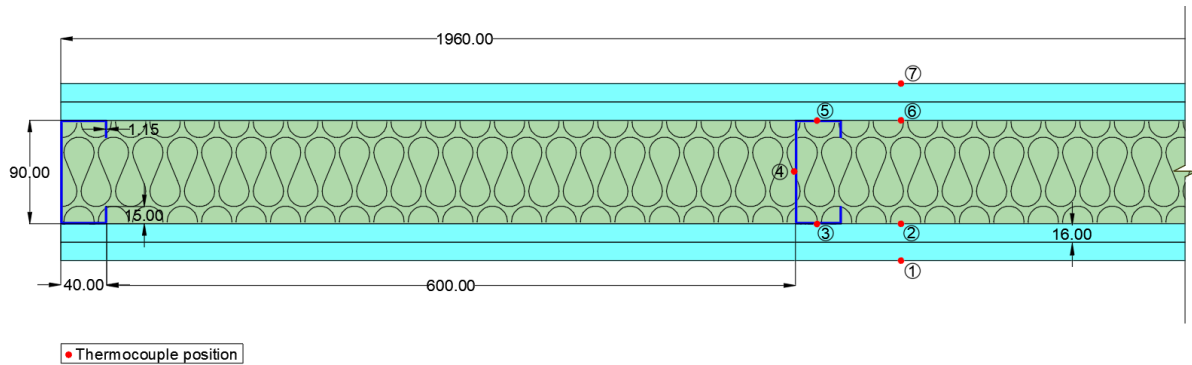
Test no.: 4

Insulation: Rockwool 100kg/m³

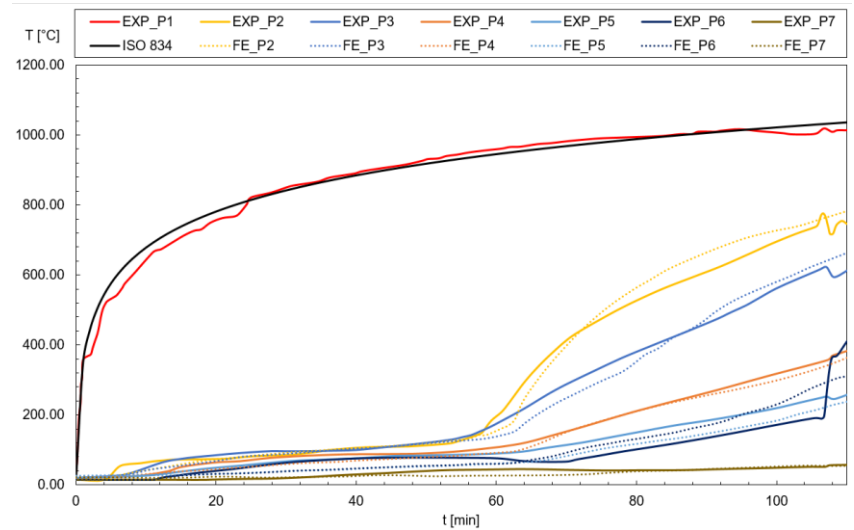
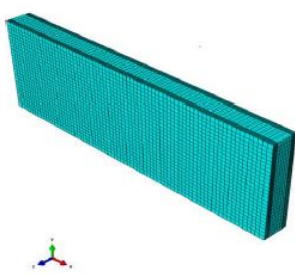
Local: Queensland University of Technology, AUS

Year: 2015

Gypsum board: 2 x 16 mm



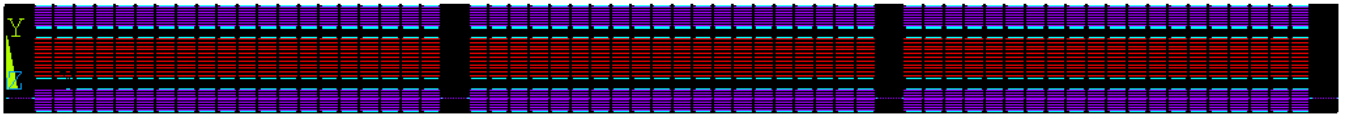
*scale drawing of the entire wall



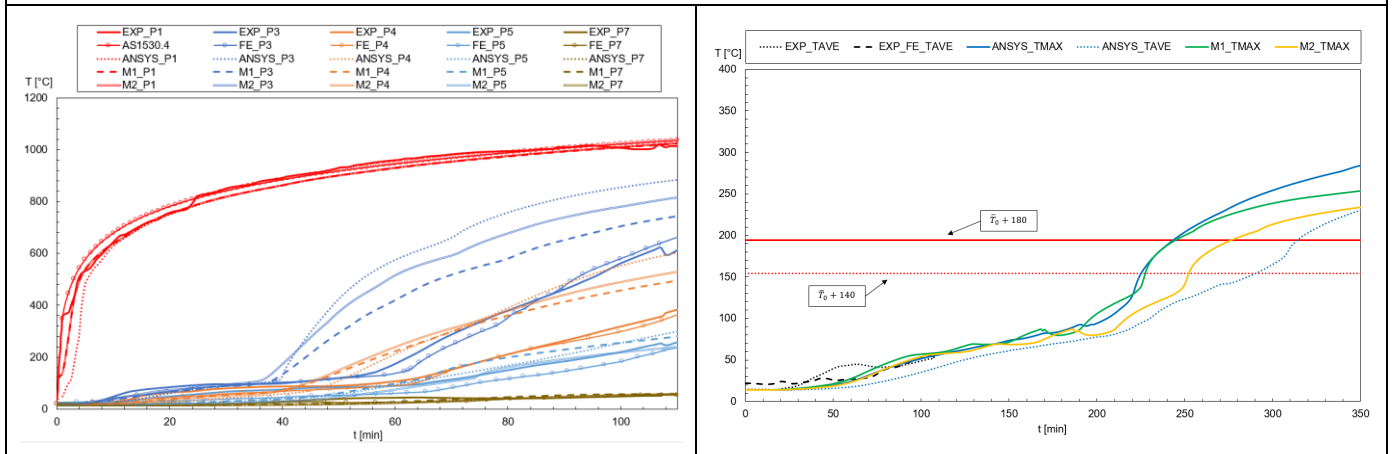
Observations:

- Dimensions in millimeters;
- Steel properties from Eurocode 3: Part 2 was used;
- Images on the left are from the experimental test and the mesh from the ABAQUS program used by the author for the finite element analysis;
- FE in the graph represents the results of the finite element analysis made by the author.

SIM. 1	WL [mm]		Matlab Fire resistance (min)		Ansys Fire resistance (min)	
	M1: 140.24	M2: 294	M1: 244	M2: 284	Ave: 289	Max: 243



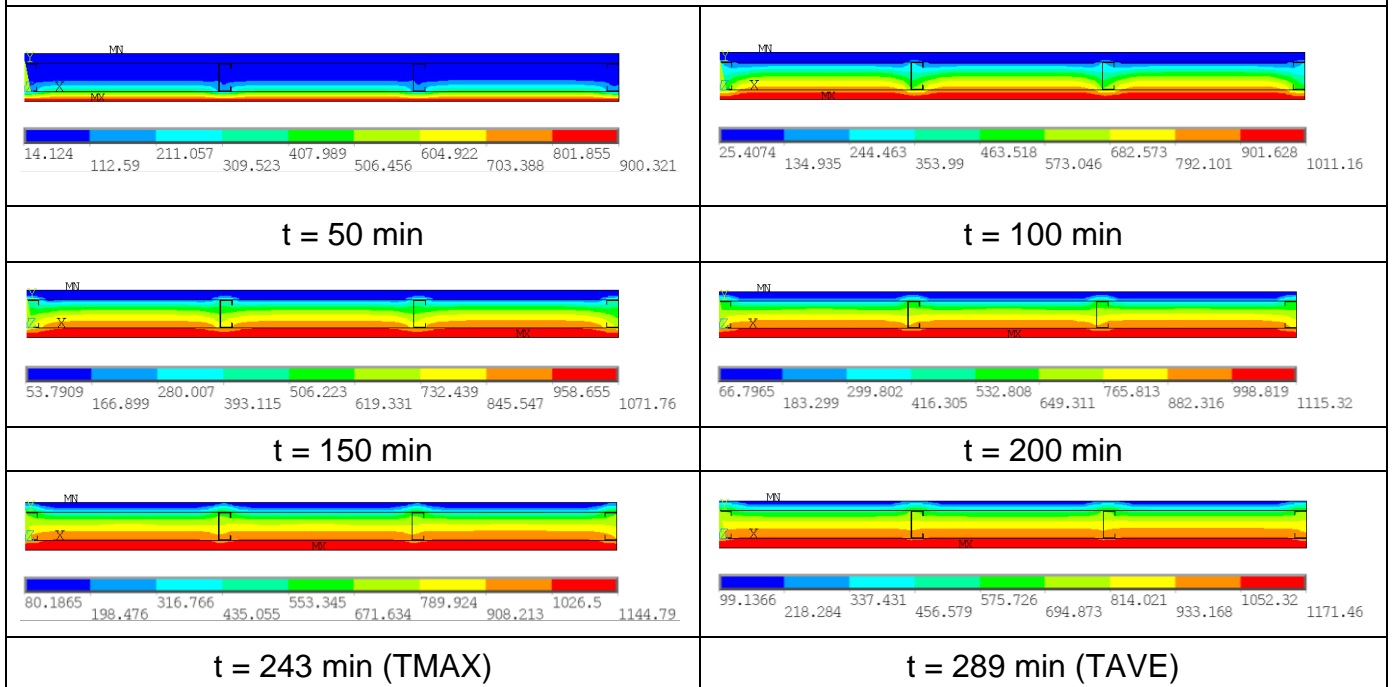
Mesh from Ansys



Comparison between all results

Unexposed curves with insulation criterion (I)

Ansys results through time



Description

Author: Rusthi, M.; Keerthan, P.; Ariyanayagam, A.; Mahendran, M. [40]

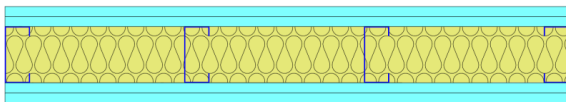
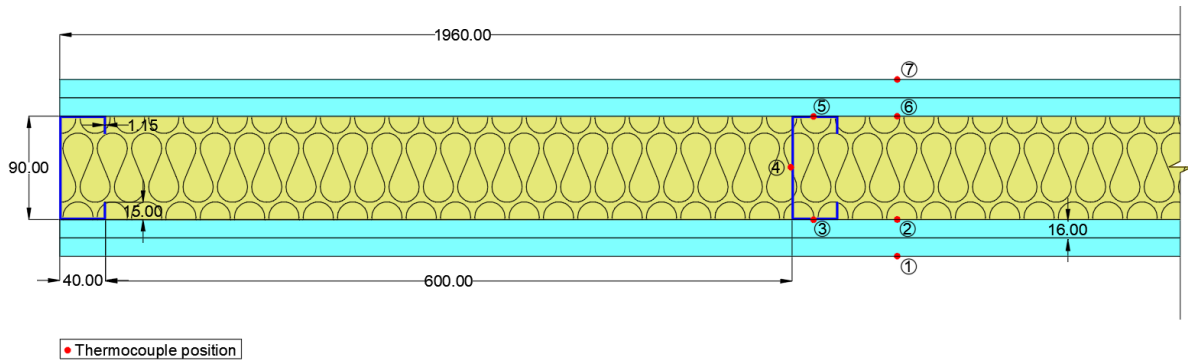
Test no.: 5

Insulation: Cellulose fibre 125kg/m³

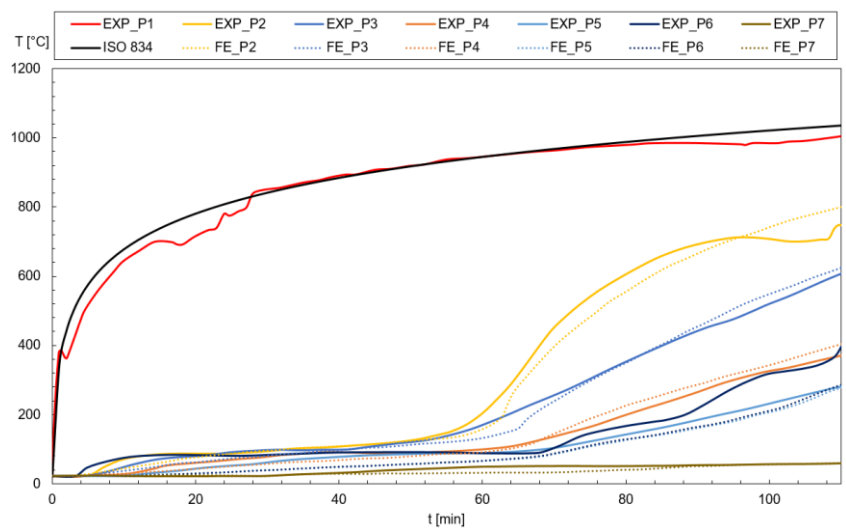
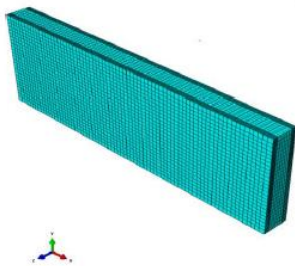
Local: Queensland University of Technology, AUS

Year: 2015

Gypsum board: 2 x 16 mm



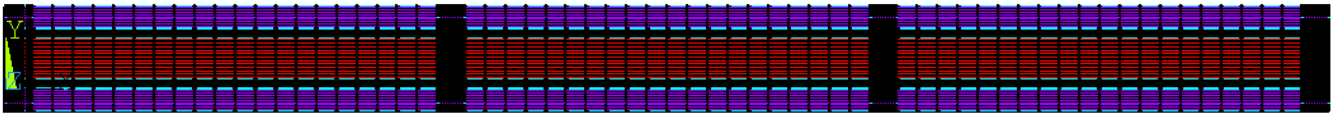
*scale drawing of the entire wall



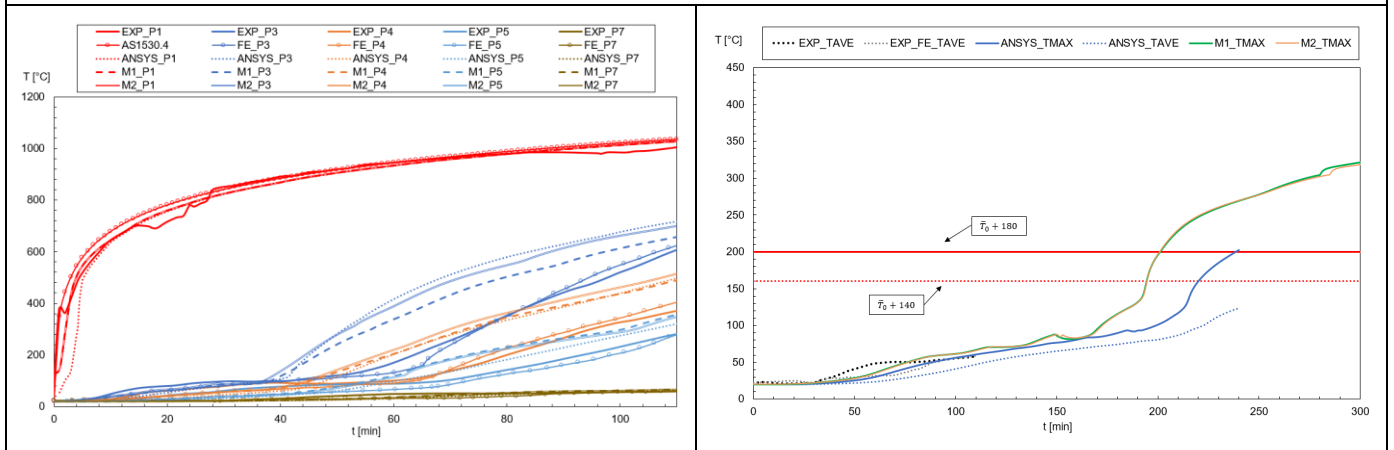
Observations:

- Dimensions in millimeters;
- Steel properties from Eurocode 3: Part 2 was used;
- Images on the left are from the experimental test and the mesh from the ABAQUS program used by the author for the finite element analysis;
- FE in the graph represents the results of the finite element analysis made by the author.

SIM. 1	WL [mm]		Matlab Fire resistance (min)		Ansys Fire resistance (min)	
	M1: 140.24	M2: 294	M1: 201	M2: 201	Ave: 201	Max: 203



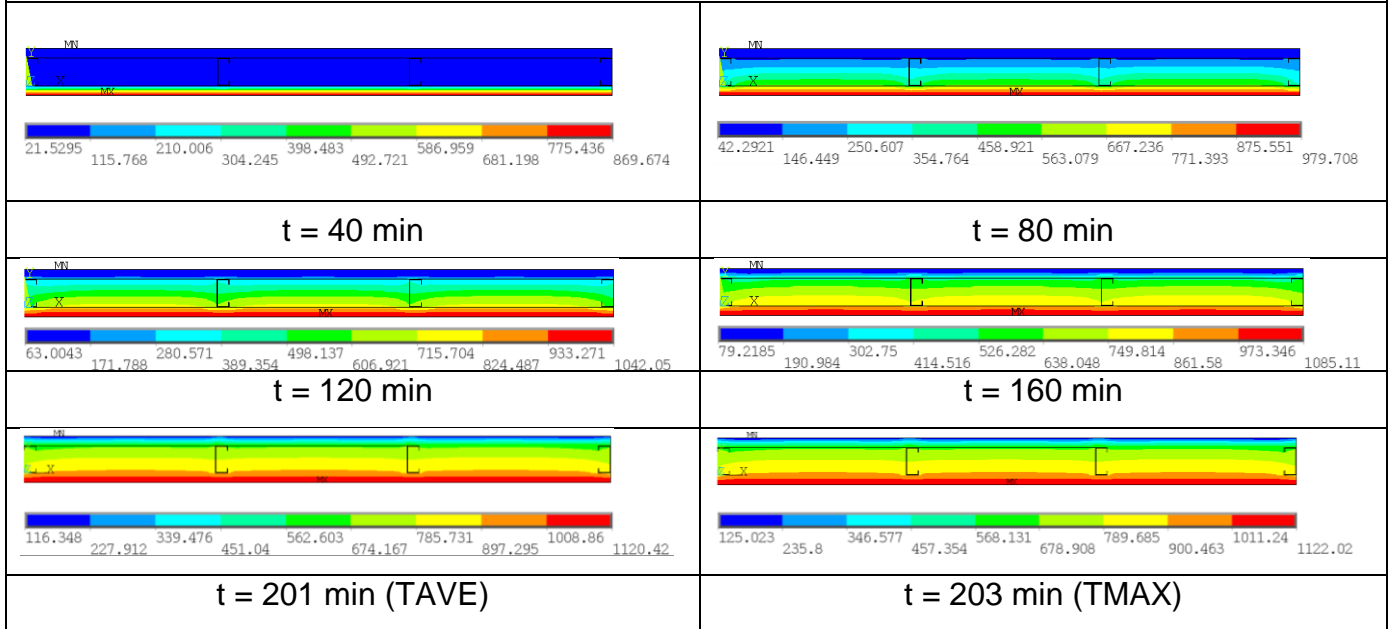
Mesh from Ansys



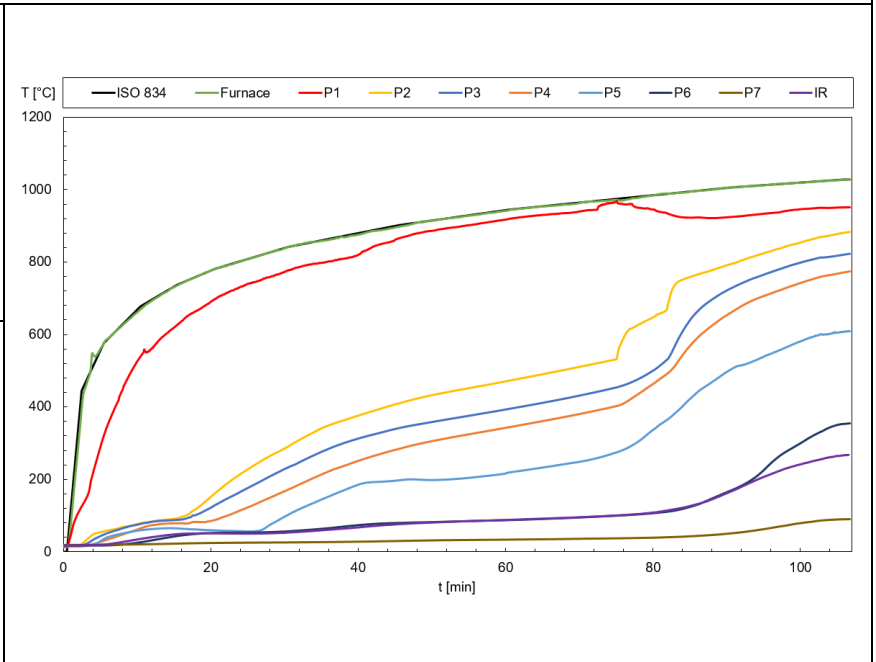
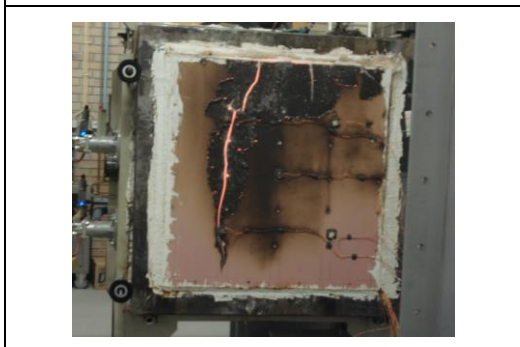
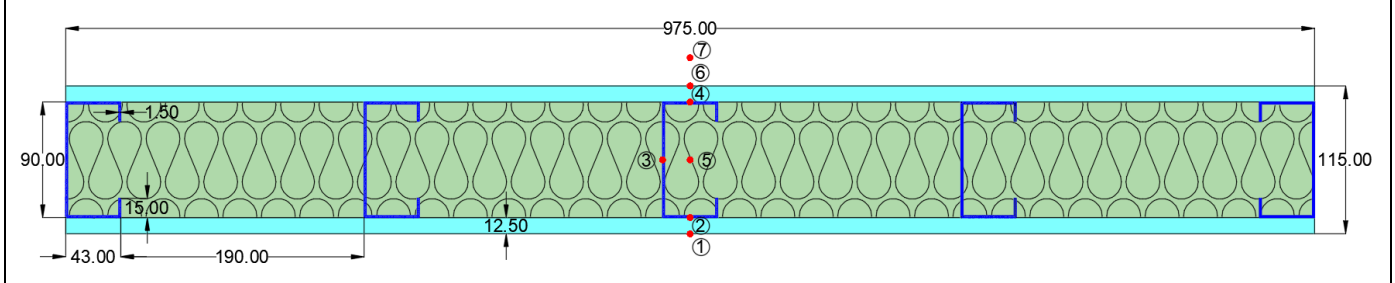
Comparison between all results

Unexposed curves with insulation criterion (I)

Ansys results through time



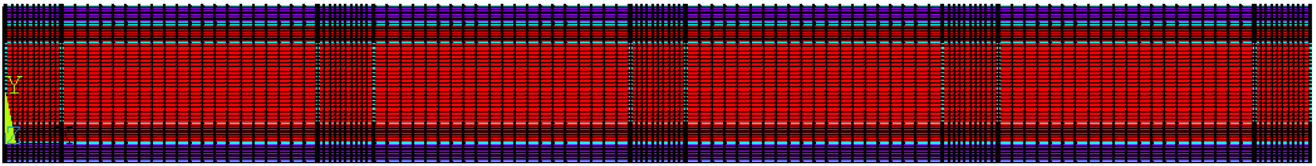
Description		
Author: Piloto, P. A. G. [44]	Test no.: 3	Insulation: Rock fibre 75kg/m ³
Local: Polytechnic Institute of Technology, PT.	Year: 2018	Gypsum board: 12.5 mm



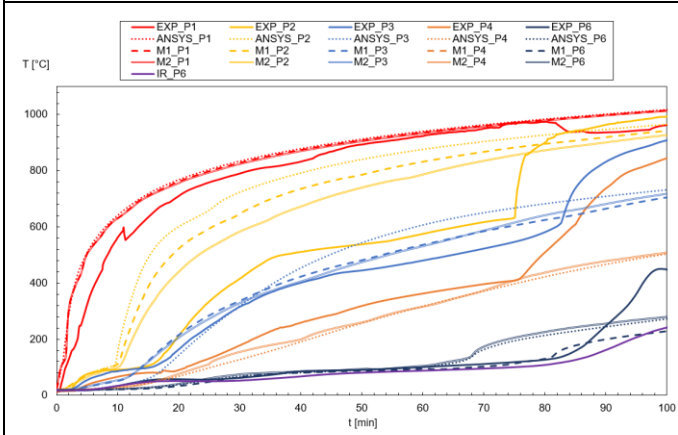
Observations:

- Dimensions in millimeters;
- Steel properties from Eurocode 3: Part 2 was used;
- IR in the graph represents the values made by an infrared thermometer of the ambient side.

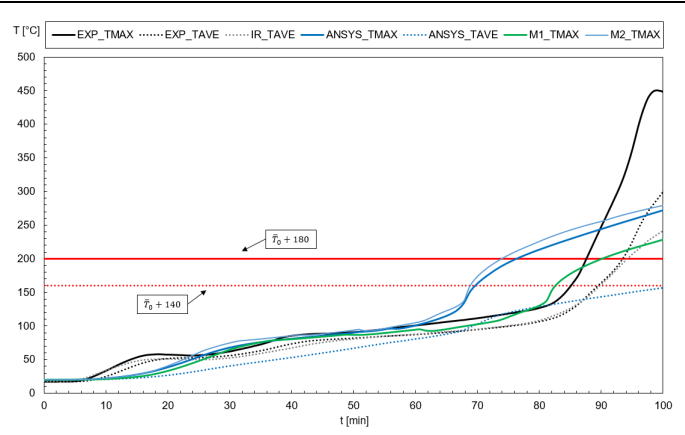
SIM. 1	WL [mm]		Matlab Fire resistance (min)		Ansys Fire resistance (min)	
	M1: 296.66	M2: 146.25	M1: 90	M2: 73	Ave: 102	Max: 76



Mesh from Ansys

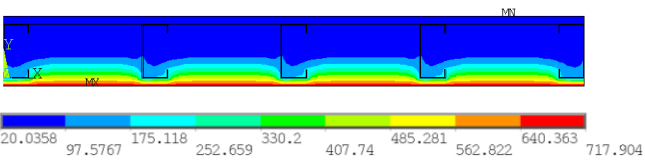


Comparison between all results

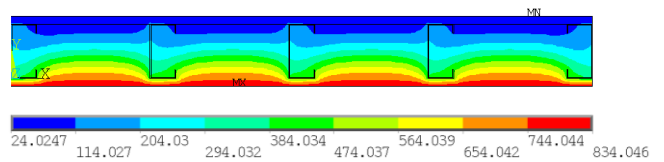


Unexposed curves with insulation criterion (I)

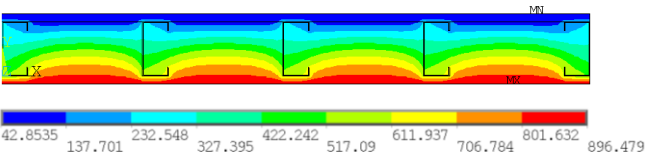
Ansys results through time



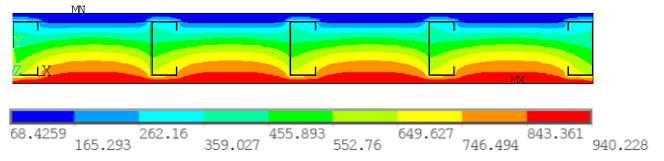
t = 15 min



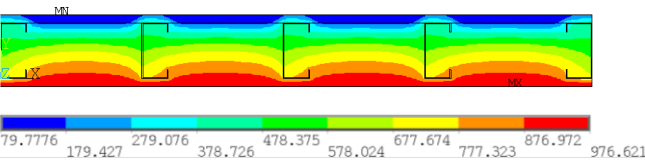
t = 30 min



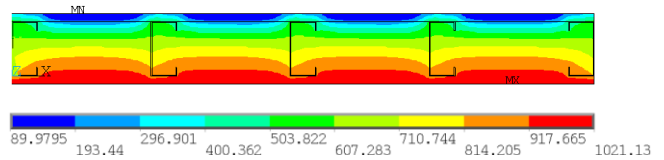
t = 45 min



t = 60 min

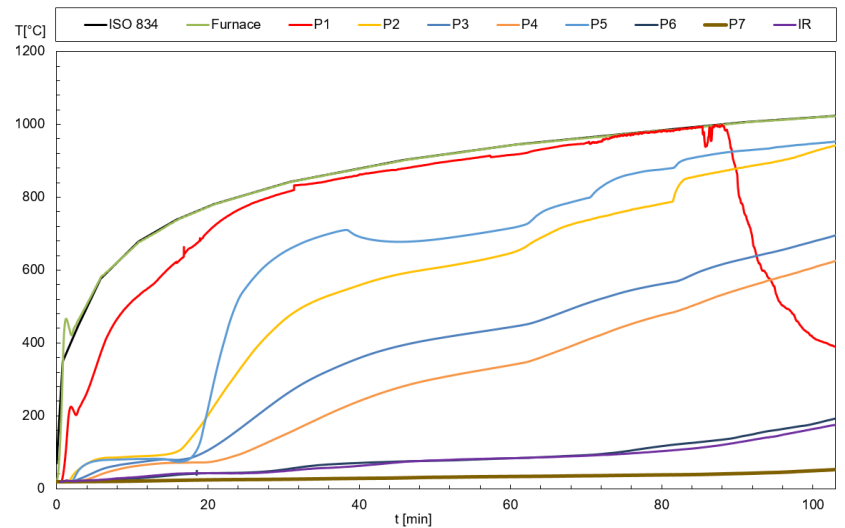
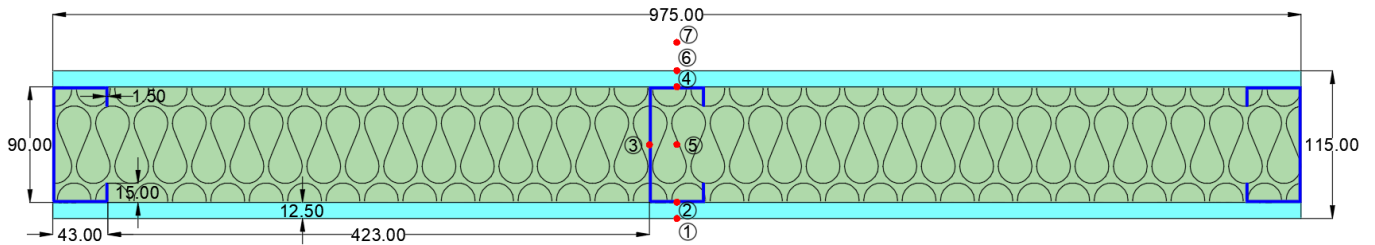


t = 76 min (TMAX)



t = 102 min (TAVE)

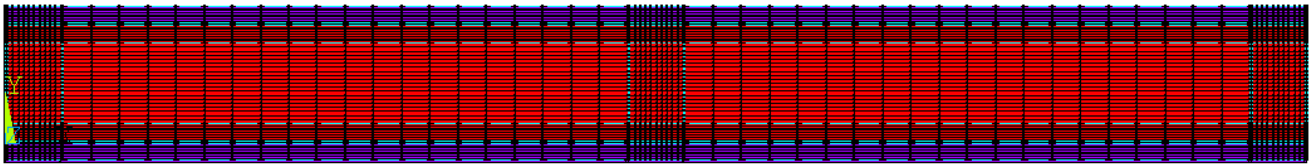
Description		
Author: Khetata, S. M.; Piloto, P. A. G., Gavilán, A. B. R. [42], [43]	Test no.: 10	Insulation: Rock fibre 75kg/m ³
Local: Polytechnic Institute of Technology, PT.	Year: 2019	Gypsum board: 12.5 mm



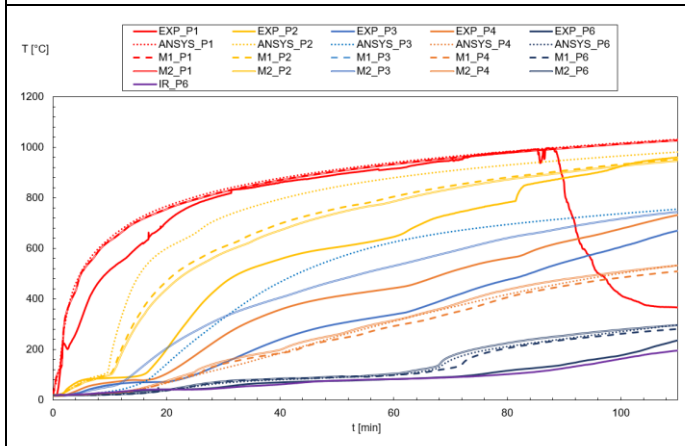
Observations:

- Dimensions in millimeters;
- Steel properties from Eurocode 3: Part 2 was used;
- IR in the graph represents the values made by an infrared thermometer of the ambient side.

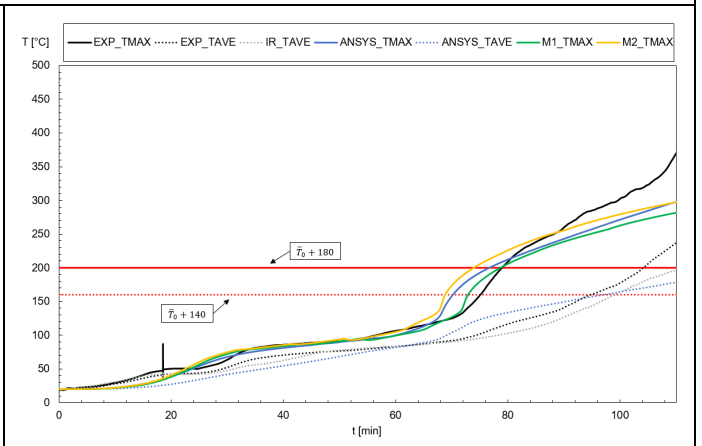
SIM. 1	WL [mm]		Matlab Fire resistance (min)		Ansys Fire resistance (min)	
	M1: 184.73	M2: 146.25	M1: 90	M2: 73	Ave: 102	Max: 76



Mesh from Ansys

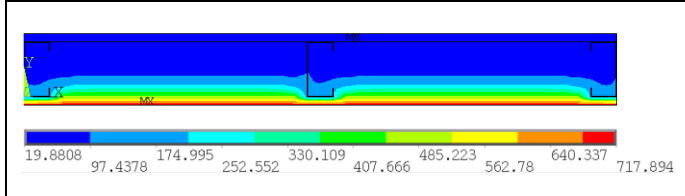


Comparison between all results

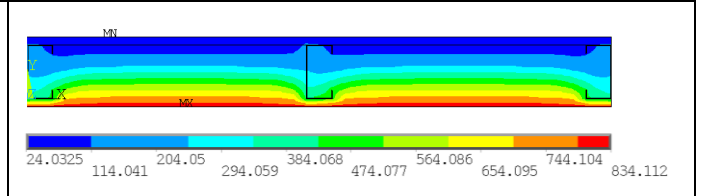


Unexposed curves with insulation criterion (I)

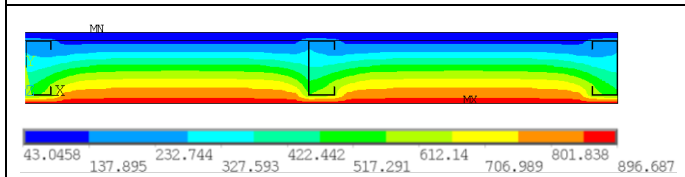
Ansys results through time



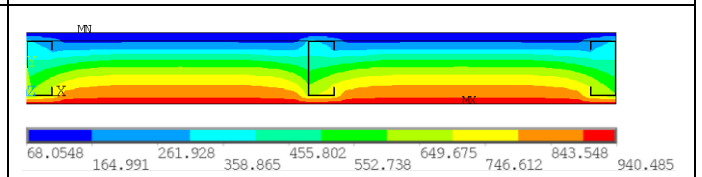
t = 15 min



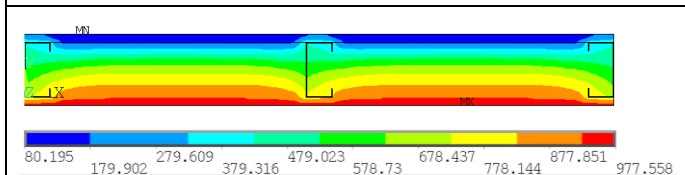
t = 30 min



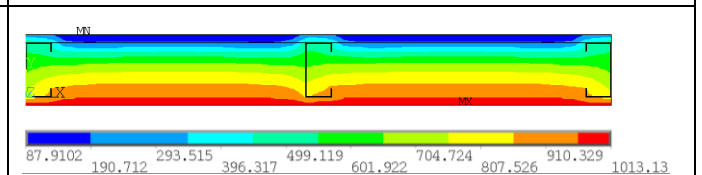
t = 45 min



t = 60 min



t = 76 min (TMAX)



t = 97 min (TAVE)

Description

Author: Khetata, S. M.; Piloto, P. A. G.,
Gavilán, A. B. R. [42], [43]

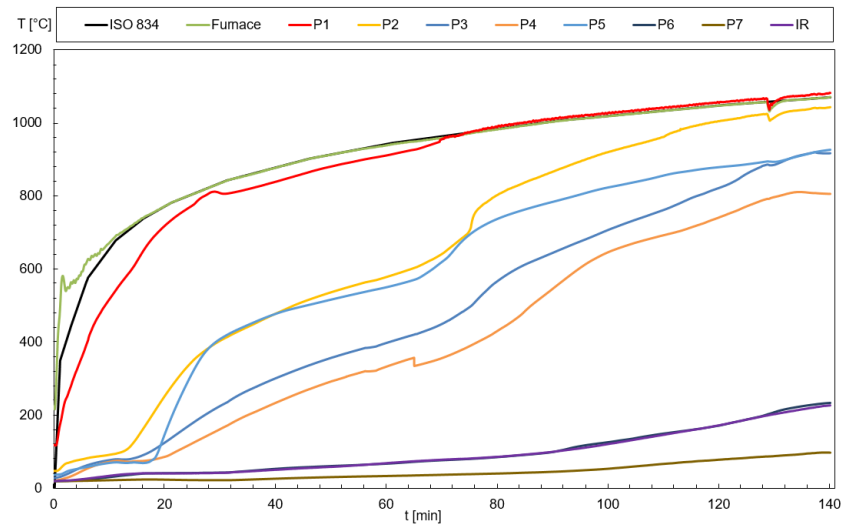
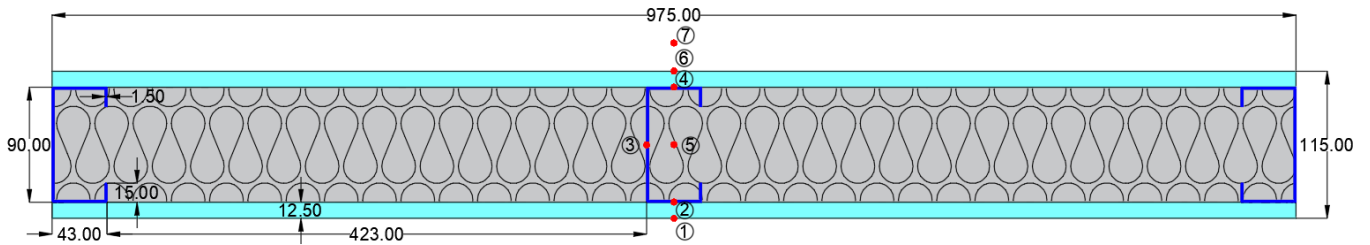
Test no.: 15

Insulation: Superwool

Local: Polytechnic Institute of
Technology, PT.

Year: 2019

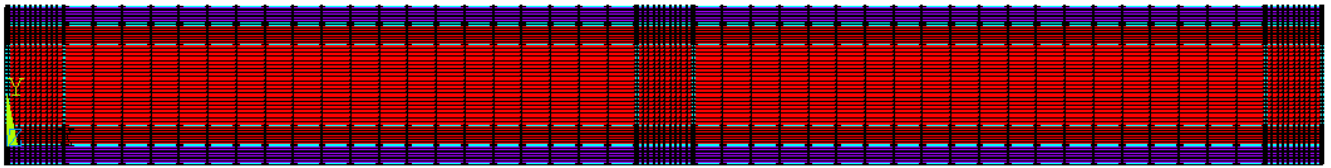
Gypsum board: 12.5 mm



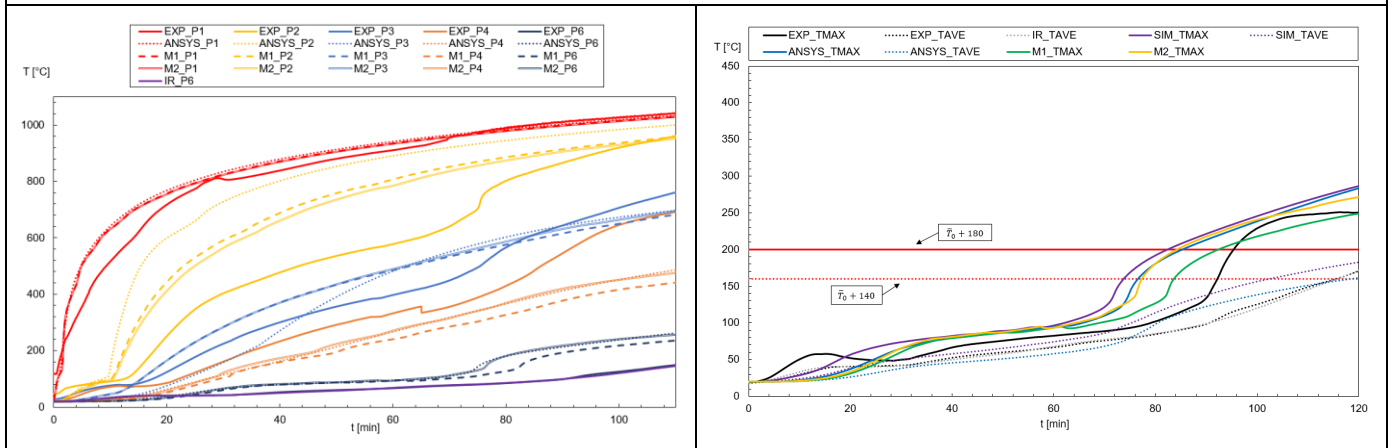
Observations:

- Dimensions in millimeters;
- Steel properties from Eurocode 3: Part 2 was used;
- IR in the graph represents the values made by an infrared thermometer of the ambient side.

SIM. 1	WL [mm]		Matlab Fire resistance (min)		Ansys Fire resistance (min)	
	M1: 184.73	M2: 146.25	M1: 92	M2: 84	Ave: 118	Max: 85



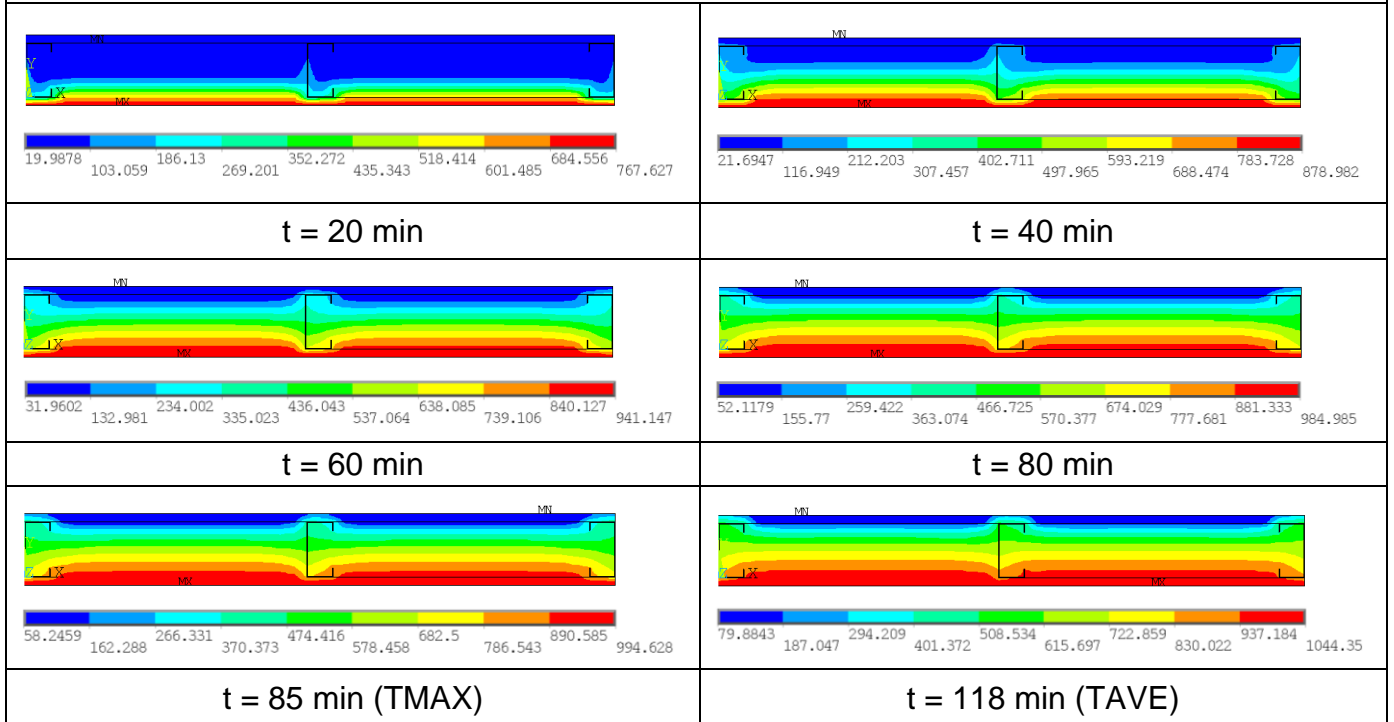
Mesh from Ansys



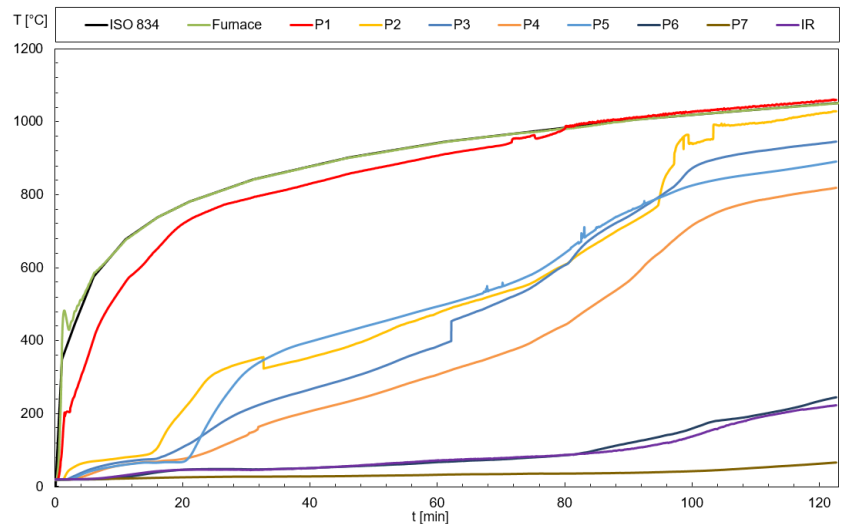
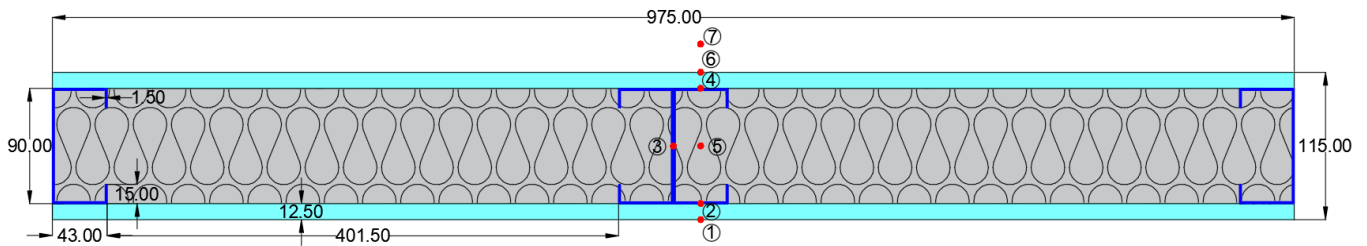
Comparison between all results

Unexposed curves with insulation criterion (I)

Ansys results through time



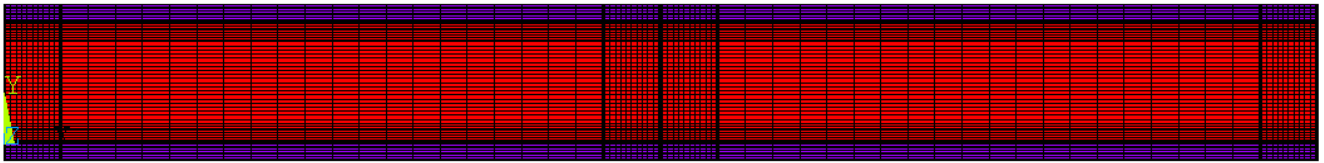
Description		
Author: Khetata, S. M.; Piloto, P. A. G.; Gavilán, A. B. R. [43]	Test no.: 16	Insulation: Superwool
Local: Polytechnic Institute of Technology, PT.	Year: 2019 (unpublished)	Gypsum board: 12.5 mm



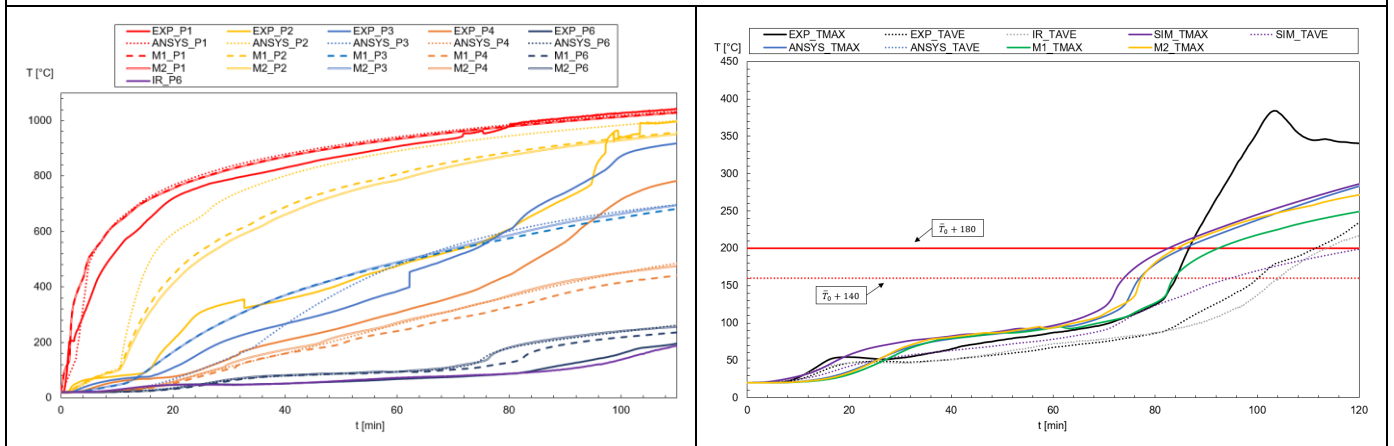
Observations:

- Dimensions in millimeters;
- Steel properties from Eurocode 3: Part 2 was used;
- IR in the graph represents the values made by an infrared thermometer of the ambient side.

SIM. 1	WL [mm]		Matlab Fire resistance (min)		Ansys Fire resistance (min)	
	M1: 184.73	M2: 146.25	M1: 92	M2: 84	Ave: 106	Max: 85



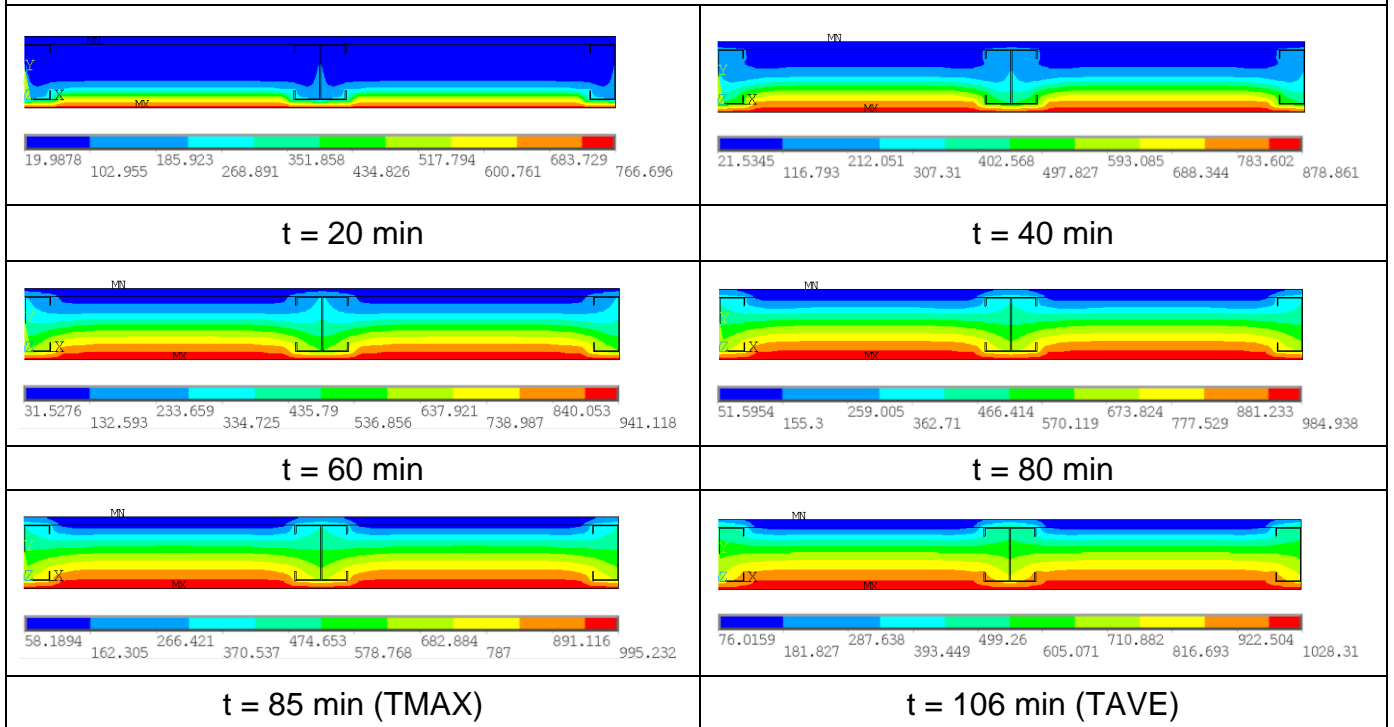
Mesh from Ansys



Comparison between all results

Unexposed curves with insulation criterion (I)

Ansys results through time



t = 20 min

t = 40 min

t = 60 min

t = 80 min

t = 85 min (TMAX)

t = 106 min (TAVE)

E. Appendix – Matlab Program

Main program – Specimen 10

```
clc;
clear all;
close all;

% variable declaration
%
% NSTEP= number of time steps
% NSTRIP= number of strip layers of materials
% MATRIX= conductivity matrix
% NODALTEMP(NTSRP)= NODAL TEMPERATURE
% TEMPINITIAL
% LOAD= load vector
% BF= width of the flange
% BW= length of the web
% BL= length of the lip
% TS= thickness of the steel profile
% TI= effective width on the left side
% BI= effective width on the right side
% TIMESTEP= time step size for incremental solution
% TOTALTIME= total time of simulation
% NSUBSTEPS=TOTALTIME/TIMESTEP
% TIME= TIME VARIABLE
% TG= thickness of the gypsum board
% ALPHACFIRE= convection coefficient for exposed side
% ALPHACUNEX= convection coefficient for unexposed side
% EPSILONFIRE= emissivity of the fire
% EPSILONM= emissivity of the material exposed to fire (Gypsum)
% TGAS= temperature of the fire
% TAMB= room temperature
% LAMDAG = conductivity of the gypsum
% ROG= specific mass of gypsum
% CPG= specific heat of gypsum
% LAMDAI= conductivity of the insulation (Rock fibre)
% ROI= specific mass of the insulation (Rock fibre)
% CPI=specific heat of the insulation (Rock fibre)
```

```

% LAMDS=conductivity of STEEL
% ROS=specific mass of the STEEL
% CPS=specific heat of the STEEL
%
% RCON56= specific resistance for heat flux by conduction from layer 5 to
layer 6
% RS156= specific resistance for heat flux by conduction through steel S1
from layer 5 to layer 6
% RS256= specific resistance for heat flux by conduction through steel S2
from layer 5 to layer 6
% RI256= specific resistance for heat flux by conduction through
insulation I2 from layer 5 to layer 6
% RS356= specific resistance for heat flux by conduction through steel S3
from layer 5 to layer 6
% RI356= specific resistance for heat flux by conduction through
insulation I3 from layer 5 to layer 6
%
% RCAP5= inverse of the capacitance of layer 5
% RG= inverse of the capacitance of gypsum
% RI15= inverse of the capacitance of the insulation (ROCKWOOL) on the
left, layer 5
% RS15= inverse of the capacitance of steel, layer 5
% RI25= inverse of the capacitance of the insulation (ROCKWOOL) on the
right, layer 5
%
% RCOND67= specific resistance for heat flux by conduction from layer 6
to layer 7
% RI167= specific resistance for heat flux by conduction through
insulation I1 from layer 6 to layer 7
% RS167= specific resistance for heat flux by conduction through steel S1
from layer 6 to layer 7
% RI267= specific resistance for heat flux by conduction through
insulation I2 from layer 6 to layer 7inverse of the capacitance of gypsum
% RS267= specific resistance for heat flux by conduction through steel S2
from layer 6 to layer 7
% RI367= specific resistance for heat flux by conduction through
insulation I3 from layer 6 to layer 7
% RI467= specific resistance for heat flux by conduction through
insulation I4 from layer 6 to layer 7
%
% RCAP6=inverse of the capacitance of layer 6
% RI16= inverse of the capacitance of the insulation (ROCKWOOL) on the
left, layer 6
% RS16= inverse of the capacitance of steel on the left, layer 6
% RI26= inverse of the capacitance of the insulation (ROCKWOOL) on the
center, layer 6

```



```

% RS26= inverse of the capacitance of steel on the right, layer 6
% RI36= inverse of the capacitance of the insulation (ROCKWOOL) on the
right, layer 6
%
% RCOND78= specific resistance for heat flux by conduction from layer 7
to layer 8
% RI178= specific resistance for heat flux by conduction through
insulation I1, on the left, from layer 7 to layer 8
% RS178= specific resistance for heat flux by conduction through steel
S1, on the left, from layer 7 to layer 8
% RI278= specific resistance for heat flux by conduction through
insulation I2, on the center, from layer 7 to layer 8
% RI378= specific resistance for heat flux by conduction through
insulation I3, on the center righth, from layer 7 to layer 8
% RI478= specific resistance for heat flux by conduction through
insulation I4, on the righth, from layer 7 to layer 8
%
% RCAP7=inverse of the capacitance of layer 7
% RI17= inverse of the capacitance of the insulation (ROCKWOOL) on the
left, layer 7
% RS17= inverse of the capacitance of steel on the left, layer 7
% RI27= inverse of the capacitance of the insulation (ROCKWOOL) on the
center, layer 7
% RI37= inverse of the capacitance of the insulation (ROCKWOOL) on the
center righth, layer 7
% RI47= inverse of the capacitance of the insulation (ROCKWOOL) on the
right, layer 7
% COND89= specific resistance for heat flux by conduction from layer 8 to
layer 9
% RI189= specific resistance for heat flux by conduction through
insulation I1, on the left, from layer 8 to layer 9
% RS189= specific resistance for heat flux by conduction through steel
S1, on the left, from layer 8 to layer 9
% RI289= specific resistance for heat flux by conduction through
insulation I2, on the center, from layer 8 to layer 9
% RI389= specific resistance for heat flux by conduction through
insulation I3, on the center righth, from layer 8 to layer 9
% RS289= specific resistance for heat flux by conduction through steel
S2, on the right, from layer 8 to layer 9
% RI489= specific resistance for heat flux by conduction through
insulation I4, on the righth, from layer 8 to layer 9
%
% RCAP8=inverse of the capacitance of layer 8
% RI18= inverse of the capacitance of the insulation (ROCKWOOL) on the
left, layer 8
% RS18= inverse of the capacitance of steel on the left, layer 8

```

```

% RI28= inverse of the capacitance of the insulation (ROCKWOOL) on the
center, layer 8
% RI38= inverse of the capacitance of the insulation (ROCKWOOL) on the
center righth, layer 8
% RI48= inverse of the capacitance of the insulation (ROCKWOOL) on the
right, layer 8
%
% RCOND910= specific resistance for heat flux by conduction from layer 9
to layer 10
% RI1910= specific resistance for heat flux by conduction through
insulation I1, on the left, from layer 9 to layer 10
% RS1910= specific resistance for heat flux by conduction through steel
S1, on the left, from layer 9 to layer 10
% RI2910= specific resistance for heat flux by conduction through
insulation I2, on the center, from layer 9 to layer 10
% RS2910= specific resistance for heat flux by conduction through steel
S2, on the center, from layer 9 to layer 10
% RS3910= specific resistance for heat flux by conduction through steel
S3, on the right, from layer 9 to layer 10
% RI3910= specific resistance for heat flux by conduction through
insulation I3, on the righth, from layer 9 to layer 10
%
% RCAP9=inverse of the capacitance of layer 9
% RI19= inverse of the capacitance of the insulation (ROCKWOOL) on the
left, layer 9
% RS19= inverse of the capacitance of steel on the left, layer 9
% RI29= inverse of the capacitance of the insulation (ROCKWOOL) on the
center, layer 9
% RS29= inverse of the capacitance of steel on the right, layer 9
% RI39= inverse of the capacitance of the insulation (ROCKWOOL) on the
right, layer 9
%
% RCAP10=inverse of the capacitance of layer 10
% RG2= inverse of the capacitance of gypsum (UNXPOSED SIDE)
% RI110= inverse of the capacitance of the insulation (ROCKWOOL) on the
left, layer 10
% RS110= inverse of the capacitance of steel from the flange, layer 10
% RI210= inverse of the capacitance of the insulation (ROCKWOOL) on the
right, layer 10
%
% TAVE12= AVERAGE TEMPERATURE OF NODALTEMP(1) AND NODALTEMP(2) USED TO
CALCULATE THE THERMAL CONDUCTIVITY
% TAVE23= AVERAGE TEMPERATURE OF NODALTEMP(2) AND NODALTEMP(3) USED TO
CALCULATE THE THERMAL CONDUCTIVITY
% TAVE34= AVERAGE TEMPERATURE OF NODALTEMP(3) AND NODALTEMP(4) USED TO
CALCULATE THE THERMAL CONDUCTIVITY

```

```

% TAVE45= AVERAGE TEMPERATURE OF NODALTEMP(4) AND NODALTEMP(5) USED TO
CALCULATE THE THERMAL CONDUCTIVITY

% TAVE56= AVERAGE TEMPERATURE OF NODALTEMP(5) AND NODALTEMP(6) USED TO
CALCULATE THE THERMAL RESISTANCE RCOND56

% TAVE67= AVERAGE TEMPERATURE OF NODALTEMP(6) AND NODALTEMP(7) USED TO
CALCULATE THE THERMAL RESISTANCE RCOND67

% TAVE78= AVERAGE TEMPERATURE OF NODALTEMP(7) AND NODALTEMP(8) USED TO
CALCULATE THE THERMAL RESISTANCE RCOND78

% TAVE89= AVERAGE TEMPERATURE OF NODALTEMP(8) AND NODALTEMP(9) USED TO
CALCULATE THE THERMAL RESISTANCE RCOND89

% TAVE910= AVERAGE TEMPERATURE OF NODALTEMP(9) AND NODALTEMP(10) USED TO
CALCULATE THE THERMAL RESISTANCE RCOND910

% TAVE1011= AVERAGE TEMPERATURE OF NODALTEMP(10) AND NODALTEMP(11) USED
TO CALCULATE THE THERMAL CONDUCTIVITY

% TAVE1112= AVERAGE TEMPERATURE OF NODALTEMP(11) AND NODALTEMP(12) USED
TO CALCULATE THE THERMAL CONDUCTIVITY

% TAVE1213= AVERAGE TEMPERATURE OF NODALTEMP(12) AND NODALTEMP(13) USED
TO CALCULATE THE THERMAL CONDUCTIVITY

% TAVE1314= AVERAGE TEMPERATURE OF NODALTEMP(13) AND NODALTEMP(14) USED
TO CALCULATE THE THERMAL CONDUCTIVITY

%

% X(NSTRIP)= result of the temperature in each layer, from 1 to 14 for a
specific time

% XFINAL(NSTRIP, NSUBSTEPS)= result of the tmeperature in each layer and
for every substep in time

%%LSF DIMENSION DEFINITION

WW=0.975;           %wall width (if necessary)
BF=0.043;           %flange length (m)
BW=0.090;           %web length (m)
BL=0.015;           %lip length (m)
TS=0.0015;          %steel profile thickness (m)
TG=0.0125;          %gypsum thickness (m)
WL=0.15*WW;         %effective width (m)
TEMPINITIAL=20;     %initial temperature for every node (°C)
TAMB=20;             %room temperature for unexposed side (°C)
TOTALTIME=14400;    %total time for simulation (s)
NSUBSTEPS=3600;     %number of time steps -> integer

NSTRIP=14;           %layer number
TIMESTEP=TOTALTIME/NSUBSTEPS;

```

```
%%Definition of parameters
```

```
TI=(WL-BF)/2;
```

```
BI=TI;
```

```
%convection coefficient
```

```
ALPHACFIRE=25.0;
```

```
ALPHACUNEX=9.0;
```

```
%emissivity coefficient
```

```
EPSILONFIRE=1.0;
```

```
EPSILONM=0.8;
```

```
%other parameters
```

```
STEFAN=5.67e-8;
```

```
MATRIX=zeros(14,14);
```

```
MATRIX1=zeros(14,14);
```

```
NODALTEMP(1,1:14)=TEMPINITIAL;
```

```
OLDNODALTEMP(1,1:14)=TEMPINITIAL;
```

```
TIME=0.;
```

```
XFINAL=zeros(NSUBSTEPS, NSTRIP);
```

```
X=zeros(NSTRIP,1);
```

```
ALPHAR=zeros(1,NSUBSTEPS);
```

```
%%Time incremental solution
```

```
for i=1:NSUBSTEPS;
```

```
    %in each time step, the vector of the nodal temperature is separated  
    into
```

```
    %old and actual
```

```

TIME=TIME+TIMESTEP;

%      %Variables initialization

%Linearization of radiation coefficient

ALPHAR(i)=EPSILONFIRE*EPSILONM*STEFAN*((TGAS(i,TIME)+273.1)+(NODALTEMP(1)
+273.1))*((TGAS(i,TIME)+273.1)^2+(NODALTEMP(1)+273.1)^2);

%%Definition of the equilibrium equations

%EQUATION 1

TAVE12=(NODALTEMP(1)+NODALTEMP(2))/2;

MATRIX(1,1)=- (ALPHAR(i)+ALPHACFIRE)*WL-LAMDAG(TAVE12)*WL/(TG/4.)-
ROG(NODALTEMP(1))*CPG(NODALTEMP(1))*WL*(TG/8.)/TIMESTEP;

MATRIX(1,2)=+LAMDAG(TAVE12)*WL/(TG/4.);

MATRIX(1,3:14)=0.;

LOAD(1)=- (ALPHAR(i)+ALPHACFIRE)*TGAS(i,TIME)*WL-
ROG(NODALTEMP(1))*CPG(NODALTEMP(1))*WL*(TG/8.)*1/TIMESTEP*NODALTEMP(1);

%EQUATION 2

TAVE23=(NODALTEMP(2)+NODALTEMP(3))/2;

MATRIX(2,1)=WL*LAMDAG(TAVE12)/(TG/4.);
MATRIX(2,2)=-WL*LAMDAG(TAVE12)/(TG/4.)-WL*LAMDAG(TAVE23)/(TG/4.)-
ROG(NODALTEMP(2))*CPG(NODALTEMP(2))*WL*(TG/4.)/TIMESTEP;
MATRIX(2,3)=LAMDAG(TAVE23)*WL/(TG/4.);

MATRIX(2,4:14)=0.;

LOAD(2)=-
ROG(NODALTEMP(2))*CPG(NODALTEMP(2))*WL*(TG/4.)*1/TIMESTEP*NODALTEMP(2);

%EQUATION 3

```

```

TAVE34=(NODALTEMP(3)+NODALTEMP(4))/2;

MATRIX(3,1)=0.;

MATRIX(3,2)=WL*LAMDAG(TAVE23)/(TG/4.);
MATRIX(3,3)=-WL*LAMDAG(TAVE23)/(TG/4.)-WL*LAMDAG(TAVE34)/(TG/4.)-
ROG(NODALTEMP(3))*CPG(NODALTEMP(3))*WL*(TG/4.)/Timestep;
MATRIX(3,4)=+LAMDAG(TAVE34)*WL/(TG/4.);

MATRIX(3,5:14)=0.;

LOAD(3)=-
ROG(NODALTEMP(3))*CPG(NODALTEMP(3))*WL*(TG/4.)*1/Timestep*NODALTEMP(3);

%EQUATION 4

TAVE45=(NODALTEMP(4)+NODALTEMP(5))/2;

MATRIX(4,1:2)=0.;

MATRIX(4,3)=WL*LAMDAG(TAVE34)/(TG/4.);
MATRIX(4,4)=-WL*LAMDAG(TAVE34)/(TG/4.)-WL*LAMDAG(TAVE45)/(TG/4.)-
ROG(NODALTEMP(4))*CPG(NODALTEMP(4))*WL*(TG/4.)/Timestep;
MATRIX(4,5)=+LAMDAG(TAVE45)*WL/(TG/4.);

MATRIX(4,6:14)=0.;

LOAD(4)=-
ROG(NODALTEMP(4))*CPG(NODALTEMP(4))*WL*(TG/4.)*1/Timestep*NODALTEMP(4);

%EQUATION 5

TAVE56=(NODALTEMP(5)+NODALTEMP(6))/2;

RI156=(TS+(BL-TS)/2)/(LAMDAL(TAVE56)*TI);
RS156=(TS+(BL-TS)/2)/(LAMDAS(TAVE56)*TS);
RS256=(TS)/(LAMDAS(TAVE56)*(BF-2*TS));
RI256=((BL-TS)/2)/(LAMDAL(TAVE56)*(BF-2*TS));

```

```
RS356=(TS+(BL-TS)/2)/(LAMDAS(TAVE56)*TS);
RI356=(TS+(BL-TS)/2)/(LAMDAI(TAVE56)*BI);
```

```
RCOND56=1/(1/RI156+1/RS156+1/(RS256+RI256)+1/RS356+1/RI356);
```

```
RG=TIMESTEP/(ROG(NODALTEMP(5))*CPG(NODALTEMP(5))*TG/8.*WL);
RI15=TIMESTEP/(ROI(NODALTEMP(5))*CPI(NODALTEMP(5))*TS*TI);
RS15=TIMESTEP/(ROS(NODALTEMP(5))*CPS(NODALTEMP(5))*TS*BF);
RI25=TIMESTEP/(ROI(NODALTEMP(5))*CPI(NODALTEMP(5))*TS*BI);
```

```
RCAP5=RG+1/(1/RI15+1/RS15+1/RI25);
```

```
MATRIX(5,1:3)=0.;
```

```
MATRIX(5,4)=+WL*LAMDAG(TAVE45)/(TG/4.);
MATRIX(5,5)=-WL*LAMDAG(TAVE45)/(TG/4.)-1/RCOND56-1/RCAP5;
MATRIX(5,6)=1/RCOND56;
```

```
MATRIX(5,7:14)=0.;
```

```
LOAD(5)=-1/RCAP5*NODALTEMP(5);
```

```
%EQUATION 6
```

```
TAVE67=(NODALTEMP(6)+NODALTEMP(7))/2;
```

```
RI167=(BW/4-TS/2)/(LAMDAI(TAVE67)*TI);
RS167=(BW/4-TS/2)/(LAMDAS(TAVE67)*TS);
RI267=(BW/4-TS/2)/(LAMDAI(TAVE67)*(BF-2*TS));
RS267=((BL-TS)/2)/(LAMDAS(TAVE67)*TS);
RI367=((BW-2*BL)/4)/(LAMDAI(TAVE67)*TS);
RI467=(BW/4-TS/2)/(LAMDAI(TAVE67)*BI);
```

```
RCOND67=1/(1/RI167+1/RS167+1/RI267+1/(RS267+RI367)+1/RI467);
```

```
RI16=TIMESTEP/(ROI(NODALTEMP(6))*CPI(NODALTEMP(6))*(BL-TS)*TI);
RS16=TIMESTEP/(ROS(NODALTEMP(6))*CPS(NODALTEMP(6))*(BL-TS)*TS);
RI26=TIMESTEP/(ROI(NODALTEMP(6))*CPI(NODALTEMP(6))*(BL-TS)*(BF-2*TS));
```

```
RS26=TIMESTEP/ (ROS (NODALTEMP (6)) *CPS (NODALTEMP (6)) * (BL-TS) *TS) ;  
RI36=TIMESTEP/ (ROI (NODALTEMP (6)) *CPI (NODALTEMP (6)) * (BL-TS) *BI) ;
```

```
RCAP6=1/ (1/RI16+1/RS16+1/RI26+1/RS26+1/RI36) ;
```

```
MATRIX (6, 1:4)=0. ;
```

```
MATRIX (6, 5)=+1/RCOND56 ;
```

```
MATRIX (6, 6)=-1/RCOND56-1/RCOND67-1/RCAP6 ;
```

```
MATRIX (6, 7)=+1/RCOND67 ;
```

```
MATRIX (6, 8:14)=0. ;
```

```
LOAD (6)=-1/RCAP6*NODALTEMP (6) ;
```

```
%EQUATION 7
```

```
TAVE78= (NODALTEMP (7) +NODALTEMP (8)) /2 ;
```

```
RI178= ( (BW-2*BL) /2) / (LAMDAI (TAVE78) *TI) ;
```

```
RS178= ( (BW-2*BL) /2) / (LAMDAI (TAVE78) *TS) ;
```

```
RI278= ( (BW-2*BL) /2) / (LAMDAI (TAVE78) * (BF-2*TS)) ;
```

```
RI378= ( (BW-2*BL) /2) / (LAMDAI (TAVE78) *TS) ;
```

```
RI478= ( (BW-2*BL) /2) / (LAMDAI (TAVE78) *BI) ;
```

```
RCOND78=1/ (1/RI178+1/RS178+1/RI278+1/RI378+1/RI478) ;
```

```
RI17=TIMESTEP/ (ROI (NODALTEMP (7)) *CPI (NODALTEMP (7)) * (BW-2*BL) /2*TI) ;
```

```
RS17=TIMESTEP/ (ROS (NODALTEMP (7)) *CPS (NODALTEMP (7)) * (BW-2*BL) /2*TS) ;
```

```
RI27=TIMESTEP/ (ROI (NODALTEMP (7)) *CPI (NODALTEMP (7)) * (BW-2*BL) /2* (BF-  
2*TS)) ;
```

```
RI37=TIMESTEP/ (ROI (NODALTEMP (7)) *CPI (NODALTEMP (7)) * (BW-2*BL) /2*TS) ;
```

```
RI47=TIMESTEP/ (ROI (NODALTEMP (7)) *CPI (NODALTEMP (7)) * (BW-2*BL) /2*BI) ;
```

```
RCAP7=1/ (1/RI17+1/RS17+1/RI27+1/RI37+1/RI47) ;
```

```
MATRIX (7, 1:5)=0. ;
```



```
MATRIX (7, 6)=+1/RCOND67;  
MATRIX (7, 7)=-1/RCOND67-1/RCOND78-1/RCAP7;  
MATRIX (7, 8)=+1/RCOND78;
```

```
MATRIX (7, 9:14)=0;
```

```
LOAD (7)=-1/RCAP7*NODALTEMP (7);
```

```
%EQUATION 8
```

```
TAVE89=(NODALTEMP (8)+NODALTEMP (9))/2;
```

```
RI189=(BW/4-TS/2)/(LAMDAI (TAVE89)*TI);
```

```
RS189=(BW/4-TS/2)/(LAMDAS (TAVE89)*TS);
```

```
RI289=(BW/4-TS/2)/(LAMDAI (TAVE89)*(BF-2*TS));
```

```
RI389=((BW-2*BL)/4)/(LAMDAI (TAVE89)*TS);
```

```
RS289=((BL-TS)/2)/(LAMDAS (TAVE89)*TS);
```

```
RI489=(BW/4-TS/2)/(LAMDAI (TAVE89)*BI);
```

```
RCOND89=1/(1/RI189+1/RS189+1/RI289+1/(RI389+RS289)+1/RI489);
```

```
RI18=TIMESTEP/(ROI (NODALTEMP (8))*CPI (NODALTEMP (8))*(BW-2*BL)/2*TI);
```

```
RS18=TIMESTEP/(ROS (NODALTEMP (8))*CPS (NODALTEMP (8))*(BW-2*BL)/2*TS);
```

```
RI28=TIMESTEP/(ROI (NODALTEMP (8))*CPI (NODALTEMP (8))*(BW-2*BL)/2*(BF-  
2*TS));
```

```
RI38=TIMESTEP/(ROI (NODALTEMP (8))*CPI (NODALTEMP (8))*(BW-2*BL)/2*TS);
```

```
RI48=TIMESTEP/(ROI (NODALTEMP (8))*CPI (NODALTEMP (8))*(BW-2*BL)/2*BI);
```

```
RCAP8=1/(1/RI18+1/RS18+1/RI28+1/RI38+1/RI48);
```

```
MATRIX (8, 1:6)=0.;
```

```
MATRIX (8, 7)=+1/RCOND78;
```

```
MATRIX (8, 8)=-1/RCOND78-1/RCOND89-1/RCAP8;
```

```
MATRIX (8, 9)=+1/RCOND89;
```

```
MATRIX (8, 10:14)=0.;
```

```
LOAD (8)=-1/RCAP8*NODALTEMP (8) ;
```

```
%EQUATION 9
```

```
TAVE910=(NODALTEMP (9)+NODALTEMP (10))/2;
```

```
RI1910=(BL/2+TS/2)/(LAMDAI (TAVE910)*TI) ;
```

```
RS1910=(BL/2+TS/2)/(LAMDAS (TAVE910)*TS) ;
```

```
RI2910=((BL-TS)/2)/(LAMDAI (TAVE910)*(BF-2*TS)) ;
```

```
RS2910=(TS)/(LAMDAS (TAVE910)*(BF-2*TS)) ;
```

```
RS3910=(BL/2+TS/2)/(LAMDAS (TAVE910)*TS) ;
```

```
RI3910=(BL/2+TS/2)/(LAMDAI (TAVE910)*BI) ;
```

```
RCOND910=1/(1/RI1910+1/RS1910+1/(RI2910+RS2910)+1/RS3910+1/RI3910) ;
```

```
RI19=TIMESTEP/(ROI (NODALTEMP (9))*CPI (NODALTEMP (9))*(BL-TS)*TI) ;
```

```
RS19=TIMESTEP/(ROS (NODALTEMP (9))*CPS (NODALTEMP (9))*(BL-TS)*TS) ;
```

```
RI29=TIMESTEP/(ROI (NODALTEMP (9))*CPI (NODALTEMP (9))*(BL-TS)*(BF-  
2*TS)) ;
```

```
RS29=TIMESTEP/(ROS (NODALTEMP (9))*CPS (NODALTEMP (9))*(BL-TS)*TS) ;
```

```
RI39=TIMESTEP/(ROI (NODALTEMP (9))*CPI (NODALTEMP (9))*(BL-TS)*BI) ;
```

```
RCAP9=1/(1/RI19+1/RS19+1/RI29+1/RS29+1/RI39) ;
```

```
MATRIX (9,1:7)=0. ;
```

```
MATRIX (9,8)=+1/RCOND89;
```

```
MATRIX (9,9)=-1/RCOND89-1/RCOND910-1/RCAP9;
```

```
MATRIX (9,10)=+1/RCOND910;
```

```
MATRIX (9,11:14)=0. ;
```

```
LOAD (9)=-1/RCAP9*NODALTEMP (9) ;
```

```
%EQUATION 10
```

```
TAVE1011=(NODALTEMP (10)+NODALTEMP (11))/2;
```

```

RG2=TIMESTEP/ (ROG (NODALTEMP (10)) *CPG (NODALTEMP (10)) * (TG/8.) *WL) ;
RI110=TIMESTEP/ (ROI (NODALTEMP (10)) *CPI (NODALTEMP (10)) * (TS) * (TI)) ;
RS110=TIMESTEP/ (ROS (NODALTEMP (10)) *CPS (NODALTEMP (10)) * (TS) *BF) ;
RI210=TIMESTEP/ (ROI (NODALTEMP (10)) *CPI (NODALTEMP (10)) * (TS) *BI) ;

RCAP10=RG2+1/ (1/RI110+1/RS110+1/RI210) ;

MATRIX (10, 1:8)=0. ;

MATRIX (10, 9)=+1/RCOND910 ;
MATRIX (10, 10)=-1/RCOND910-LAMDAG (TAVE1011) *WL/ (TG/4.) -1/RCAP10 ;
MATRIX (10, 11)=+LAMDAG (TAVE1011) *WL/ (TG/4.) ;

MATRIX (10, 12:14)=0. ;

LOAD (10)=-1/RCAP10*NODALTEMP (10) ;

%EQUATION 11

TAVE1112= (NODALTEMP (11) +NODALTEMP (12)) /2 ;

MATRIX (11, 1:9)=0. ;

MATRIX (11, 10)=+LAMDAG (TAVE1011) *WL/ (TG/4.) ;
MATRIX (11, 11)=-LAMDAG (TAVE1011) *WL/ (TG/4.) -
LAMDAG (TAVE1112) *WL/ (TG/4.) -
ROG (NODALTEMP (11)) *CPG (NODALTEMP (11)) * (TG/4.) *WL/TIMESTEP ;
MATRIX (11, 12)=+LAMDAG (TAVE1112) *WL/ (TG/4.) ;

MATRIX (11, 13:14)=0. ;

LOAD (11)=-
ROG (NODALTEMP (11)) *CPG (NODALTEMP (11)) *WL* (TG/4.) *1/TIMESTEP*NODALTEMP (11)
;

%EQUATION 12

```

```

TAVE1213= (NODALTEMP (12) +NODALTEMP (13)) /2;

MATRIX (12, 1:10)=0.;

MATRIX (12, 11)=+LAMDAG (TAVE1112) *WL/ (TG/4.);
MATRIX (12, 12)=-LAMDAG (TAVE1112) *WL/ (TG/4.) -
LAMDAG (TAVE1213) *WL/ (TG/4.) -
ROG (NODALTEMP (12)) *CPG (NODALTEMP (12)) * (TG/4.) *WL/TIMESTEP;
MATRIX (12, 13)=+LAMDAG (TAVE1213) *WL/ (TG/4.);

MATRIX (12, 14)=0.;

LOAD (12)=-
ROG (NODALTEMP (12)) *CPG (NODALTEMP (12)) *WL* (TG/4.) *1/TIMESTEP*NODALTEMP (12)
;

%EQUATION 13

TAVE1314= (NODALTEMP (13) +NODALTEMP (14)) /2;

MATRIX (13, 1:11)=0.;

MATRIX (13, 12)=+LAMDAG (TAVE1213) *WL/ (TG/4.);
MATRIX (13, 13)=-LAMDAG (TAVE1213) *WL/ (TG/4.) -
LAMDAG (TAVE1314) *WL/ (TG/4.) -
ROG (NODALTEMP (13)) *CPG (NODALTEMP (13)) * (TG/4.) *WL/TIMESTEP;
MATRIX (13, 14)=+LAMDAG (TAVE1314) *WL/ (TG/4.);

LOAD (13)=-
ROG (NODALTEMP (13)) *CPG (NODALTEMP (13)) *WL* (TG/4.) *1/TIMESTEP*NODALTEMP (13)
;

%EQUATION 14

MATRIX (14, 1:12)=0.;

MATRIX (14, 13)=+LAMDAG (TAVE1314) *WL/ (TG/4.);
MATRIX (14, 14)=-LAMDAG (TAVE1314) *WL/ (TG/4.) -ALPHACUNEX*WL-
ROG (NODALTEMP (14)) *CPG (NODALTEMP (14)) * (TG/8.) *WL/TIMESTEP;

```

```

LOAD(14)=-ALPHACUNEX*TAMB*WL-
ROG(NODALTEMP(14))*CPG(NODALTEMP(14))*WL*(TG/8.)*1/TIMESTEP*NODALTEMP(14)
;
%
    %SOLVING SYSTEM OF EQUATIONS

X=inv(MATRIX)*LOAD';

for k=1:NSTRIP
    XFINAL(i,k)=X(k);
    NODALTEMP(k)=XFINAL(i,k);
end

end %time cycle

T=table((1:TIMESTEP:TOTALTIME)', XFINAL);
writetable(T, 'specimen10.txt')

```

Fire Curve – TGAS

```

function [ TGAS ] = TGAS(i, TIME)

TGAS=20.0+345.*log10(8.0*TIME/60.0+1.0);

end

```

Material Properties – Gypsum

```
function [ LAMDAG ] = LAMDAG(TEMP)

if (TEMP<100.0)
    LAMDAG=0.25;
elseif (TEMP>=100.0) && (TEMP<400.0)
    LAMDAG=0.12;
elseif (TEMP>=400.0) && (TEMP<800.0)
    LAMDAG=0.00035*TEMP-0.01;
else
    LAMDAG=0.0013*TEMP-0.77;
end

end
```

```
function [ ROG ] = ROG(TEMP)

if (TEMP<80.0)
    ROG=698;
else
    ROG=576;
end

end
```

```

function [ CPG ] = CPG(TEMP)

if (TEMP<78.0)
    CPG=6.146*TEMP+1377;
elseif (TEMP>=78.0) && (TEMP<85.0)
    CPG=150*TEMP-9858;
elseif (TEMP>=85.0) && (TEMP<97.0)
    CPG=262*TEMP-19501;
elseif (TEMP>=97.0) && (TEMP<124.0)
    CPG=476*TEMP-40311;
elseif (TEMP>=124.0) && (TEMP<139.0)
    CPG=154507-1097*TEMP;
elseif (TEMP>=139.0) && (TEMP<148.0)
    CPG=16601-105*TEMP;
elseif (TEMP>=148.0) && (TEMP<373.0)
    CPG=1189-1.27*TEMP;
elseif (TEMP>=373.0) && (TEMP<430.0)
    CPG=714;
elseif (TEMP>=430.0) && (TEMP<571.0)
    CPG=1151-1.014*TEMP;
elseif (TEMP>=571.0) && (TEMP<609.0)
    CPG=1.877*TEMP-501;
elseif (TEMP>=609.0) && (TEMP<662.0)
    CPG=44.2*TEMP-26300;
elseif (TEMP>=662.0) && (TEMP<670.0)
    CPG=3000;
elseif (TEMP>=670.0) && (TEMP<685.0)
    CPG=103570-150*TEMP;
else
    CPG=571.0;
end

end

```

Material Properties – Insulation (Rock fibre)

```
function [ LAMDAI ] = LAMDAI (TEMP)

if (TEMP<=375)
    LAMDAI=0.00019*TEMP+0.045;
elseif (TEMP>375 && TEMP<=376)
    LAMDAI=-0.005*TEMP+1.99125;
elseif (TEMP>376 && TEMP<=600)
    LAMDAI=0.00031808*TEMP-0.008348214;
elseif (TEMP>600 && TEMP<=680)
    LAMDAI=0.00078125*TEMP-0.28625;
elseif (TEMP>680 && TEMP<=1050)
    LAMDAI=0.000851351*TEMP-0.333918918;
elseif (TEMP>1050 && TEMP<=1200)
    LAMDAI=6.83E-4*TEMP-1.58E-4;
end

end
```

```
function [ ROI ] = ROI (TEMP)

ROI= 75;

end
```

```
function [ CPI ] = CPI (TEMP)

if (TEMP<=80)
    CPI=1.875*TEMP+800;
elseif (TEMP>80 && TEMP<=500)
    CPI=0.833333333*TEMP+883.3333333;
elseif (TEMP>500 && TEMP<=1000)
    CPI=0.52*TEMP+1040;
else
    CPI=0.52*TEMP+1040;
end

end
```


Material Properties - Steel

```
function [ LAMDAS ] = LAMDAS (TEMP)
```

```
if (TEMP<800.0)
```

```
    LAMDAS=54-0.0333*TEMP;
```

```
else
```

```
    LAMDAS=27.3;
```

```
end
```

```
end
```

```
function [ ROS ] = ROS (TEMP)
```

```
ROS=7850;
```

```
end
```

```
function [ CPS ] = CPS (TEMP)
```

```
if (TEMP<600.0)
```

```
    CPS=425.0+0.773*TEMP-1.69E-3*TEMP^2+2.22E-6*TEMP^3;
```

```
elseif (TEMP>=600.0) && (TEMP<735.0)
```

```
    CPS=666+13002/(738-TEMP);
```

```
elseif (TEMP>=735.0) && (TEMP<900.0)
```

```
    CPS=545+17820/(TEMP-731);
```

```
else
```

```
    CPS=650.0;
```

```
end
```

```
end
```